# Electromagnetic Dissociation as a Tool for Nuclear Structure and Astrophysics

Gerhard Baur,[1][*] Kai Hencken,[2][†] Dirk Trautmann[2][‡]

[1]Forschungszentrum Jülich, D-52425 Jülich, Germany
[2]Universität Basel, CH-4056 Basel, Switzerland

February 5, 2008

## Abstract

Coulomb dissociation is an especially simple and important reaction mechanism. Since the perturbation due to the electric field of the (target) nucleus is exactly known, firm conclusions can be drawn from such measurements. Electromagnetic matrixelements and astrophysical $S$-factors for radiative capture processes can be extracted from experiments. We describe the basic elements of the theory of nonrelativistic and relativistic electromagnetic excitation with heavy ions. This is contrasted to electromagnetic excitation with leptons (electrons), with their small electric charge and the absence of strong interactions. We discuss various approaches to the study of higher order electromagnetic effects and how these effects depend on the basic parameters of the experiment. The dissociation of neutron halo nuclei is studied in a zero range model using analytical methods. We also review ways how to treat nuclear interactions, show their characteristics and how to avoid them (as far as possible). We review the experimental results from a theoretical point of view. Of special interest for nuclear structure physics is the appearence of low lying electric dipole strength in neutron rich nuclei. Applications of Coulomb dissociation to some selected radiative capture reactions relevant for nuclear astrophysics are discussed. The Coulomb dissociation of $^8$B is relevant for the solar neutrino problem. The potential of the method especially for future investigations of (medium) heavy exotic nuclei for nuclear structure and astrophysics is explored. We conclude that the Coulomb dissociation mechanism is theoretically well understood, the potential difficulties are identified and can be taken care of. Many interesting experiments have been done in this field and many more are expected in the future.

[*]E-mail: g.baur@fz-juelich.de
[†]E-mail: k.hencken@unibas.ch
[‡]E-mail: dirk.trautmann@unibas.ch

arXiv:nucl-th/0304041v2  1 Jul 2003

# Contents

# 1   Introduction

Nuclear reactions at high energy are very complicated in general, due to the strong interactions between the colliding hadrons. However, in the special case of very peripheral collisions the nuclei do not touch each other and the short range strong forces between the collision partners are avoided. The reaction mechanism becomes simple and unambiguous conclusions can be drawn from such experiments. In very peripheral collisions the nuclei interact with each other through the time-dependent electromagnetic field caused by the moving nuclei. Especially for heavy nuclei these fields are very strong and various interesting effects can occur. It is the purpose of this review to describe them. We discuss how these collisions are treated theoretically and how they are applied to nuclear structure and nuclear astrophysics problems. Coulomb excitation has been a very powerful tool in the past to study electromagnetic matrix-elements in nuclei. Classical review papers exist, see, e.g., [1, 2]. For collision energies below the Coulomb barrier the condition of no nuclear interactions of the nuclei with each other is very well fulfilled and valuable nuclear structure information has been obtained. An important example is the investigation of nuclear rotational and vibrational collective motion by means of Coulomb excitation [1]. Such studies are also of special interest for the investigation of exotic nuclei at the radioactive beam facilities which have become available in the past decades all over the world. Nuclei (far) away from the valley of stability (neutron– or proton–rich) can now be investigated experimentally. They have widened considerably the landscape of nuclear physics and also made possible novel studies in nuclear astrophysics. New phenomema like halo nuclei have been discovered. Electromagnetic excitation and dissociation is again a very powerful tool in this case. They are expected to play an even more important role in the future at the new facilities being proposed presently around the world (GSI, Germany [3], RIA, USA [4, 5], RIKEN, Japan [6]).

The condition that the hadrons do not touch each other can be fulfilled either by using bombarding energies well below the Coulomb barrier, or by going to very forward scattering angles in *intermediate*, ($v \lesssim c$, $\gamma \gtrsim 1$) and *relativistic* ( $v \approx c$, $\gamma \gg 1$) collisions. These forward angles (classically) correspond to impact parameters larger than the sum of the nuclear radii for high beam energies. The two cases are shown schematically in Figs. 1 (a) and (b).

It is very important to note that with increasing beam energy higher lying states can be excited with the Coulomb excitation mechanism. This can lead to Coulomb dissociation, in addition to Coulomb excitation of particle-bound states. This was reviewed some time ago in [7]. It has become more and more clear, that such investigations are also well suited for secondary (radioactive) beams. An (unstable) fast projectile nucleus can interact with a high $Z$ target nucleus. In this way the interaction of an unstable particle with a (quasireal or equivalent) photon can be studied. A similar method is used in particle physics, where it is known as the *Primakoff effect* [8, 9].

Since the electric field of a nucleus with high charge number $Z$ is much stronger than, e.g., the one of an electron, the nucleus can be a very suitable electromagnetic probe for certain cases. One can study, e.g., higher order phenomena, which are inaccessible with conventional electromagnetic probes like the electron. The excitation of the double phonon giant dipole resonance observed at GSI [10, 11] is an example.

We now give a guided tour through the content of this review: we start with a general discussion of the theory of Coulomb excitation and dissociation. Due to the time-dependent electromagnetic field the projectile is excited to a bound or continuum state, which can subsequently decay. Since the electromagnetic interaction is very well known, rather precise unambiguous information can be obtained from such experiments. If first order electromagnetic excitation is the dominant effect, experiments can directly be interpreted in terms of electromagnetic matrix elements which also enter, e.g., in radiative capture cross-sections. It is therefore very important to know the conditions of validity of the first order theory and how to assess quantitatively the higher order effects.

We especially mention two aspects of multiple electromagnetic excitation: it is a way to excite new
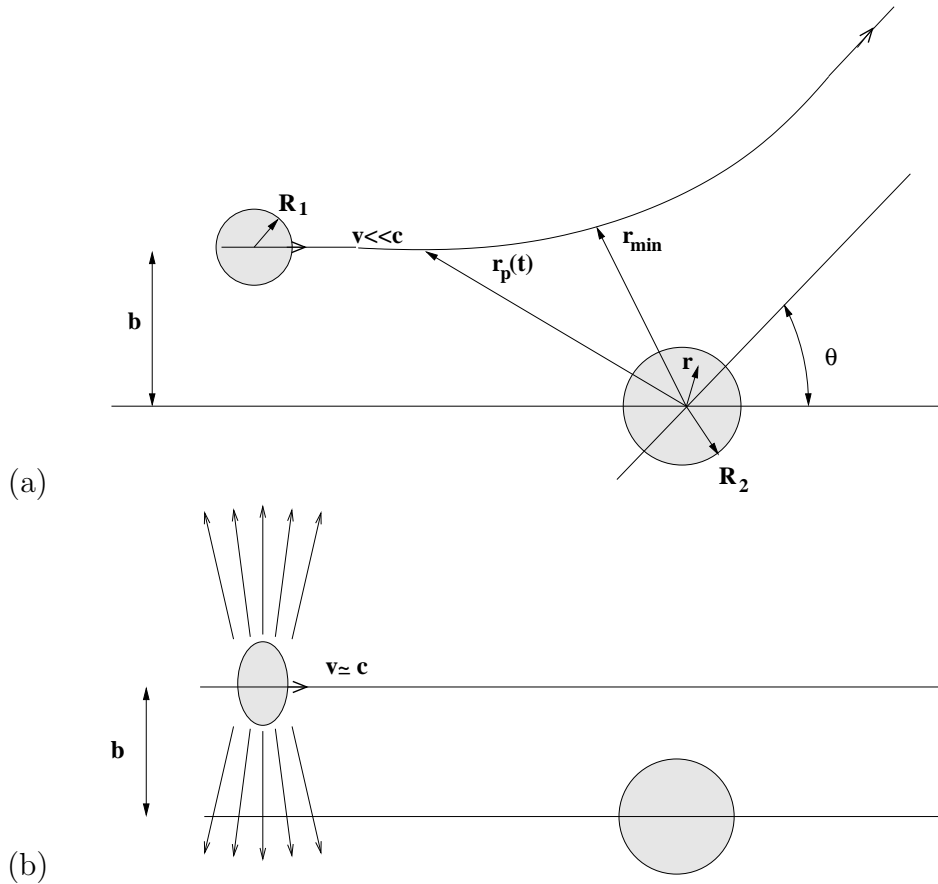
Figure 1: (a) A projectile with charge $Z_1 e$ is scattered on a target nucleus. The projectile velocity is nonrelativistic ($v \ll c$). The minimum distance of closest aproach of the Rutherford trajectory is $r_{min} > R_1 + R_2$, the sum of the nuclear radii. (b) A projectile with velocity $v \lesssim c$ passes by a target nucleus with an impact parameter $b > R_1 + R_2$. The Rutherford orbit is very close to a straight line.

nuclear states, like the double phonon giant dipole resonance [12]; but it can also be a correction to the one-photon excitation [13, 14, 15]. The theoretical methods to treat these problems are discussed in Sec. 3. They range from higher order perturbation theory to Glauber calculations, CDCC (Continuum Discretized Coupled Channel) and solving numerically the time-dependent Schrödinger equation.

Breakup reactions are at least a three-body problem, which is very complicated in general, and the long range character of the Coulomb interaction adds to the complication. We discuss here the Coulomb dissociation of neutron halo nuclei as an illustrative example. We can study analytically a rather simple model of the dissociation of a two-particle system (deuteron, neutron halo nucleus) bound by a zero-range force in the nuclear Coulomb field. This sheds light on the conditions of validity of the usual treatment of the semiclassical Coulomb excitation theory and of the importance of higher order effects. This is done in Sec. 4.

Coulomb excitation is a very useful tool to determine nuclear electromagnetic matrix-elements. This is of interest for nuclear structure and nuclear astrophysics [16, 17, 18, 12]. In the following we illustrate the theoretical concepts and discuss examples of experimental results and their theoretical interpretation. The emphasis is more on theory. As theorists we cannot give a detailed treatment of nor do full justice to the ingenious experimental developments which make possible the precision studies at these extreme forward angles. We refer to the previous reviews, see e.g. [17, 18] and to the new proposals for future facilities like [3] or [4].

In Sec. 6 we review the results that have been obtained on nuclear structure from intermediate

energy electromagnetic excitation in the past years. We briefly mention the Primakoff effect in particle physics, where the nuclear Coulomb field is used to study the interaction of fast (unstable) particles with the quasireal photons due to the Coulomb field of a nucleus. We also mention the very large effects of electromagnetic excitation in relativistic heavy ion collisions in fixed target experiments. These effects become quite spectacular at the heavy ion colliders RHIC and LHC with the very high values of the Lorentz parameter. Recently experimental results from RHIC have become available.

In the next section we discuss applications to radiative capture reactions (the time reversed process of photodissociation) of astrophysical interest. This subject has been reviewed before [18]. This field is rapidly expanding; this is essentially due to the new experimental possibilities world-wide. Future applications are given in Sec. 8. We discuss new possibilities, like the investigation of $r-$ and $rp$–process nuclei, which will be produced with high intensity at the future RIA facilities, and the experimental study of two-particle capture processes by means of Coulomb dissociation. We close with conclusions and an outlook in Sec. 9. This review grew out of a series of lectures given by one of us in the frame of the "European Graduate School Basel-Tübingen", for the transparencies see [19].

# 2   Theory of Electromagnetic Dissociation

First we briefly recall the basic points of the theory of nonrelativistic (NR) Coulomb excitation. Excellent reviews exist, see e.g. [1]. It is usually a very good approximation to treat the relative motion between projectile and target classically (*semiclassical approximation*). It is also well understood how one can obtain the semiclassical limit from the quantal theory [2]. We want to concentrate here on intermediate and relativistic energies. In these cases one can replace the Rutherford trajectory by a straight line to a good approximation. In contrast to low energy Coulomb excitation retardation is now an important effect and the long wave-length approximation is not necessarily a good approximation. Deviations from the straight line approximation have to be and can be assessed quantitatively. In collisions above the Coulomb barrier strong interactions between the nuclei cannot be avoided. However at very forward angles, corresponding to large impact parameters, such nuclear effects can become negligible. Even then there can be some kind of nuclear effects at a certain level of accuracy: there is diffraction due to the wave nature of the projectile. However, essentially due to the small de Broglie wavelength of the projectile this effect is quite small. These questions will be addressed in Sec. 5 below.

## 2.1   *Nonrelativistic (NR) Projectile Velocity*

We discuss briefly the basic ideas of (NR) Coulomb excitation. The condition of *no nuclear contact* is ensured by using bombarding energies below the Coulomb barrier. In the semiclassical theory the projectile moves on a classical Rutherford trajectory, see Fig. 1(a), giving rise to a time dependent external electromagnetic field. Nonrelativistic semiclassical Coulomb excitation theory is a classical textbook example of the application of time-dependent perturbation theory, see, e.g., [20] or [21].

The excitation of the target nucleus is due to the static Coulomb interaction, or more generally, (see [1], Eq. (II.1.2)) the mutual electromagnetic interaction between the ions. For NR collisions we can *neglect retardation*, and the electromagnetic interaction can be written as

$$W(1,2) = \int \int d^3r_1 d^3r_2 \frac{\rho_1(\vec{r_1})\rho_2(\vec{r_2}) - \vec{j_1}(\vec{r_1}) \cdot \vec{j_2}(\vec{r_2})/c^2}{|\vec{r_1} - \vec{r_2}|}, \tag{1}$$

where $\rho_i(\vec{r_i})$, $\vec{j_i}(\vec{r_i})$ are the charge and current densities for the projectile $(i = 1)$ and the target nucleus $(i = 2)$, respectively. For non-overlapping charge-densities one can express $W(1,2)$ in terms of the electromagnetic multipole moments of the two nuclei. The full expression is given in [1]. We give here

only the most important terms, that is the *monopole-monopole* and *monopole-multipole* interactions and neglect the less important multipole-multipole interactions.

We are especially interested in target excitation. In this case we can assume that nucleus 1 is a point charge, we have $\rho_1(\vec{r}_1) = Z_1 e \delta(\vec{r}_p(t)) - \vec{r}_1)$. We can specialize to the coordinate system $(\vec{r}, \vec{r}_p)$, where $\vec{r}$ is the target coordinate (measured from the center of mass of the target) and $\vec{r}_p(t)$ is the relative coordinate between the center of masses of the two nuclei, see Fig. 1(a). In the semiclassical theory $\vec{r}_p(t)$ is a classical time-dependent parameter. The charge operator $\rho(\vec{r})$ is given by

$$\rho(\vec{r}) = e \sum_i \delta(\vec{r} - \vec{r}_i), \tag{2}$$

where the $\vec{r}_i$ denote the proton coordinates.

Neglecting the multipole-multipole interactions we can write the electromagnetic interaction as

$$W(1,2) = V(1, \vec{r}_p(t)) + V(2, \vec{r}_p(t)) + \frac{Z_1 Z_2 e^2}{r_p(t)}. \tag{3}$$

The last term is the monopole-monopole Coulomb potential between projectile and target which is responsible for the Coulomb trajectory of the projectile. The quantity $V(2, \vec{r}_p(t))$ gives rise to target excitations and $V(1, \vec{r}_p(t))$ to projectile excitations, respectively.

The monopole–electric-multipole interaction can be obtained from the expansion

$$\frac{1}{|\vec{r} - \vec{r}_p|} = 4\pi \sum_{\lambda\mu} \frac{1}{2\lambda+1} \frac{r^\lambda}{r_p^{\lambda+1}} Y_{\lambda\mu}^*(\hat{r}) Y_{\lambda\mu}(\hat{r}_p), \tag{4}$$

where we have made use of the condition of *no nuclear contact* so that always $r < r_p$. In this way, the variables $r$ and $r_p$ are separated.

The total time-dependent interaction relevant for the target excitations is given by the sum $V(2, \vec{r}_p(t))$ = $V_E(2, \vec{r}_p) + V_M(2, \vec{r}_p)$, where we can write the quantities $V_E$ (electric interaction) and $V_M$ (magnetic interaction), see Eqs. (II.1.12) and (II.1.13) in [1], as

$$V_E(2, \vec{r}_p) = \sum_{\lambda \geq 1, \mu} \frac{4\pi Z_1 e}{2\lambda+1} M(E\lambda, -\mu)(-1)^\mu r_p^{-\lambda-1} Y_{\lambda\mu}(\hat{r}_p) \tag{5}$$

$$V_M(2, \vec{r}_p) = \sum_{\lambda \geq 1, \mu} \frac{4\pi Z_1 e}{2\lambda+1} \frac{i}{\lambda} M(M\lambda, -\mu)(-1)^\mu \frac{\dot{\vec{r}}_p}{c} r_p^{-\lambda-1} \vec{L} Y_{\lambda\mu}(\hat{r}_p). \tag{6}$$

The electromagnetic interaction can be parametrized completely in terms of the electromagnetic multipole matrix-elements $M(\pi\lambda\mu)$. In the long wave length limit they are defined as

$$M(E\lambda\mu) = \int d^3 r \rho(\vec{r}) \, r^\lambda \, Y_{\lambda\mu}(\hat{r}) \tag{7}$$

$$M(M\lambda\mu) = \frac{-i}{c(\lambda+1)} \int d^3 r \vec{j}(\vec{r}) \cdot \left[ r^\lambda \, \vec{L} \, Y_{\lambda\mu}(\hat{r}) \right], \tag{8}$$

with $\vec{L} = -i\vec{r} \times \vec{\nabla}$. Especially we have $M(E00) = Z_2 e/\sqrt{4\pi}$, where $Z_2$ is the electric (monopole) charge of the target nucleus.

The condition of no nuclear contact is vital to this approach. In this case we obtain the complete separation into the electromagnetic matrixelements of the target. For $r > r_p$ the strong interaction between the nuclei would come into play and would severely modify the results. This is discussed in detail in Sec. 5 (and also in [22, 23]).

There are a few dimensionless parameters which characterize the electromagnetic excitation: we define the *adiabaticity parameter* as the ratio between the *collision time* and the *excitation time*

$$\xi = \frac{\tau_{coll}}{\tau_{exc}}. \tag{9}$$

We can estimate the collision time to be $\tau_{coll} = r_{min}/(\gamma v)$ and we have $\tau_{exc} = \hbar/\Delta E$, where $\Delta E = \hbar\omega$ is the nuclear excitation energy. From this we get

$$\xi = \frac{\omega r_{min}}{\gamma v}. \tag{10}$$

For NR collisions we have $\gamma \approx 1$, whereas in the relativistic case (see below) the Lorentz parameter $\gamma$ can be much larger than one and the collision time can become very small due to the Lorentz contraction. For adiabaticity parameters $\xi \gg 1$ the system can follow the adiabatic ground state and no excitation occurs [20] (with probability $\sim \exp(-\xi)$). This means also that in NR Coulomb excitation one can only excite nuclear states for which the long-wavelength limit is valid: Due to the adiabaticity condition $\xi \lesssim 1$ we have $\omega r_{min} \ll v$. This leads to $kR_2 \ll 1$, where $k = \omega/c$ and $R_2$ denotes the size of the nucleus (see Fig. 1(a)), since $r_{min} > R_2$ and $v < c$. On the other hand, for relativistic collisions the collision time can be very small and one is able to excite states for which the long wavelength limit is no longer valid.

A second parameter is the *strength parameter*, which is defined as the strength of the interaction potential times its duration (in units of $\hbar$):

$$\chi = \frac{V_{int}\tau_{coll}}{\hbar}. \tag{11}$$

Here $V_{int}$ denotes a typical value of the interaction potential. For a multipole interaction of order $\lambda$, this value of the interaction potential is typically $e \langle f \| M(E\lambda) \| i \rangle / r_{min}^{\lambda+1}$ (NR case), the strength parameter $\chi$ is therefore estimated to be

$$\chi = \frac{Z_1 e < f \| M(E\lambda) \| i >}{\hbar v r_{min}^{\lambda}}. \tag{12}$$

(The relativistic case will be discussed below: in this case, the collision time has a $\gamma^{-1}$-dependence; the interaction $V_{int}$ is proportional to $\gamma$ and $\chi$ becomes independent of $\gamma$.) The strength parameter for the monopole-monopole case is the Coulomb parameter, which is given by

$$\eta = \frac{Z_1 Z_2 e^2}{\hbar v}. \tag{13}$$

In order to obtain the equation describing the time evolution of the system under the influence of the electromagnetic field, we expand the wave function of the target nucleus into the complete set of eigenstates of the target Hamiltonian $\Phi_n$ with energy $\hbar\omega_n$.

$$\Psi(t) = \sum_n a_n(t) \exp(-i\omega_n t)\Phi_n, \tag{14}$$

One finds the following system of coupled equations (see, e.g., Eq. (5.29) of [1]) for the excitation amplitudes $a_n(t)$

$$i\hbar \dot{a}_n = \sum_m \langle n|V(t)|m\rangle \exp[i(\omega_n - \omega_m)t]\, a_m(t), \tag{15}$$

where the time-dependent electromagnetic interaction is denoted by $V(t)$. A formal solution can be given using the time ordering operator $\mathcal{T}$ as (see Eq. (II.3.13) of [1])

$$a_n(\infty) = \langle n| \mathcal{T} \exp\left(-\frac{i}{\hbar} \int_{-\infty}^{+\infty} dt \tilde{V}(t)\right) |0\rangle, \tag{16}$$

where the interaction $\tilde{V}$ is given by

$$\tilde{V}(t) = \exp(iH_0 t/\hbar)V(t)\exp(-iH_0 t/\hbar) \tag{17}$$

and $H_0$ is the Hamiltonian of the nuclear system.

We mention two important limits: if the electromagnetic interaction $V(t)$ is weak enough (strength parameter $\chi \ll 1$), it can be treated in first order (*one photon exchange*) and one obtains an expression which factorizes into the orbital integrals and the electromagnetic matrixelements. One has [1]

$$a_n = \frac{4\pi Z_1 e}{i\hbar} \sum_{\lambda\mu} \frac{(-1)^\mu}{2\lambda+1} < n|M(E\lambda, -\mu)|0 > S_{E\lambda\mu}. \tag{18}$$

The orbital integrals $S_{\pi\lambda\mu}$ can be calculated from the kinematics of the process [1] (We have given here only the electric part of the excitation, $\pi = E$, the magnetic part $\pi = M$ can be found in [1]). Thus the experimentally determined excitation probabilities (or cross-sections) are directly proportional to the reduced transition probabilities $B(\pi\lambda)$ (see Eq. (4), p. 93 of [1]).

Another important limit is the *sudden approximation*, where the collision time $\tau_{coll} = r_{min}/\gamma v$ is much smaller than the nuclear excitation time $\tau_{exc} = 1/\omega$, i.e., the adiabaticity parameter $\xi$ is much smaller than one. But the strength parameter $\chi$ can have arbitrary values. In this case, we have $\tilde{V} \approx V$ and we can neglect the time ordering in Eq. (16) and the electromagnetic interaction can be summed to all orders. For large values of $\xi$ and $\chi$ one may use an adiabatic representation of the Schrödinger equation, see [1]. It is also often useful to solve Eq. (15) numerically in these cases. (The case of the excitation of a harmonic oscillator can be treated exactly analytically, see below.) In contrast to the NR case considered in this subsection the velocity for intermediate energy and relativistic collisions $v$ is close to $c$, and the strength parameter $\chi$, see Eq. (12), cannot be too large in these cases and higher order effects tend to be small, see also Sec. 2.2. This is in contrast to Coulomb excitation below the barrier, where $v \ll c$ and $\chi$ can be much larger than one. An example is the excitation of a rotational band in deformed nuclei [1], more details will be given in Sec. 3.

Although we have shown above that we can treat the electromagnetic interaction in the limit of no retardation for NR collisions, one may also treat the electromagnetic interaction in its full relativistic form, taking retardation effects into account. This is done, e.g., in [2] using the Coulomb gauge. In addition to the contribution from the instantaneous Coulomb interaction (*longitudinal photons*) one gets the one photon exchange contribution due to the $H_{int} = \vec{j} \cdot \vec{A}$ interaction (*transverse photons*). The multipole expansion of the vector potential $\vec{A}$ is performed, and it is found [2] that the instantaneous Coulomb interaction is canceled by a certain term (see Eq. (139) in the appendix) and only the contribution from transverse photon remains. Again there is a factorization into an orbital integral and an electromagnetic matrixelement; this time it is the full electromagnetic multipole matrix element (see Eqs. (141) and (142)) in the appendix, where the wave number is equal to $k = \omega/c$, i.e., *at the photon point* (*please note that the long wavelength approximation is not made in this case*). One may say that (NR) Coulomb excitation is due to longitudinal (Coulomb) photons, yet it is true that the nuclear structure information is entirely contained in electromagnetic matrixelements *at the photon point* $k = \omega/c$. (For more details see the appendix.)

There is an important difference of Coulomb excitation to electron inelastic scattering. In inelastic electron scattering the photon is *virtual* (spacelike, i.e., $|\vec{k}| > \omega$), and one can study electromagnetic matrixelements as a function of momentum transfer. In this way, e.g., the spatial distribution of the nuclear charge can be investigated. Also monopole transitions can occur.

The matrixelements occurring in Coulomb excitation determine the interaction of real (*transverse*, $q^2 = 0$) photons with the nuclear system. The equivalence of the current and charge matrix-elements (see Eqs. (7) and (141)) in the long wavelength limit is sometimes called "Siegert's theorem", see e.g. p. 89ff of [21]. From the above it is clear that the condition of no nuclear contact is the more basic

condition than the long wave length limit. In the following discussion of relativistic electromagnetic excitation, the long wavelength limit does not generally apply. Yet, due to the condition of no nuclear contact, the information about nuclear structure is again entirely contained in the electromagnetic matrixelements at the photon point.

Before going to intermediate energy and relativistic energy electromagnetic excitation let us mention the straight line limit of the NR Coulomb excitation theory: From the standard formalism of Coulomb excitation using Rutherford trajectories one can also obtain this limit by going to small scattering angles $\theta$. There remains a characteristic difference between the straight line theory and the straight line limit of the Rutherford trajectory: a factor $\exp(-\pi\xi/2)$, see Eq. (II.E.79) of [2]. This factor can be traced back to the influence of Coulomb repulsion; the impact parameter $b$ should be replaced by an effective impact parameter. This is explained in detail in [2]and [24]. We come back to this in the next section, where the relativistic case is discussed.

## 2.2 *Equivalent Photon Method, Theory of Relativistic Coulomb Excitation*

### 1. Basic Idea

The equivalent photon method was introduced by Fermi in a classic paper in 1924 [25, 26], see also the translation by Gallinaro and White [27]. He considered only the NR case, the relativistic generalisation was subsequently given by Weizsäcker and Williams [28, 29]. This method is lucidly described in the textbook of Jackson [30], so let us only summarize very briefly the idea:

We consider the classical straight line motion of a charged particle with charge $Ze$ and impact parameter $b$ (see Fig. 1(b)). This motion gives rise to a time-dependent electromagnetic field at a given point (the target nucleus). The Fourier-transform of the electric field is *"compared to the corresponding electric field of a suitable spectrum of light"* [25]. In this way, Fermi introduced the idea of *"äquivalente Strahlung"* (equivalent photons). In this method only the $E1$-multipole is treated correctly, since the spatial variation of the electric field strength over the nuclear volume is neglected. Higher multipoles ($E2$, $E3$, ..., $M1$, $M2$, ...) show a different behaviour (see, e.g., [7] and below). Higher multipole contributions are given correctly only in the limit $\gamma \to \infty$ in this approach.

In the equivalent photon approximation the cross section for an electromagnetic process is written as

$$\sigma = \int \frac{d\omega}{\omega}\, n(\omega)\sigma_\gamma(\omega). \tag{19}$$

where $\sigma_\gamma(\omega)$ denotes the appropriate cross section for the photo-induced process and $n(\omega)$ is the equivalent photon number. The equivalent photon number in the case of a point particle is given in terms of the modified Bessel functions $K_n$ as:

$$n(\omega) = \frac{2Z_1^2\alpha}{\pi}\frac{c^2}{v^2}\left[\xi K_0(\xi)K_1(\xi) - \frac{v^2\xi^2}{2c^2}(K_1^2(\xi) - K_0^2(\xi))\right], \tag{20}$$

where $\xi = \omega b_{min}/\gamma v$. The minimum impact parameter is denoted by $b_{min} = R_1 + R_2$. Eq. (20) is well approximated by

$$n(\omega) = \frac{2}{\pi}Z_1^2\alpha \ln\frac{\gamma v}{\omega b_{min}} \tag{21}$$

for $v \sim c$ and $\xi \ll 1$.

For $\xi \gg 1$ one can use the asymptotic expression for the modified Bessel functions and obtain a spectrum which decreases exponentially with $\xi$:

$$n(\omega) \approx \frac{Z_1^2\alpha}{2}\exp(-2\xi). \tag{22}$$

9

Already from this simple approach the major properties can be read off: the equivalent photon spectrum is very soft, it shows essentially an $1/\omega$ dependence. There is an adiabatic cutoff at $\omega = \gamma v/b_{min}$. There is a $(c/v)^2$ dependence, which gives a large photon flux for small beam velocities. However, this is restricted to small photon energies, $\omega < \gamma v/b_{min}$.

## 2. Semiclassical straight line approximation and exact multipole decomposition

In the above method equivalent photon numbers of higher ($E2$, $E3$, ..., $M1$, $M2$,...) electromagnetic multipoles are in general not treated properly. A beautiful analytic expression which treats all multipoles exactly was given in [24], see also [7]. We discuss it briefly now.

In the relativistic case, retardation can no longer be neglected. One can use, e.g., the Liénard-Wiechert potential (see Eq. (143)) in order to describe the (retarded) electromagnetic interaction [24], corresponding to the Lorentz gauge. In the multipole expansion the condition $r < r_p$ is used and again (see appendix for more details) one can separate the first order amplitude into an *orbital part* and a *structure part*, which consists of the electromagnetic matrix elements at the photon point (*no long wave length limit is made*). We give only the final formula here:

$$a_{fi} = -i\frac{Z_1 e}{\gamma \hbar v} \sum_{\pi l m}(-1)^m \sqrt{2l+1}\left(\frac{\omega}{c}\right)^l G_{\pi l m}\left(\frac{c}{v}\right) K_m\left(\frac{\omega b}{\gamma v}\right)\langle I_f M_f|\, M(\pi l - m\,|I_i M_i\rangle, \qquad (23)$$

where the functions $G_{\pi l m}$ can be expressed in terms of the associated Legendre polynomials, see [24].

This formula is the basis for the analysis of electromagnetic excitation. The dependence on the electromagnetic multipolarity $\pi l$, the impact parameter $b$ and the Lorentz factor $\gamma$ is clearly exposed. We note that the above equation is a first order result, i.e. the strength parameter $\chi$ should be much smaller than one. In the straight line relativistic case we can write $\chi$ as (see Eq. (1.6) of [24])

$$\chi \sim \frac{Z_1 e < f|M(E\lambda)|i >}{\hbar v b^\lambda}. \qquad (24)$$

We may define an *intermediate energy region* where $\gamma v/c = \gamma\beta = \sqrt{\gamma^2 - 1} =\lesssim$ 1–2. In this region there are relativistic effects, see [31], but also effects from the Coulomb repulsion. This region is of special interest to us: at GSI we have $\gamma\beta \sim$ 1–2, at MSU, RIKEN, and GANIL there is $\beta\gamma \lesssim 0.5$.

While in the nonrelativistic theory the Coulomb repulsion of the ions is included in the Rutherford trajectory, the problem for the relativistic case (where we have assumed a straight line trajectory) is more delicate. A very interesting approach to treat the classical trajectory in a relativistic Coulomb problem can be found in [31, 32].

It was shown in [24] that a simple redefinition of the impact parameter accounts well for Coulomb repulsion:

$$b' = b + a_0\frac{\pi}{\gamma}. \qquad (25)$$

An alternative procedure is suggested in [33, 34] where the following substitution is made:

$$b' = a_0 + \sqrt{a_0^2 + b^2}. \qquad (26)$$

This amounts to replacing the asymptotic impact parameter $b$ by the distance of closest approach in small angle scattering. The quantity $a_0$ is given in the NR, as well as, in the relativistic case by $a_0 = \hbar\eta/(kv)$ with $\hbar k = \gamma m_a v$ the momentum of the projectile nucleus. Recently the effects of retardation on the electromagnetic excitation in intermediate energy collisions were carefully studied in [35]

We note some further properties: The high energy $\gamma \to \infty$ limit is investigated in [24]. The question of which value of the magnetic quantum number $m$ gives the largest contribution to a given transition depends on the value of $k$. For small values of $k$ the amplitudes for $m = \pm l$ are largest. The excitation

amplitude is proportional to $1/b^l$. Integrating over $b$ this leads to the logarithmic rise of the cross section with $\gamma$ only for $l = 1$, i.e., for dipole transitions ($E1$, $M1$). Higher multipoles on the other hand tend to a constant in this approximation (i.e. neglecting the $m = \pm 1$ contribution). For large impact parameters $kb > l$ the largest contribution is due to $m = \pm 1$. This contribution corresponds to the Weizsäcker-Williams approximation, where the excitation corresponds to the absorption of a photon traveling in the beam direction with helicity $m = \pm 1$ (see the Eqs. (2.20)–(2.23) in [24]). Now there is the logarithmic rise of the cross section for all multipolarities, albeit only for extremely high values of $\gamma$.

### 3. Validity of the Semiclassical Method:

It is well known that for Coulomb parameters $\eta \gg 1$ the semiclassical approximation can be used. This can be seen from the following argument: two different transverse momenta $q_T$ are associated with an impact parameter $b$: The Coulomb repulsion gives a (classical) momentum transfer to the nucleus perpendicular to the beam direction. It is given by $q_{T,Coul} = 2\eta\hbar/b$. Due to quantal diffraction we have a transverse momentum $q_{T,diff} = \hbar/b$ associated with the impact parameter $b$. The semiclassical approximation is appropriate as long as the Coulomb push $q_{T,Coul}$ is much larger than the uncertainties associated with the wave nature of the particle, i.e., $q_{T,Coul} \gg q_{T,diff}$, or $\eta \gg 1$. A more refined derivation of this condition can be found in [36] and also in App. B of [1]. Another condition for the validity of the semiclassical approximation is $\Delta E/E \ll 1$, i.e., the energy loss due to the excitation is small. This is well fulfilled due to the adiabaticity condition Eq. (10).

From the criterion for the validity of the semiclassical approximation (i.e. $\eta \gg 1$) we find: for highly charged ions with $Z_1 Z_2 > 137$ (like the Pb–Pb system) the semiclassical approximation is valid for all velocities $v$, whereas in general we should satisfy the condition $Z_1 Z_2 > 137 v/c$ or $v/c < Z_1 Z_2/137$; for sufficiently low velocities the semiclassical approximation becomes always applicable.

## 2.3   *Quantum Mechanical Treatment of Projectile Motion: PWBA and Glauber Method*

For cases where the Coulomb parameter $\eta$ is smaller than one the semiclassical approximation is not valid. Well-known prominent examples are electron or proton scattering on light target nuclei. In these cases one uses fully quantal approaches like PWBA or Glauber theory [7, 15]. The nuclear interaction with the nucleus can often be taken into account using the black disk approximation. Characteristic diffraction effects arise, see also [37, 18] and [15].

For $\eta \gg 1$ one can obtain the semiclassical limit starting from a quantum-mechanical approach [1]. In Glauber theory this can be done as follows, e.g., see [38] (see also Eqs. (73)-(80) of [34]). The excitation amplitude has the form (see Eq. (73) of [34])

$$f^{\mu}_{inel}(\theta) = ik \int_0^{\infty} db\, b\, J_\mu(qb) \exp[i\chi(b)]\, a_\mu(b). \tag{27}$$

The eikonal phase for a Coulomb potential can be written as $\chi(b) = 2\eta ln(kb)$. The inelastic excitation amplitude is denoted by $a_\mu$ (cf. Eq. (16) or (18)) where $\mu$ denotes the $z$-component of the angular momentum transfer to the nucleus. The integrand in Eq. (27) oscillates rapidly as a function of $b$. In the semiclassical approximation we obtain the main contribution for those values of $b$ where the phase is stationary.

We can approximate the Bessel function for large values of $qb$ as

$$J_\mu(qb) \approx \frac{1}{\sqrt{2\pi qb}}\left[\exp\left(iqb - i\pi\frac{\mu + 1/2}{2}\right) + \exp\left(-iqb + i\pi\frac{\mu + 1/2}{2}\right)\right]. \tag{28}$$

We use the stationary phase (saddle point) approximation

$$\int db\, G(b) \exp\left[i\Phi(b)\right] \approx \sqrt{\frac{2\pi i}{|\Phi''(b_0)|}}\, G(b_0) \exp(-i\pi/4) \exp\left[i\Phi(b_0)\right], \tag{29}$$
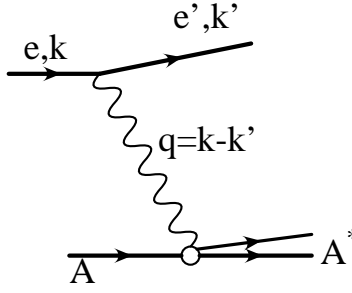
Figure 2: One-photon excitation e.g. in the $(e, e')$ reaction. In PWBA there is a definite four-momentum transfer $q_\mu = k_\mu - k'_\mu$ to the nucleus. In contrast to this there is no definite value of $q$ in the Coulomb excitation due to the large number of additionally exchanged elastic photons.

where a phase $\exp(-i\pi/4)$ needs to be chosen for our case, where $\Phi''(b_0) = -q^2/(2\eta) < 0$ and which is valid for slowly varying functions $G(b)$. The point of stationary phase is denoted by $b_0$, it is determined from the condition

$$\Phi'(b_0) = 0. \tag{30}$$

With

$$\Phi(b) = -qb + 2\eta ln(kb). \tag{31}$$

the condition Eq. (30) leads to

$$b_0 = \frac{2\eta}{q}, \tag{32}$$

i.e., the classical connection between impact parameter and scattering angle, or momentum transfer. We obtain

$$f^\mu_{inel}(\theta) \approx \frac{ik}{\sqrt{q}} \sqrt{\frac{ib_0}{|\Phi''(x_0)|}} \exp\left[i\chi(b_0) + i\pi\mu/2\right] a_\mu(b_0), \tag{33}$$

Finally we obtain

$$\frac{d\sigma_{inel}}{d\Omega} = \frac{d\sigma_{Rutherford}}{d\Omega} P(b_0), \tag{34}$$

where $P(b_0) = \frac{1}{2I_i+1} \sum_{m_i,m_f} |a_\mu|^2$, analogous to the expression in the nonrelativistic case [2, 1].

The main difference of electromagnetic excitation in hadron-hadron scattering, as opposed to electron- (lepton-) hadron scattering, is due to the strong absorption at impact parameters less than the sum of the two nuclear radii. Thus, for $\eta \gg 1$ the semiclassical method is very suitable to take these effects into account, because the impact parameter is the relevant variable and not the momentum transfer. Neglecting strong absorption effects it can be shown that (first order) SCA and PWBA give identical results for total cross sections (where the limit of the momentum transfer $q_{max}$ must be extended to $\infty$; this is in general a good approximation as the contribution to the cross section for large $q$ is rather small ). For the nonrelativistic case this is shown, e.g., in [39], the relativistic generalization is given by [7]. Likewise the equivalence of the coupled channel semiclassical theory and Glauber theory (i.e., with the electromagnetic interaction treated to all orders) is given in [40]. It should be noted however that *differential cross sections* are different in the PWBA and SCA approaches, and thus the appropriate theory should be used in each individual case.

In the PWBA there is a definite four-momentum transfer $q_\mu = k_\mu - k'_\mu$, that is, a definite energy transfer $\omega = q_0$ and a definite three-momentum transfer $\vec{q} = (\vec{q_T}, q_l)$. To a good approximation $q_l$ is given by the minimum momentum transfer $q_l = q_{min} = \omega/v$ for small angle scattering and small energy loss. The invariant mass of the photon is $Q^2 = -q^2 = q_T^2 + (\omega/(\gamma v))^2$. We always have $Q^2 > 0$: the exchanged photon is *virtual* (spacelike).

12

In contrast to this, the photon, which is exchanged in Coulomb excitation, contains a sum over virtual photon momenta; they conspire in such a way that only an electromagnetic matrix-element survives, which corresponds to the interaction with a real photon $Q^2 = 0$ (see appendix for details).

In principle, heavy ion electromagnetic excitation can also be treated within field theory. This is however rather complicated and has to our knowledge never fully been done in practice. Due to the validity of the semiclassical approximation it is also not necessary to do so. Let us indicate how one would proceed [41, 42]: There are infinitely many graphs which have elastic photon exchanges between the two ions. For small angle scattering and high energies one can make use of an relativistic eikonal approach [43, 44]. In this approach infinitely many Feynman graphs are summed. The result can again be expressed in terms of an expression in impact parameter space with a relativistic eikonal $\chi$. The semiclassical approach can be recovered in exactly the same way as already explained above. From the saddle point (stationary phase) approximation one obtains again the relation $b = 2\eta/q$. For $b < b_{min} = R_1 + R_2$ there is nuclear contact and and graphs which involve the strong interaction have to be added, see [44]. In the case of nucleus-nucleus collisions the black disk model can be applied. This means that the eikonal $\chi$ is a very large imaginary number for $b < b_{min} = R_1 + R_2$.

# 3 Higher Order Effects

The importance of higher order effects is governed by the strength parameter $\chi$. This parameter is proportional to $1/v$, see Eq. (12) and Eq. (24) above. For slow collisions the Coulomb field acts for a long time and this parameter can be quite large. E.g., rotational bands in deformed nuclei can be very well excited in this way and this has been a fruitful field of research [1]. For collisions with $v \lesssim c$ higher order effects tend to be small. The strength parameter $\chi$ will soon reach its lower limit, which we have for $v = c$ in Eq. (12) and Eq. (24).

Let us deal in the first subsection with a very interesting higher order electromagnetic excitation process at intermediate and relativistic energies: the excitation of the Multiphonon Giant Dipole Resonance, especially the Double Phonon Giant Dipole resonance (DGDR). In the following subsection we will discuss a more disturbing effect: corrections of one-photon exchange effects due to multiphoton exchange (a similar problem exists for $(e, e')$ scattering named *dispersion corrections* see, e.g. [21]).

## 3.1 *Multiphonon Giant Dipole Resonances*

The Giant Dipole Resonance (GDR) is a collective mode par excellence. This can directly be seen from the fact that the energy-weighted TRK-sum rule (Eq. (109) below) is exhausted by this mode. With its large $B(E1)$-value this transition is very strongly excited electromagnetically in intermediate energy heavy ion collisions. For heavy systems the excitation probability in grazing collisions is of the order of 30 percent. From this one can conclude directly that higher order effects must play a role. This was the situation in the middle of the eighties, and the question was to which states does the GDR couple most strongly. There is the Axel-Brink hypothesis that a GDR is built on any nuclear (excited) state. In this spirit a multiphonon harmonic oscillator model was adopted in [12, 45] and higher order electromagnetic excitation was calculated within this model. In the harmonic oscillator model the interaction can be included to all orders and a Poisson distribution of the multiphonon states is found, as is well known, see, e.g., [1]. We give some key steps in the derivation of this result, see also [46].

In terms of the corresponding creation and destruction operators $a^\dagger$ and $a$ the Hamiltonian of a harmonic oscillator is given by

$$H = \hbar\omega(a^\dagger a + \frac{1}{2}),\tag{35}$$

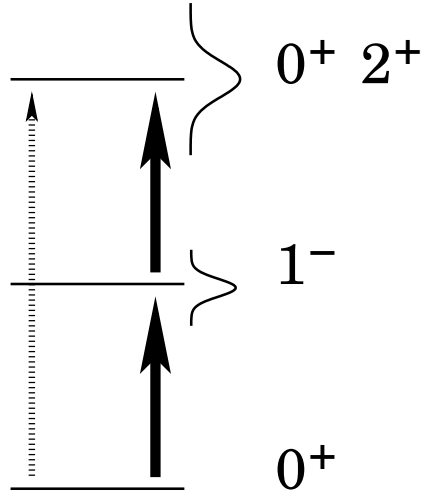where $\omega$ denotes the energy of the oscillator. We have the boson commutation rules $[a, a^\dagger] = 1$ and

Figure 3: One- and two-photon excitation of the DGDR. The one-photon excitation to the DGDR is forbidden ($0^+ \rightarrow 0^+$) or strongly hindered ($0^+ \rightarrow 2^+$).

$[a, a] = [a^\dagger, a^\dagger] = 0$, respectively. Only one mode is shown explicitly, in general one has to sum (integrate) over all the possible modes.

We assume that the interaction $V$ is linear in the creation and destruction operators:

$$V(t) = f(t)(a + a^\dagger). \tag{36}$$

In this case we can calculate $\tilde{V}$ (Eq. (17)) explicitly using the boson commutation rules given above and the expansion

$$\tilde{V}(t) = V(t) + it[H_0, V(t)] + \frac{(it)^2}{2!}[H_0, [H_0, V(t)]] + \cdots. \tag{37}$$

One finds

$$\tilde{V}(t) = f(t) \left( a^\dagger e^{-i\omega t} + a e^{i\omega t} \right). \tag{38}$$

Now we can convince ourselves that the commutator of $\tilde{V}$ at different times $t$ and $t'$ is a pure $c$-number. In this case we can disregard the time ordering operator in Eq. (16) and obtain an exact analytical answer, up to an unimportant overall phase factor (for details see, e.g., [1]).

This leads to the excitation of a so-called coherent state, see [47, 48]. For the excitation of multi-phonon states this is explicitly shown, e.g., in [49]. One has

$$a_n = < n|e^{-i(u*a^\dagger + ua)}|0 > = \frac{(-iu^*)^n}{\sqrt{n!}} e^{-\frac{1}{2}uu^*}, \tag{39}$$

where $u$ is the $c$-number

$$u = \int_{-\infty}^{\infty} dt\, f(t) \exp(-i\omega t) \tag{40}$$

In order to show this the operator identity $e^{A+B} = e^A e^B e^{-\frac{1}{2}[A,B]}$ was used, which is valid for two operators $A$ $(= -iu^*a^\dagger)$ and $B$ $(= -iua)$ for which the commutator is a $c$-number.

The excitation probability $P_N(b)$ of an $N$-phonon state is given by

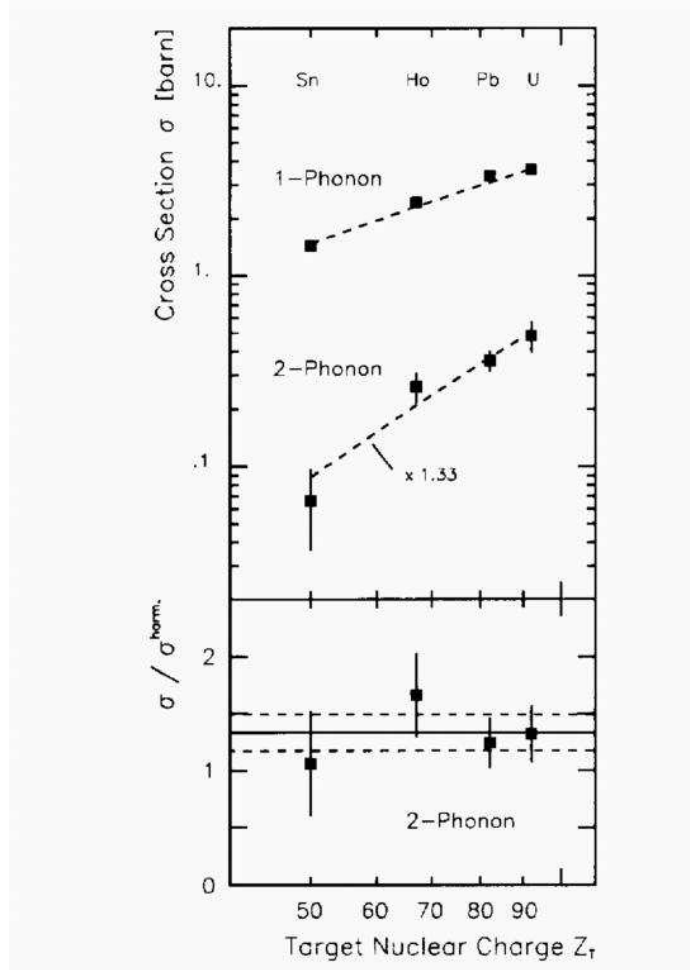$$P_N(b) = \frac{\left[P^{(1)}(b)\right]^N \exp\left[-P^{(1)}(b)\right]}{N!}, \tag{41}$$

14

Figure 4: (upper panel) Integrated experimental cross sections for the one-phonon GDR and the DGDR in $^{208}$Pb obtained from different targets of nuclear charge $Z$. In case of the DGDR the calculated values are multiplied by a factor of 1.33 to fit to the experimental data. (lower panel): ratio of the experimental cross sections for the DGDR in $^{208}$Pb to the harmonic approximation. The mean value and its error are indicated by solid and dashed lines , respectively. Taken from [50], Fig. 2 there, where further details can be found.

where $P^{(1)}(b)$ is the excitation probability of the GDR for an impact parameter $b$ calculated in first order perturbation theory. It is given by [7]

$$P^{(1)}(b) = \frac{2\alpha^2 Z_1^2 N_2 Z_2}{A_2 m_N \omega} \frac{1}{b^2}, \tag{42}$$

where the energy $\omega$ of the resonance is given by $\omega = 80A^{-1/3}$MeV and where $N_2$ and $A_2$ are the neutron and mass number of the nucleus, which is excited.

Certainly the most difficult question at that time was the width of the multi-phonon states (It still is today.)

Subsequently detailed experiments [51, 52] were carried out at GSI and the two-photon excitation of the DGDR was clearly observed in a two step excitation process, see Fig. 3. Generally, the experiments also confirmed the simple theoretical approach. In Fig. 4 we show the dependence of GDR and DGDR excitation on the charge number $Z$ of the target. For the GDR we have a one-photon exchange, i.e., there is a $Z^2$ dependence. For the DGDR we have a two-photon exchange, i.e., a $Z^4$ dependence, essentially in agreement with the experimental result [50].

However, interesting differences to the harmonic model showed up, which motivated various groups to do more detailed theoretical calculations. Most conspicuously, the width of the DGDR tends to be somewhat less than twice the width of the one-phonon GDR. The DGDR is a remarkable example of a large amplitude collective motion with damping. We refer in this respect to the reviews [11] and [53], where also further references can be found. The influence of the damping on the GDR- and DGDR-excitation cross sections was investigated in [54], a more sophisticated approach was adopted in [55]. This work also puts the approach of Carlson et al. [56, 57] on a firmer theoretical basis. A schematic model which treats the coherent (collective) excitation modes and their coupling to more complicated states was considered in [58].

It would also be very interesting to study the DGDR in deformed nuclei like $^{238}$U. What will the splitting of the DGDR be due to the nuclear deformation? What is the influence of the nuclear shape on the minimum impact parameters? Clearly, a closer look at these problems would be very interesting in the future.

Due to the very collective nature of the GDR, the electromagnetic couplings in this case are very strong. As we have seen in this section, interesting effects follow from this. Even at the relativistic heavy ion colliders RHIC and LHC the GDR, and possibly also DGDR, play an interesting role, which is briefly discussed in Sec. 6.2.

Finally we mention that multiphonon states were also reviewed in [59], where emphasis is also put on the nuclear excitation mechanism (which becomes important for lower beam energies) and quadrupole phonons. Multiphonon states were first investigated in pion-charge exchange reactions [60].

## 3.2  *Corrections to One-Photon Exchange*

Now we turn to cases where the higher order effects are less pronounced. But still they are there and they are essentially a correction to the most interesting dominant first order effect. There are various methods to take higher order electromagnetic effects into account theoretically. If the coupling is strong, a coupled channels approach is appropriate (see Eq. (15)), sometimes higher (especially second) order perturbation theory is sufficient. There is a sum over all intermediate states $n$, which are (considered to be) important [1]. Another approach is to integrate the time-dependent Schrödinger equation directly for a given model Hamiltonian [61, 62, 63, 64]. In this way all orders are taken into account.

If the collision is sudden ($\xi \ll 1$), one can neglect the time ordering $\mathcal{T}$ in the usual perturbation approach, see Eq. (16) (*sudden approximation*). The interaction is again summed to infinite order. In order to obtain the excitation cross section one has to calculate the matrix element of this operator between the initial and final state. Intermediate states $n$ do not appear explicitly.

In order to see the typical effects and how they depend on the relevant parameters we now study higher order effects in the simple model of [13]. Let us briefly describe this model. It will be discussed also in the following section, where this model is discussed in the so-called post-form DWBA (*distorted wave Born approximation*). (The method used here is more closely related to the *prior-form DWBA*.)

We assume a target nucleus with charge $Z$ (to avoid unnecessary complications we assume an infinite mass for a pedagogical discussion, this is however not essential). We want to describe the breakup of a bound state $a = (c + n)$ with binding energy $E_0$ in the Coulomb field of this target. There is the Coulomb interaction $V_c = Z_c Z e^2 / r_c$ between the target and the core $c$. We assume a zero range interaction between the core and the neutron. This can be viewed as a deep square well potential with depth $V$ extending up to a radius $a$ with $a^2 V$ held constant when $a \to 0$. In this potential an $s$-wave bound state can exist.

In order to calculate the breakup process $Z + (c + n) \to Z + c + n$ we assume that the $(c + n)$-system moves on a straight line trajectory with velocity $v$ and impact parameter $b$ in a semiclassical model. We restrict ourselves to electric dipole transitions. The $E1$ and $E2$ effective charges are given by $Z_{eff}^{(l)} = Z_c \left[ \frac{m_n}{m_n + m_c} \right]^l$, $l = 1, 2, \cdots$. Due to the smallness of $Z_{eff}^{(2)}$ it is a good approximation to neglect

the $E2$ transitions for the neutron-core case (This is in contrast to the proton-core case to be discussed below). Analytical results were obtained for $1^{st}$ and $2^{nd}$ order electromagnetic excitation for small values of the adiabaticity parameter $\xi$. We are especially interested in collisions with small impact parameters, where higher order effects tend to be larger than for the very distant ones. In this case the adiabaticity parameter $\xi$ is small. For $\xi = 0$ (*sudden approximation*) we have a closed form solution. (This is a special example of the general formula, see Eq. (16) but without the time-ordering operator). In Eq. (37) of [13] the angle integrated breakup probability is given. We expand this expression in a scaling parameter

$$y = \frac{2ZZ_c e^2 m_n}{\hbar v (m_n + m_c) b\kappa} = \frac{m_n \eta}{(m_n + m_c) b\kappa}, \tag{43}$$

where the parameter $\kappa$ is related to the binding energy $E_0$ by

$$E_0 = \frac{\hbar^2 \kappa^2}{2\mu}. \tag{44}$$

and the reduced mass $\mu$ is given by

$$\mu = \frac{m_n m_c}{m_n + m_c}. \tag{45}$$

This parameter $y$ is directly related to the strength parameter $\chi$. We define another scaling parameter

$$x = \frac{q_{rel}}{\kappa}, \tag{46}$$

where the wave number $q_{rel}$ is related to the energy $E_{rel}$ of the continuum final state by

$$E_{\text{rel}} = \frac{\hbar^2 q_{rel}^2}{2\mu}. \tag{47}$$

In leading order (LO) we obtain

$$\frac{dP_{LO}}{dq_{rel}} = \frac{16}{3\pi\kappa} y^2 \frac{x^4}{(1+x^2)^4}. \tag{48}$$

The next to leading order (NLO) expression is proportional to $y^4$ and contains a piece from the $2^{nd}$ order $E1$ amplitude and a piece from the interference of $1^{st}$ and $3^{rd}$ order. We find [65]

$$\frac{dP_{NLO}}{dq_{rel}} = \frac{16}{3\pi\kappa} y^4 \frac{x^2 (5 - 55x^2 + 28x^4)}{15(1+x^2)^6}. \tag{49}$$

These are very simple and transparent results for the Coulomb dissociation of neutron-halo nuclei. There are two scaling parameters $x$ and $y$. The parameter $x$ controls the shape of the relative energy distribution, whereas the parameter $y$ plays the role of the strength parameter. We have given these formulae explicitly, since they show most of the important features in a simple analytical formula: as is to be expected, $y$ is proportional to the target charge $Z$ and the effective $E1$-charge $Z_c m_n/(m_n + m_c)$. It is proportional to $1/v$, again this is the special case of a general result. We also have the $1/b$ dependence characteristic of $E1$ transitions.

The integration over $x$ and the impact parameter $b$ can also be performed analytically in good approximation, for details see [65]. We can insert the corresponding values for the Coulomb dissociation experiments on $^{11}$Be and $^{19}$C [67, 66] in the present formulae. We find that the ratio of the NLO contribution to the LO contribution in the case of Coulomb dissociation on $^{19}$C [66] is given by $-2\%$. This is to be compared to the results of [68], where a value of about $-35\%$ was found (A further discussion of this is found in [65]). A version of the theoretical model used in [68], see also [69], is discussed below in Sec. 4.
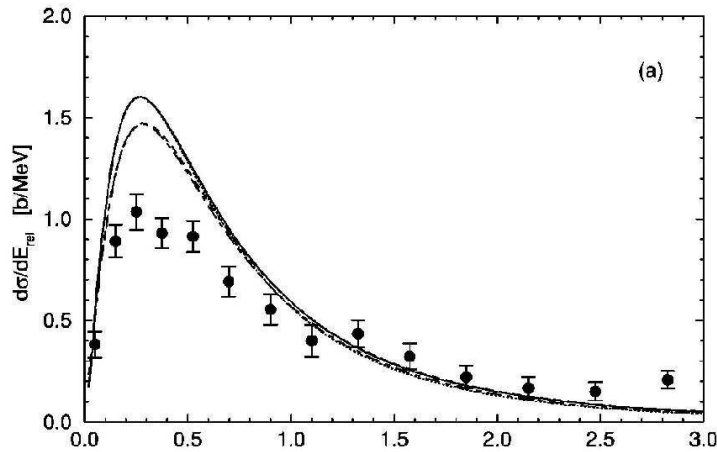
Figure 5: Differential cross sections integrated over scattering angle from $0^0$ to $3^0$ for the Coulomb dissociation of 67 $A$MeV $^{19}$C scattered on $^{208}$Pb as a function of the relative energy. The solid line shows the results of the LO expression (Eq. (48)), the dashed one includes also the NLO contribution (Eq. (49)). The dotted line shows the results of a semiclassical calculation for $E1$ only in first order, the dashed-dotted line (which almost coincides with the (dashed) LO+ NLO results) for the numerical solution of the Schödinger equation with $E1$. Both $1^{st}$ order calculations (solid and dotted line) are also in close agreement with each other. The points are the experimental results from [66]. Reproduced from Fig. 3 of [65]. Copyright (2001) by the American Physical Society.

In Fig. 5 we show a comparison of theoretical and experimental differential cross sections for Coulomb dissociation of $^{19}$C , see Fig. 3 of [65]. In this figure, LO and NLO results (Eqs. (48) and (49)) are also compared to full dynamical calculations (solution of the time-dependent Schrödinger equation).

Let us now deal with the breakup of a proton-core system as another typical case. Examples are $^{8}$B = $^{7}$Be + $p$ or $^{17}$F = $^{16}$O + $p$. In this case, the $E1$-effective charge is small and the $E2$-effective charge is large, as compared to the neutron-core case. The effective charges are given by $Z_{eff}^{(l)} = Z_c(\frac{-m_p}{m_p+m_c})^l + Z_p(\frac{m_c}{m_p+m_c})^l$ ($l = 1, 2, ...$) where $m_p$ and $m_c$ are the masses of the proton and the core, $Z_c$ is the charge number of the core and $Z_p = 1$. Also in view of the importance of the $^{8}$B Coulomb dissociation for the solar neutrino problem (more see below in Sec. 7) this case has been studied extensively with all the methods available, which we now briefly survey. In most models, some nuclear structure quantities enter and it is a pity that somewhat different assumptions (for example about $E1$ or $E2$ matrix elements) are used in the different calculations by the various groups. This makes the comparison of the different reaction calculations somewhat more difficult. How does one separate the effects from the nuclear structure input and the effects of the different approximations in the reaction theory? Yet, quite a conclusive picture has emerged. Using perturbation theory, higher order effects in the Coulomb dissociation of $^{8}$B were studied in [14, 15]. This approach works best for the high beam energies. Results are given in Fig. 23, see Sec. 7 below.

The CDCC (*Coupled Discretized Continuum Channels*) method was also applied, for recent references see [70, 71]. The effects of $E2$ and higher order excitations are included. Since the relative motion of the projectile and target, with its huge number of partial waves is treated in a quantum mechanical way, this kind of method becomes numerically more and more involved for high energies. In [72] it was seen that (not unexpectedly, since the corresponding $\eta$-value is much larger than 1) the semiclassical approximation compares well to corresponding fully quantal calculations at sub-barrier energies. This is a great simplification in the numerical evaluation. At higher energies, where also nuclear (grazing)
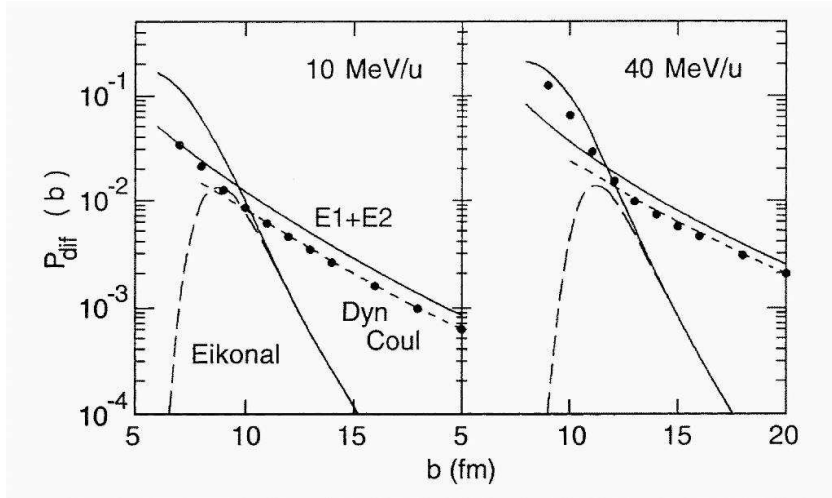
18

Figure 6: Diffraction dissociation probabilities of the $^{17}$F ground state at 10 and 40 $A$MeV on a $^{208}$Pb target. The points are the results of the full dynamic calculation. The long-dashed and steep solid line is the result of an eikonal calculation with and without core-absorption effects. The flatter solid line is the result of a first order calculation including $E1$ and $E2$ contribution. The short dashed line is the result of the dynamic calculation including only the Coulomb interaction. Taken from [22], Fig. 5 there.

collisions can become important, a Glauber approach is very useful [34].

Instead of expanding the wave function into the nuclear basis states one may also study the time-development of the nuclear wave function directly. With modern powerful computational methods it is now possible to solve the time-dependent Schrödinger equation very efficiently [73, 22, 62, 74, 75]. It may be considered to be a drawback of these approaches that they rely on choosing a specific (simple) nuclear Hamiltonian, like a particle-core model with a phenomenological interaction between them. However, it will cover the essential aspects of the problem in most cases. In practice such approaches turn out to be very useful and also give us some general insight into, e.g., the importance of higher order effects.

Esbensen and Bertsch [22] investigated the two-body $(p+^{16}$O)breakup of $^{17}$F on Ni and Pb targets at 10-40 $A$MeV. Higher order, as well as, nuclear effects are important and we report on some of their results now. A *"dynamic polarization (Barkas) effect"* is found. It is essentially due to the interference of a (first order) $E1$ amplitude and a (second order) $E1$-$E2$ amplitude. The effect is proportional to $Z^3$. In Fig. 6 we show the breakup probabilities of $^{17}$F on a Pb target at 10 and 40 $A$MeV as a function of the impact parameter.

In [1] one may find various approaches to study deviations from the sudden approach, see, e.g., the discussion in Sec. II.3. It would be of interest to further explore this in the future.

In summary we may say that higher order effects are well under control. After all we have a fair knowledge about nuclear structure and a very good knowledge of how to treat the electromagnetic interaction. Due to present days' computing power many quite involved calculations have become possible and they are essential for the analysis of the experimental data. Simple models and analytical solutions are also useful: they show the dependence on the various parameters.

# 4 Analytically Solvable Model for the Coulomb Breakup of Neutron Halo Nuclei

Breakup processes in nucleus-nucleus collisions are complicated, in whatever way they are treated. They constitute at least a three-body problem, which is further complicated due to the long range Coulomb force. Exact treatments (like the Faddeev-approach) are therefore prohibitively cumbersome. On the other hand, many approximate schemes have been developed in the field of direct nuclear reactions, and these approaches have been used with considerable success [76]. In this context we wish to investigate a realistic model for the Coulomb breakup of a neutron halo nucleus. This model has already been mentioned in the previous section. With the operation of exotic beam facilities all over the world, these reactions (previously restricted essentially to deuteron induced reactions) have come into focus again. The Coulomb breakup of these nuclei is of interest also for nuclear astrophysics, since the breakup cross section can be related to the photo-dissociation cross section and to radiative capture reactions relevant for nuclear astrophysics [18], see Sec. 7 below.

In this section we study the Coulomb breakup of a neutron-halo nucleus with a zero-range neutron-core interaction. A full quantum mechanical treatment can be done with two different treatments of the final state. In the so-called *prior-form* the Hamiltonian $H$ is split in the initial and final channel into

$$H = H_f^{prior} + V_f^{prior}, \tag{50}$$

where

$$H_f^{prior} = T + V_a + V_{cn} \tag{51}$$

and

$$V_f^{prior} = V_c + V_n - V_a, \tag{52}$$

where $V_i$ denotes the interaction of $i = c$, $n$ with the target nucleus and $V_{cn}$ is the relative core-neutron interaction. The interaction $V_a$ is an optical model interaction of the $a = (c + n)$ bound state with the target nucleus. The final state is a product of the wave function of the center of mass (with the coordinate vector $\vec{R}$) and the relative wave function of the unbound $(c + n)$ system [76].

In the so-called *post-form* the Hamiltonian $H$ is split in the final channel into

$$H = H_f^{post} + V_f^{post}, \tag{53}$$

where

$$H_f^{post} = T + V_n + V_c \tag{54}$$

and

$$V_f^{post} = V_{nc}. \tag{55}$$

The interactions $V_n$ and $V_c$ are treated to all orders in this way, whereas the relative interaction between $c$ and $n$ is only treated in first order. In the previous section we have studied the *prior-form* DWBA (in its semiclassical limit, i.e. for large values of the Coulomb parameter $\eta$). Accordingly we have used a decomposition into a c.m. motion of the projectile system and its relative wave function in the initial and final channel.

An important benefit of the present model is that it can be solved analytically in the CWBA (neglecting the nuclear interaction of the projectile with the target we can call the DWBA the *Coulomb Wave Born Approximation* CWBA), see Sec. 4.2. Analytic expressions also exist for the PWBA limits of both prior- and post-form, which we can compare with each other. Thus this model constitutes an ideal *theoretical laboratory* to investigate the physics of breakup reactions. We can study certain limiting cases and its relation to the semiclassical approximation, which is mainly used in the analysis of experiments. Especially the effect of *postacceleration* (to be explained in more detail below) can be

studied in a unique way in this approach. We will first study the plane wave limits of both the prior- and post-form and compare them with the semiclassical limit. The question of higher-order effects will then be discussed in the full CWBA approach.

## 4.1 *Theoretical Model, Plane Wave Approximations and Qualitative Discussion*

We consider the breakup of a particle $a = (c + n)$ (deuteron, neutron-halo nucleus) consisting of a loosely bound neutral particle $n$ and the core $c$ (with charge $Z_a = Z_c$) in the Coulomb field of a target nucleus with charge $Z$

$$a + Z \rightarrow c + n + Z. \tag{56}$$

To simplify the kinematical relations we assume in this section that the target is infinitely heavy (this is not necessary, see below). We assume that the $a = (c + n)$ system is bound by a zero range force, see Sec. 3. The potential $V_{cn}$ is adjusted to give one $s$-wave bound state with a binding energy $E_0$. Neglecting the nuclear interaction of $c$ and $n$ with the target (*pure Coulomb* case) the Hamiltonian of the system is given by

$$H = T_n + T_c + \frac{Z Z_c e^2}{r_c} + V_{cn}(r). \tag{57}$$

The bound-state wave function of the system is given by

$$\phi_0 = \sqrt{\frac{\kappa}{2\pi}} \frac{\exp(-\kappa r)}{r}, \tag{58}$$

where the quantity $\kappa$ is related to the binding energy $E_0$, see Eq. (44) above.

The incoming particle $a$ has a momentum $\vec{q}_a$ and the momenta of the outgoing particles $c$ and $n$ are denoted by $\vec{q}_c$ and $\vec{q}_n$, respectively; see also Fig. 7 below. It is useful to introduce also the relative and c.m. momenta $\vec{q}_{rel}$ and $\vec{q}_{cm}$ which are related to $\vec{q}_c$ and $\vec{q}_n$ in the following way:

$$\vec{q}_{rel} = \frac{m_c \vec{q}_n - m_n \vec{q}_c}{m_n + m_c} \tag{59}$$

$$\vec{q}_{cm} = \vec{q}_c + \vec{q}_n. \tag{60}$$

These momenta are further constrained by energy conservation

$$\frac{q_a^2}{2m_a} - \frac{\kappa^2}{2\mu} = \frac{q_c^2}{2m_c} + \frac{q_n^2}{2m_n} = \frac{q_{cm}^2}{2(m_c + m_n)} + \frac{q_{rel}^2}{2\mu}. \tag{61}$$

From the experimental point of view it is interesting to mention at this point a *magnifying glass effect*: for a given scattering angles of the particle $c$ and $n$ there is a minimum relative energy $E_{rel}^{min}$. The relative energy $E_{rel} = q_{rel}^2/(2\mu)$ is a small quantity, close to $E_{rel}^{min}$. It can be determined accurately from the measurement of the momenta $\vec{q}_c$ and $\vec{q}_n$ (which are both large), see, e.g., [16] and Fig. 4 of [17].

It is interesting to write down the amplitude for the breakup reaction in Born (plane wave) approximation. This approximation is valid for small values of the Coulomb parameter $\eta_a$. This parameter characterizes the strength of the Coulomb interaction. In the applications considered here $\eta_a$ is usually much larger than one, but still, this example will expose many characteristic features of the breakup process. In the prior-form we split the Hamiltonian, see above, into $H = H_0 + V_c$ with $H_0 = T + V_{cn}$ (i.e. we we set $V_a = 0$). Accordingly we have in the initial state a plane wave for the c.m. motion and a bound state wave function; in the final state we have again a plane wave of the c.m. motion and the relative continuum wave function, which in the zero-range approximation is given by

$$|\vec{q}_{rel}\rangle = \exp(i\vec{q}_{rel} \cdot \vec{r}) - \frac{\exp(i q_{rel} r)}{(\kappa + i q_{rel})r}, \tag{62}$$

i.e., only the $s$-wave is modified by the short range potential $V_{cn}$. Using the Bethe integral

$$\frac{1}{r_c} = \frac{1}{\left|\vec{R} - \frac{m_n}{m_a}\vec{r}\right|} = \frac{1}{2\pi^2}\int d^3q \frac{\exp\left[i\vec{q}\cdot(\vec{R} - \frac{m_n}{m_a}\vec{r})\right]}{q^2}, \tag{63}$$

we can separate the matrix element into the relative and c.m. coordinates. The $T$-matrix in the Born approximation (PWBA) is found to be

$$T^{Born} = 4\pi \frac{ZZ_c e^2}{q^2} a_{fi}(\vec{\Delta}p), \tag{64}$$

where $\Delta p$ is related to the momentum transfer (or *Coulomb push*) to the target nucleus

$$\vec{q} = \vec{q}_a - \vec{q}_{cm} = \vec{q}_a - \vec{q}_c - \vec{q}_n \tag{65}$$

by $\vec{\Delta}p = (m_n/m_a)\vec{q}$. This *Coulomb push* has a perpendicular component $q_\perp$ and a component in the beam direction $q_\parallel$. For high energies we have $q_\parallel = \omega/v$ (corresponding to the *minimum momentum transfer*). The amplitude $a_{fi}$ can be calculated analytically, see, e.g., Eqs. (33), (34) of [13]. It is found to be

$$a_{fi} = \sqrt{8\pi\kappa}(a_{FT} + a_S). \tag{66}$$

The quantity $a_{FT}$ is essentially the Fourier transform of the Yukawa wave function, given by

$$a_{FT} = \frac{1}{(\vec{q}_{rel} - \vec{\Delta}p)^2 + \kappa^2} \tag{67}$$

and $a_S$ takes the $s$-wave scattering part of the continuum wave into account:

$$a_S = \frac{i(\kappa + iq_{rel})}{2|\Delta p|(\kappa^2 + q_{rel}^2)} \ln \frac{\kappa + i(q_{rel} + |\Delta p|)}{\kappa + i(q_{rel} - |\Delta p|)}. \tag{68}$$

We are interested in forward angle scattering at high energies. The value of $q_\parallel$ is usually small and we have $q \approx q_a\theta$ where $\theta(\ll 1)$ is the scattering angle. We can introduce the modulus of the elastic scattering Coulomb amplitude

$$f_{coul} = \frac{2\eta_a q_a}{q^2} \approx \frac{2\eta_a}{q_a\theta^2}. \tag{69}$$

We find $T = (2\pi/m_a)f_{coul}a_{fi}$. For very small values of $q$, or equivalently $\Delta p$, the terms $a_{FT}$ and $a_S$ nearly cancel each other (the bound and the continuum wave functions are orthogonal) and the dipole term will be dominant. We find

$$a_{fi}(\vec{q}_{rel}, \vec{\Delta}p) \approx \sqrt{8\pi\kappa}\frac{2\vec{q}_{rel}\cdot\vec{\Delta}p}{(q_{rel}^2 + \kappa^2)^2}. \tag{70}$$

We can compare this expression with two others: the semiclassical straight line expression [13] in Sec. 3 above and the Born limit of the post form CWBA.

First, we recall the results of [13] and Sec. 3 above. In this approach the semiclassical straight line approximation is used. It is valid for high beam energies and for $\eta_a \gg 1$. In the *semiclassical approach* (corresponding to the *prior form* decomposition of $H$), one now calculates (*impact parameter dependent*) breakup amplitudes $a_{fi}(b)$; the breakup amplitude is given by

$$f_{breakup} = f_{coul}a_{fi} \tag{71}$$

and the cross section is

$$d\sigma/d\Omega = d\sigma_{ruth}/d\Omega \ |a_{fi}(b)|^2, \tag{72}$$

where

$$\frac{d\sigma_{ruth}}{d\Omega} = |f_{coul}|^2. \tag{73}$$

The impact parameter $b$ is related to the *Coulomb push* by the semiclassical relation $b = 2\eta_a/q$. We see that the formula for the Born approximation is the same as the one derived for the semiclassical sudden limit. Please keep in mind however that the ranges of validity of the two approaches, do not overlap: for the Born approximation we have $\eta_a \ll 1$ while the semiclassical approximation requires $\eta_a \gg 1$. In the sudden limit we have $\omega = 0$ and there is only a transverse momentum transfer $q_\perp$. The breakup amplitude in the sudden limit is given by, see Eq. (33) of [13]

$$a_{fi} = \langle q| \exp(i\vec{\Delta}p \cdot \vec{r}) |0\rangle . \tag{74}$$

It should be kept in mind that in [13] only the electric dipole component is considered. The above equation leads to

$$a_{fi} = i\vec{\Delta}p \cdot \langle q| \vec{r} |0\rangle \tag{75}$$

in lowest order of $\Delta p$ or $q$. This expression is the same as Eq. (70). In this case there is no interaction between the $c$ and $n$ in the final state $p-$wave. In higher orders of $q$, however, this interaction will show up.

Now we compare these *prior form* expressions to the *post-form* DWBA scheme. In the prior form we have a c.m.-motion (either *classical* or *quantal*) of the center of mass (with coordinate vector $\vec{R}$) of the $(c+n)$-system (either in the ground- or excited state) in the Coulomb field $ZZ_ce^2/R$. If this potential is neglected because of the high projectile energies, one has a plane wave or a straight line trajectory. The relative wave function of the $(c-n)$-system is governed by the internal Hamiltonian $H_{cn} = T_{cn} + V_{cn}$.

In the post-form the Hamiltonian in the final state is split as in Eqs. (53)–(55). I.e., we take the Coulomb interaction between $Z$ and $c$ fully into account in the final state (i.e., postacceleration effects are fully considered) and treat $V_{cn}$ to lowest order only. In our model there is no resonance structure in the $c + n$ continuum. We can expect that $V_{cn}$ is not so important. This is clearly a good assumption for the deuteron and will also hold for other neutron halo systems. Similarly a c.m. Coulomb wave function is used for the initial state. In the final state the broken up system is treated in a different way, more appropriate if there are strong postacceleration effects. This is, e.g., found to be the case for low energy deuteron breakup, see [77, 78]. For this see the next subsection.

We first give explicitly the (Born) plane wave limit [79] of the post-form DWBA (or CWBA). The Born approximation in this case is obtained by substituting for the full Coulomb wave functions in Eq. (85) below their $1^{st}$ order expansions in $V_c$. We find (see Eq. (3) of [79])

$$T = D_0 f_{coul} 4\pi \left[ \frac{1}{q_a^2 - (\vec{q}_n + \vec{q}_c)^2} + \frac{m_c}{m_a} \frac{1}{(q_c^2 - (\vec{q}_a - \vec{q}_n)^2)} \right], \tag{76}$$

where the *zero-range constant* is given by

$$D_0 = \frac{\hbar^2}{2\mu} \sqrt{8\pi\kappa}. \tag{77}$$

As above, $f_{coul}$ is the modulus of the Coulomb scattering amplitude Eq. (69).

This expression shows a similarity to the Bethe-Heitler formula for bremsstrahlung $Z + e^- \rightarrow Z + e^- + \gamma$. The Bethe-Heitler formula has two terms which correspond to a Coulomb interaction of the electron and the target followed by the photon emission and another one, where the photon is emitted first and then the electron scatters from the nucleus. Now we have a Coulomb scattering of the incoming
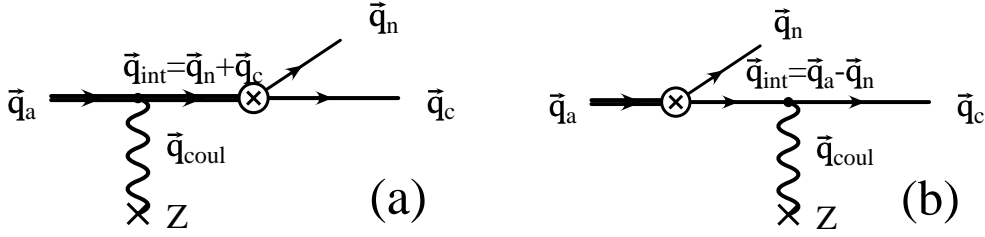
Figure 7: The two bremsstrahlung type of graphs, which describe the Coulomb breakup in the post-form Born approximation. Three-momentum conservation at each vertex determines the intermediate momenta $\vec{q}_{\text{int}}$.

particle followed by breakup $a = (c + n) \rightarrow c + n$ and another term, where the projectile $a$ breaks up into $c + n$, and subsequently, $c$ is scattered on the target $Z$.

The two terms in the parenthesis correspond to the two graphs shown in Fig. 7.

It is useful to rewrite the denominators of Eq. (76) in terms of the relative and c.m. variables $q_{rel}$ and $\Delta p$ (Eqs. (60) and (65)) as

$$q_a^2 - q_{cm}^2 = \frac{m_a^2}{m_n m_c}(q_{rel}^2 + \kappa^2) \tag{78}$$

and

$$q_c^2 - (\vec{q}_a - \vec{q}_n)^2 = -\frac{m_c + m_n}{m_n}(\kappa^2 + (\vec{q}_{rel} - \vec{\Delta}p)^2)), \tag{79}$$

where we have used the energy conservation Eq. (61) to obtain this result. For the $T$-matrix we obtain

$$T = \sqrt{8\pi\kappa}\frac{2\pi f_{coul}}{m_a}\left(\frac{1}{q_{rel}^2 + \kappa^2} - \frac{1}{(\vec{q}_{rel} - \vec{\Delta}p)^2 + \kappa^2}\right). \tag{80}$$

For small values of $\Delta p$, or equivalently $q$, the two terms almost cancel.

We can expand this equation in the small parameter $\Delta p$. In lowest order we obtain

$$T = \sqrt{8\pi\kappa}f_{coul}\frac{2\pi}{m_a}\frac{2\vec{\Delta}p \cdot \vec{q}_{rel}}{(\kappa^2 + q_{rel}^2)^2}. \tag{81}$$

We can compare this to the limit of small $\vec{\Delta}p$ in the prior form PWBA, Eqs (64) and (70). We see that these limits agree with each other.

For *larger* values of $q$ characteristic differences will appear: in Eq. (64) the $n$-$p$ final state interaction in the $l = 0$ channel is treated properly. This is not the case for Eq. (76) or (80). In this equation, on the other hand the Coulomb force on the core $c$ in the final state is treated properly.

In the Born approximation it is only the momentum transfer $\vec{q} = \vec{q}_a - \vec{q}_c - \vec{q}_n$ and not the momentum $q_a$ itself which enters into the matrix element. In the semiclassical approximation, on the other hand, the quantity $v_a = q_a/m_a$ appears explicitly. This quantity enters in the adiabaticity parameter $\xi$, a concept not present in the plane wave approach. The (nonrelativistic) adiabaticity parameter (see Eq. (10)) is given by

$$\xi = \omega b/v_a = \frac{2\eta_a\omega/v_a}{q} = \frac{2\eta_a q_{\parallel}}{q_{\perp}}. \tag{82}$$

We have $q_{\parallel} = \omega/v_a$ and, for not too large impact parameters, $q_{\perp} \sim q$. As we know, for large values of the adiabaticity parameter, i.e. when $2\eta_a q_{\parallel} \gg q_{\perp}$, the breakup probability is suppressed exponentially with $\xi$. In the next subsection we will also encounter a simple limit of the full CWBA expression, very

much related to the plane wave (Born) treatment of the post form CWBA given above. It is valid for small values of $\xi$ and *arbitrary* values of $\eta_a$. We will also treat the case of large values of $\eta_a$ and $\xi$ there.

It is an interesting and difficult task to specify more clearly the ranges of validity of the post and prior formulations. In the simplest high energy limit we have just found that there are regions where both approaches agree with each other. For low energy deuteron breakup the post-form CWBA is very reasonable, whereas the prior form is very poor [80]. What about high energies? In second order of $\Delta \vec{p}$ differences show up. Which of the two approximations is reasonable, and in which region of parameter space? The relevant parameters are $x$, $y$, and $\xi$, what is the range of validity of $x$- and $y$-scaling? In this context we mention a recent paper [81], where final state three-body Coulomb effects are discussed for the $^{208}\mathrm{Pb}(^8\mathrm{B},^7\mathrm{Be} + p)^{208}\mathrm{Pb}$ Coulomb breakup reaction.

## 4.2   CWBA

In the post-form CWBA the Hamiltonian is split in two ways corresponding to the initial and final states. We have $H = H_i + V_i$ where

$$H_i = T + V_{nc}(r) + V_a(R) = T_R + T_r + V_{nc}(r) + \frac{ZZ_ce^2}{R}, \tag{83}$$

i.e., the initial state separates in the $\vec{r}$ and $\vec{R}$ coordinates. In the final state we have $H = H_f + V_f$ with

$$H_f = T + V_c(r_c) = T_{r_c} + T_{R_{n-(Ac)}} + \frac{ZZ_ce^2}{r_c}. \tag{84}$$

The $T$-matrix for the reaction Eq. (56) can be written as [82]

$$T = \left\langle \chi^{(-)}_{\vec{q}_c} \psi_{\vec{q}_n} \middle| V_{nc} \middle| \chi^{(+)}_{\vec{q}_a} \phi_0 \right\rangle = D_0 \int d^3R \chi^{(-)}_{\vec{q}_c}(\vec{R}) e^{-i\vec{q}_n \cdot \vec{R}} \chi^{(+)}_{\vec{q}_a}(\vec{R}), \tag{85}$$

with the *zero range constant* $D_0$ as given in Eq. (77) above.

In order to compare with experimental data, one has to take the finite target mass $m_A$ into account in a standard way. For this one replaces the momenta of the previous section (where the target mass was assumed to be infinite) by the ones with the correct kinematics and the masses $m_a$, $m_c$, and $m_n$ would have to be replaced by the reduced masses $(m_a m_A)/(m_a + m_A)$, $(m_c m_A)(m_A + m_c)$ and $(m_n(m_A + m_c))(m_n + m_c + m_A)$, respectively. Note that if we would have included also an interaction $V_n$ such a separation would not have been possible.

The initial state is given by the incoming Coulomb wave function $\chi^{(+)}_{\vec{q}_a}$ with momentum $\vec{q}_a$ and the halo wave function $\phi_0$. The final state is given by the independent motion of the core described by the outgoing Coulomb wave function $\chi^{(-)}_{\vec{q}_c}$ in the Coulomb field of the target nucleus $Z$ with asymptotic momentum $\vec{q}_c$ and the free neutron with momentum $\vec{q}_n$, described by a plane wave.

In these wave functions the Coulomb interaction is taken into account correctly to all orders. The present *post-form* description, Eqs. (85), includes therefore the effects of *postacceleration*. *Postacceleration* can be viewed as a higher order electromagnetic effect, see Sec. 3 and refers to the fact that (at low beam energies) the core $c$ has a larger final state energy than what one would get from sharing the kinetic energy among the fragments according to their mass ratio. *Postacceleration* arises in a purely classical picture of the breakup process. This is nicely discussed in [83] (We show their Fig. 5 here as our Fig. 8). The nucleus $a = (c + n)$ moves up the Coulomb potential, loosing the appropriate amount of kinetic energy. At the *breakup point* (marked as *"breakup occurs here"*, see Fig 8), this kinetic energy (minus the binding energy) is supposed to be shared among the fragments according to their mass ratio (assuming that the velocities of $c$ and $n$ are equal). Running down the Coulomb barrier, the charged particle $c$ alone (and not the neutron) gains back the Coulomb energy, resulting in its *postacceleration*.
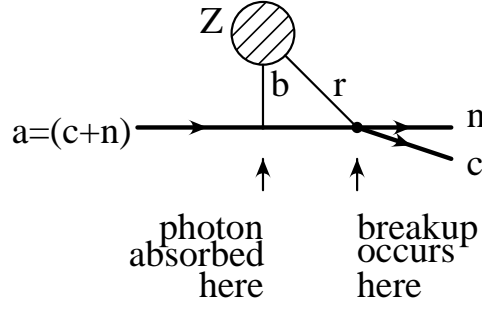
Figure 8: A schematic classical view of Coulomb-breakup, as adapted from [83]. The distance from the target nucleus to the breakup point is denoted by $r$.
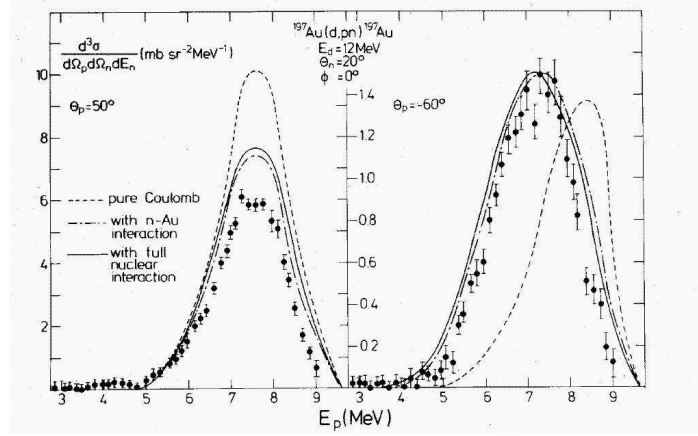


Figure 9: Comparison of calculations and measurement for the deuteron breakup coincidence cross section on $^{197}$Au at $E_d = 12$ MeV (Fig. 4 of [87]). The postacceleration effect can clearly be seen, as the maximum of the proton energy ($\sim 7.5$ MeV) is larger than the one of the neutron ($\sim 2.5$ MeV). The experimental data are taken from [78].

Of course this picture is based on the purely classical interpretation of this process, and will be modified in a quantal treatment, where such a *breakup point* does not exist. The correct semiclassical limit of the theory in this case can be found, e.g., in [84]. A purely classical formula for this postacceleration, where the *breakup point* corresponds to the distance of closest approach — i.e., $b = r$ in Fig. 8 — is given in [85]. Postacceleration is clearly observed in low energy deuteron breakup, in the theoretical calculations, as well as, in the corresponding experiments, see Fig. 9 and also, e.g., [86, 87].

The formula Eq. (85) is also useful for the description of the Coulomb dissociation of halo nuclei at high beam energies, see [88]. Within this theory postacceleration effects become negligibly small in the high energy region. This is seen in the numerical calculations [88] and in the analytical investigations to be described below. It can, e.g., be applied to $^{11}$Be and $^{19}$C Coulomb dissociation experiments [66, 67] (We disregard here the importance of finite range effects).

On the other hand the $1^{st}$ order semiclassical Coulomb excitation theory was widely applied in the past years to the Coulomb dissociation of high energy neutron halo nuclei, see, e.g., [89]. The theory corresponds to the *prior form*, mentioned above. The question of higher order electromagnetic effects was studied recently in [65] within this framework. These effects were found to be small, for zero range, as well as, finite range wave functions of the $a = (c + n)$-system. Higher order effects were recently studied in a post-form DWBA approach [68, 69], which was already discussed in Sec. 3.

26

We now show that the full CWBA amplitude is directly related to the Born approximation, Eq. (76) or the semiclassical result, see Eq. (70). This is true (with modifications to be discussed below) not only for $\eta_a \ll 1$ but also for arbitrary values of $\eta_a$ and $\eta_c$. For this to be the case, the beam energy must be high (compared to the binding energy $E_0$) and the two fragment must be scattered to forward angles.

As was discussed above, the plane-wave approximation to the post-form DWBA has some similarity to the bremsstrahlung process. Replacing the neutron by a photon the diagrams of Fig. 7 are analogous to the bremsstrahlung diagrams in lowest order. The electron-photon vertex corresponds to the $(c + n) \to c + n$ breakup amplitude, the neutral massless photon to the massive neutron. In the case of bremsstrahlung it is well known [90] that *for arbitrary values of $\eta$, even for $\eta \gg 1$*, one obtains the Born approximation result, as long as the scattering is into a narrow cone in the forward direction. This leads one to suspect that higher order effects are not very large in the case of high energy Coulomb dissociation also, where the fragments are emitted into the forward direction.

The $T$-matrix can be evaluated analytically in this model due to the well known Nordsieck formula [91]. Using this formula one obtains the $T$-matrix Eq. (85) in terms of a hypergeometric function $F$ as well as its derivative $F'$. The argument of the hypergeometric function $F$ (and $F'$) is given by [77, 88]:

$$\zeta_0 = \frac{2q^2(q_a q_c + \vec{q}_a \cdot \vec{q}_c) - 4(\vec{q} \cdot \vec{q}_a)(\vec{q} \cdot \vec{q}_c)}{(q^2 - 2\vec{q} \cdot \vec{q}_a)(q^2 + 2\vec{q} \cdot \vec{q}_c)}. \tag{86}$$

We observe that the parameter $\zeta_0$ is found to be negative and $-\zeta_0 \gg 1$ for perpendicular momentum transfers $q_\perp \gg 2\eta_a q_\parallel$ (nonadiabatic case) and beam energy large compared to the binding energy.

This was already noticed in the numerical evaluation of the process: the hypergeometric series therefore does not converge and an analytic continuation had to be used. Here we use this fact to our advantage and make a linear transformation to get the argument of the hypergeometric function close to zero. The transformation we are using leads to the argument of the hypergeometric function $z = 1/(1 - \zeta_0)$ (Eq. (15.3.7) of [92]). In this respect our approach differs from the one used in the bremsstrahlung case, where a transformation giving an argument close to one is used. Using only the lowest order term in the hypergeometric series one obtains after some algebra (up to an overall phase)

$$T \approx 4\pi \ D_0 \ f_{coul} \ e^{-\frac{\pi}{2}\xi}\left[e^{-i\phi}\frac{1}{q_a^2 - (\vec{q}_n + \vec{q}_c)^2} + e^{+i\phi}\frac{m_c}{m_a} \ \frac{1}{q_c^2 - (\vec{q}_n - \vec{q}_a)^2}\right]. \tag{87}$$

Hereby, the relative phase is $\phi = \sigma_0(\eta_c) - \sigma_0(\eta_a) - \sigma_0(\xi) - \xi/2 \log|\zeta_0|$. The $\sigma_0(\eta) = \arg \Gamma(1 + i\eta)$ are the usual Coulomb phase shifts, and $\xi = \eta_c - \eta_a{}^1$.

The correspondence to the Born result Eq. (76) is clearly seen. One only has an additional prefactor $e^{-\frac{\pi}{2}\xi}$ and a relative phase $e^{\pm i\phi}$ between the two terms. The phase $\phi$ is $O(\xi)$. Since $v_c \sim v_a$ the quantity $\xi$ is usually very small and so is $\phi$ for the cases of, e.g., [66, 67]. The prefactor is also well known in the semiclassical theory, where it accounts for the replacement of the *Coulomb bended* trajectories with the straight line trajectories. Both corrections vanish in the limit $\xi \to 0$ and the result coincides with the usual Born approximation (*even if $\eta_a$ and $\eta_c$ are not small*).

Above we have established the correspondence of the full CWBA result with the (Born) plane wave result and with the semiclassical result in the sudden limit. One may expect also to find a connection between the two theories in the adiabatic limit, corresponding to $q_\perp < 2\eta_a q_\parallel$.

For $\eta_a, \eta_c \gg 1$ one can define a classical path for both $a$ and $c$ in the initial and final state. (For high beam energies, the straight line approximation can be applied and the impact parameter $b$ is given by $b = 2\eta_a/q_\perp$. The adiabatic case corresponds to the case of large impact parameters $b > 1/q_\parallel$.) For

---

[1]The parameter $\xi$ is the one used commonly in NR Coulomb excitation. The parameter $\xi$ as introduced above (see Eq. (10) in Sec. 2) corresponds to the parameter $\xi(\theta)$, see, e.g., p. 6 of [1] in the literature on NR Coulomb excitation. Instead of the scattering angle $\theta$ we use the corresponding impact parameter $b$.

the adiabatic regime ($q_\perp < 2\eta_a q_\parallel$) the well known exponential decrease with the adiabaticity parameter is observed in the numerical calculations. In this case, the inequality $-\zeta_0 \gg 1$ is no longer generally satisfied.

The semiclassical limit can be obtained with analytical methods in this case also. Such a method is valid in both the adiabatic and nonadiabatic case as long as $\eta_a, \eta_c \gg 1$.

We use two methods to show this result: in the first approach we use the confluence

$$_1F_1(\alpha, \gamma, x) = \lim_{\beta \to \infty} {}_2F_1(\alpha, \beta, \gamma, \frac{x}{\beta}) \tag{88}$$

together with some relations of [92] to relate hypergeometric functions to (modified) Bessel functions, which appears also in the semiclassical limit.

A second approach makes use of the partial wave expansion of the neutron plane wave. The semiclassical limit is made by approximating the radial wave function with the WKB approximation. In the case of the plane wave expansion the resulting sum over $l$ can then by done and an analytic expression can be found for the absolute value of the matrixelement $T$ [93].

A similar situation is encountered in the theory of bremsstrahlung and Coulomb excitation, see Sec. II E of [2]. There a fully quantal expression for the differential cross-section for dipole Coulomb excitation is given in II E.62. It looks similar to the corresponding expression for Coulomb breakup (see [77]). The semiclassical version of this formula is found in II E.57. It is noted there that it can be obtained from the quantal expression by letting both $\eta_a$ and $\eta_c$ go to infinity and perform a confluence in the hypergeometric functions.

Postacceleration effects are also important for Coulomb dissociation studies of radiative capture reactions of astrophysical interest. We expect that our present investigations will shed light on questions of postacceleration and higher order effects in these cases also. Postacceleration was studied numerically in [94]; as expected these effects turned out to be small at high energies.

We also note the following important physics point: in the post-form DWBA we can introduce in a straightforward way neutron-target interactions [87]. One may say that breakup is a kind of *"transfer into the continuum"*, see also [95, 96]. On the other hand, in the prior form DWBA the final state wave function is the product of a c.m. motion and an internal $n$-core wave function, governed by the interaction $V_{nc}$. In this case the breakup process may be viewed as an inelastic excitation of the bound $(c + n)$-system into the continuum.

# 5 Nuclear Effects, Coulomb-Nuclear Interference

A common problem for the Coulomb dissociation method is the influence of the strong interaction between projectile and target. For heavy target nuclei Coulomb excitation often dominates due to the coherence factor $Z^2$, whereas the total nuclear cross section increases with $R^2 \sim A^{2/3}$ , direct reactions (elastic nuclear breakup is a special case) scale with $R \sim A^{1/3}$, see, e.g., [97], as they take place in a ring area around the nucleus.

A good method to avoid the nuclear interaction altogether is to use beam energies below the Coulomb barrier, which suppresses nuclear effects very effectively. As was discussed above in Sec. 1, one can access only low energy nuclear states in this way. We are mainly interested in higher lying states and higher beam energies are necessary. Again, we can suppress nuclear effects, this time by going to forward scattering angles. This corresponds, in a semiclassical picture, to trajectories where the nuclei do not touch each other. The (total) electromagnetic excitation probability falls off at least with $1/b^2$; it is maximal for grazing impact parameters, where also the nuclear effects set in. For too large impact parameters, the adiabatic cutoff sets in and the excitation probability drops exponentially to zero. I.e. we have the same problem as Wilhelm Tell [98], who had the task to hit a rather well defined spot, with

grave consequences in the case of failure. By the wave nature of the projectile nuclear effects cannot be totally avoided, they will enter somehow, but often this effect is negligible. Even for small scattering angles there can be some effect coming from the interference of that part of the wave function that is bent by the Coulomb interaction with that part of the wave function, which is diffracted by the "black disc" of the target. This will lead to diffraction patterns, see the discussion in [99].

It should be kept in mind that one does understand nuclear effects, at least in a semiquantitative way. It is certainly best to choose the experimental conditions (beam energy, scattering angle,...) in such a way that these effects are virtually negligible. Such considerations can be based on the good knowledge of nuclear effects. As a second best approach they can be taken into account with confidence by using the results of some kind of nuclear reaction theory. Direct (nuclear) reactions have been extensively studied in the past decades and it can safely be said that one understands rather well their main characteristic features, but not as well as Coulomb excitation itself. This section is devoted to these nuclear processes, Coulomb-nuclear interference and the theoretical methods used to describe them. These methods sometimes involve heavy computing. Entire conferences are devoted to this subject [100], which we only briefly summarize here.

## 5.1  *Various Kinds of Nuclear Reaction Mechanisms*

Nuclear breakup is dominant for light target nuclei and is used by itself as a tool to explore the structure of exotic nuclei, especially nuclear halo systems. In a nuclear projectile-target interaction all of the fragments (typically two) can emerge while the nucleus remains in the ground state. This is called *diffractive breakup* and it is a reaction mechanism which leads to the same final state as Coulomb dissociation. In addition to *diffractive breakup* (*diffractive dissociation*) there is also *stripping* and *absorption*. In *stripping reactions*, only part of the fragments comes out of the reaction in the very forward direction, while the rest is absorbed; also all fragments can interact violently with the target and are absorbed, see [101, 102, 103] for details.

Stripping reactions have been the "workhorse" of the study of halo systems in nuclear reactions, mainly due to the fact that they can be interpreted in a simple (sometimes too simple) way: in the so-called *transparent limit* the longitudinal momentum distribution of the core after stripping is related to the momentum space probability distribution of the halo nucleon. This picture was more refined in recent years [75, 97, 104] in order to incorporate the so-called *core-shadowing effects*. The longitudinal momentum distribution is related to the *momentum-distribution at the surface,*, that is, to the Wigner transform at the surface [105].

Diffractive breakup leads to the same final state as Coulomb excitation. As all fragments are generally measured in order to reconstruct, e.g., their relative excitation energy, it is only this process which needs to be considered as a background to Coulomb excitation. We concentrate in the following on this process. We refer here to a number of reviews [106, 107, 108, 109, 110] of direct nuclear reactions with exotic nuclei.

## 5.2  *DWBA*

Nuclear effects can be treated in complete analogy to the DWBA approach explored for Coulomb excitation above. The pure-Coulomb wave function $\Psi$ is replaced by the one where an optical potential between projectile and target acts in addition to the Coulomb potential. In addition one has to add the nuclear excitation, treated in first order here, for higher order effects see also the discussion below in Sec. 5.4.

The $T$-matrix for inelastic scattering in the DWBA is given by, see, e.g., Eq. (7) of [111]:

$$T = \int d^3R \Psi_f^{(-)*}(\vec{R}) \, F_{fi}(\vec{R}) \, \Psi_i^{(+)}(\vec{R}),$$
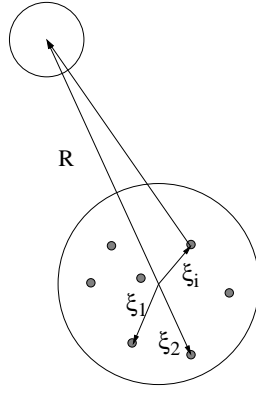
(89)

Figure 10: The potential $V(\vec{R}, \xi)$ is given by the sum of the (Coulomb and nuclear) interactions between the individual components of the target with the projectile $V_i(\vec{R} - \xi_i)$.

The c.m. distorted waves functions are denoted by $\Psi_{f,i}^{(\pm)}$. The nuclear form-factor $F_{fi}(R)$ is given by

$$F_{fi}(\vec{R}) = \int d\xi \; \phi_f^*(\xi) \; V(\vec{R}, \xi) \; \phi_i(\xi), \tag{90}$$

where $\xi$ denotes the internal coordinates, see Fig. 10. The initial and final internal wave functions are $\phi_{i,f}(\xi)$. The projectile-target interaction is given by

$$V(\vec{R}, \xi) = \sum_i V_i(\vec{R} - \vec{\xi}_i). \tag{91}$$

We see that nuclear effects enter in two ways: first there is an influence on the distorted waves of the c.m. motion $\Psi_{f,i}^{\pm}$ due to the nuclear interaction. Second there is an additional breakup component due to the nuclear form-factor $F$. This form-factor can be expanded in terms of multipoles and added to the Coulomb multipoles.

At lower energies the interactions of protons, neutrons, and also light ions with different target nuclei have been analysed and tabulated [112], so that they are usually well known. At higher energies (few 100 MeV) the knowledge of the phenomenological optical potentials is rather sparse. Often global parametrisations (fitting optical potentials for protons and neutrons) are used for a whole range of energies and targets, see, e.g., [113], or for individual target nuclei, see [114] for a recent reference. The interaction between the projectile nucleus and the target (or some fragments with the target) are then calculated within a folding approach of the projectile density with the proton-target and neutron-target optical potentials.

$$V(\vec{r}) = \int d^3r_1 \rho_1(r_1) V_{NA}(|\vec{r} - \vec{r}_1|), \tag{92}$$

where $V_{NA}$ is the nucleon-target potential.

Another way is to use a double folding approach over *both* densities (projectile and target). The nuclear interaction is then given by

$$V(r) = \int d^3r_1 d^3r_2 \rho_1(r_1) \rho_2(r_2) V_{NN}(|\vec{r} - \vec{r}_1 + \vec{r}_2|), \tag{93}$$

where $V_{NN}$ is the nucleon-nucleon potential.

Only the nucleon-nucleon interaction $V_{NN}$ is needed in addition to the nuclear densities $\rho_{1,2}$. A typical example of this approach is the DDM3Y interactions [115, 116], based on a fit of the nucleon-nucleon interaction in nuclear matter [117] together with an assumed density dependence. Only the real (elastic) part of the potential can be found in this way and the imaginary part needs to be adjusted. In

many cases it is chosen for simplicity to be proportional to the real part, with a proportionality factor in the range of 0.5–0.9. This proportionality is in general only a first approximation; especially at lower energies there are corrections, which can be described by a polarisation potential, see e.g., [118].

## 5.3 *Eikonal DWBA*

At high energies the partial wave decomposition of the wave function of projectile and target $\Psi_{f,i}^{\pm}$ is rather cumbersome. High energy methods, like the *eikonal approach* ("Glauber method"), are more useful and at the same time accurate. The wave nature of the projectile is still taken fully into account and leads to characteristic diffraction effects. The use of eikonal wave functions for the initial and final states in the DWBA matrixelement is discussed in [38], where also its relation to the semiclassical case is explored. Higher order effects can be treated within a coupled channels method [34], a corresponding computer program is described there. In this approach the differential cross section can be written as (see also Eq. (27)):

$$f_{inel}^{\mu} = ik \int_0^{\infty} b\,db\,J_{\mu}(qb)\exp(i\chi(b))a_{\mu}(b). \tag{94}$$

The index $\mu$ denotes the angular momentum transfer to the target in the beam direction. The *excitation amplitudes* $a_{\mu}(b)$ are calculated in the semiclassical straight line approximation for impact parameter $b$. The eikonal phase $\chi(b) = \chi_C(b) + \chi_N(b)$ takes Coulomb, as well as, nuclear effects into account. It involves the Coulomb phase given by

$$\chi_C(b) = -2\eta K_0(kb) \approx 2\eta ln(kb) \tag{95}$$

and a nuclear phase, which can be calculated from an optical model potential $U_{opt}(r)$ as

$$\chi_N(b) = -\frac{1}{\hbar v} \int_{-\infty}^{\infty} dz\,U_{opt}(r = \sqrt{b^2 + z^2}). \tag{96}$$

The simplest way to take nuclear effects into account is the *"black disk model"*, where one sets $\exp i\chi = 0$ for $b < R_1 + R_2$ and $\chi = \chi_C$ for $b > R_1 + R_2$. This is justified due to the strong imaginary part of the nuclear interaction at these energies.

Diffraction effects in this black disk model are studied numerically in [38] and [37]. In Figs. 1 and 2 of [37] the importance of nuclear diffraction can be seen. A reduced integral is defined there in Eq. (8); it depends on the characteristic parameters $\eta$ and $\xi$. Plots are given for a reduced scattering angle $\theta/\theta_{gr}$ where $\theta_{gr} = 2\eta\theta_{diff}$ and the diffraction angle is given by $\theta = 1/(kR)$. It can be seen in theses figures that for $\eta \gg 1$ the semiclassical approximation is very good, especially for small values of $\xi$.

A model which takes into account the smoothness of the surface is discussed in [33], where surface normalized Gaussians are used for the density of the nuclei. In this way analytic expressions for the eikonal phase can be found of the form

$$\chi(b) = \chi_0 \exp\left[-b^2/(a_1^2 + a_2^2)\right], \tag{97}$$

with

$$\chi_0 = \frac{\pi^2 \bar{\sigma}_{NN} \rho_1(0)\rho_2(0)a_1^3 a_2^3}{10(a_1^2 + a_2^2)} \tag{98}$$

and $a_i$ and $\rho_i(0)$ are adjusted to reproduce the experimental nuclear density at the surface of the nucleus; for a tabulation see [33]. $\bar{\sigma}_{NN}$ denotes the average nucleon-nucleon cross section.

An advantage of the (Glauber) eikonal approach is the fact, that one does not need a nuclear potential in order to derive the eikonal phase. Scattering at high energies is concentrated in the forward

31

direction. A knowledge of the elastic scattering amplitude $f_{el}(q)$ is sufficient, as it is related via a Fourier transform to the eikonal phase

$$\exp\left[i\chi(b)\right] - 1 = \frac{i}{2\pi k} \int d^2q f_{el}(q) \exp(-i\vec{q}\vec{b}). \tag{99}$$

In order to determine the eikonal phase in nucleus-nucleus scattering $\chi_{AA}$ the so called $t\rho\rho$ formalism can be used, where the interaction is described through a folding of the densities together with the nucleon-nucleon scattering amplitude [119], cf. to Eq. (93). In terms of the nucleon-nucleon profile function $\Gamma_{NN}(b) = 1 - S_{NN}(b) = 1 - \exp\left[i\chi_{NN}(b)\right]$ it can be written as

$$\chi_{AA}(\vec{b}) = i \int d^3r_1 d^3r_2 \rho(r_1)\rho(r_2)\Gamma_{NN}(\vec{r}_{\perp 1} - \vec{r}_{\perp 2} - \vec{b}), \tag{100}$$

This is related to the double-folding approach, see Eq. (93). In the limiting case of a zero-range interaction one gets

$$\Gamma_{NN}(\vec{x}) = \delta^{(2)}(\vec{x})\frac{1}{2}(1 - i\alpha_{NN})\sigma_{NN}, \tag{101}$$

where $\sigma_{NN}$ is the total nuclear cross section and $\alpha_{NN}$ the ratio of the real to imaginary part of the forward scattering amplitude. Parameterizations of this forward amplitude can be found in the literature [120].

The $t\rho\rho$ formalism, which is often also called the *optical limit approximation* can be derived from the multiple particle Glauber formalism by taking the first term of the *cumulant expansion*. One wants to find an eikonal $\chi_{AA}$, which reproduces the elastic scattering amplitude of the microscopic multiple scattering model, see Eqs. (103) and (104) below,

$$\exp\left[i\chi_{AA}(\vec{b})\right] = \langle 0| \prod_i S_i(b_i) |0\rangle. \tag{102}$$

By taking the logarithm of both sides and expanding to first order in powers of $\Gamma_{NN}$, see also [121], one obtains Eq. (100) above. In this way the interaction is approximately included in all orders. A discussion of this approach can be found also in [122, 123, 105].

## 5.4  *Higher Order Effects*

Whereas the Coulomb interaction is long ranged and often the major contribution comes from larger impact parameters, where the interaction is not strong and first order theories are adequate, the nuclear interaction is short ranged and strong. Therefore higher order effects can become important and should be taken into account.

Within the eikonal DWBA higher order effects in $F(R)$ can be taken into account as discussed above, e.g., in the (semiclassical) coupled channel approach as given in [34]. In the case of the deuteron, $^6$Li and other halo systems, quite elaborate calculations have also been made in terms of the CDCC (*continuum discretized coupled channel*) see [124, 125], or [126, 127, 128]. In both approaches one needs to identify the dominant structures especially in the continuum in order to restrict oneself to a manageable number of channels to be incorporated in the calculation.

A theory which is well suited for intermediate and high energy nuclear breakup of halo nuclei is the Glauber multiple scattering theory [121, 122]. In this approach one uses the eikonal approximation together with the sudden limit to describe the elastic, as well as, inelastic scattering from the ground state to a state $m$ as

$$f_{m0}(q) = \frac{k}{2\pi i} \int d^2b \exp(i\vec{q}\vec{b}) \int d\xi \phi_m^*(\xi)\phi_0(\xi) \left(S(b, \xi_\perp) - 1\right), \tag{103}$$
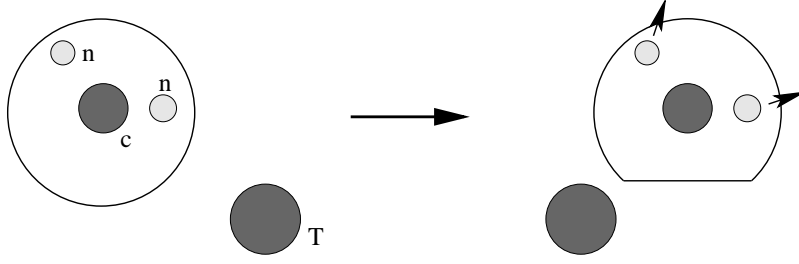
Figure 11: The "wounded nucleus" picture of nuclear elastic breakup (*diffractive breakup*) of a halo nucleus. Due to the strong absorptive (imaginary) part of the nuclear interaction, those parts of the wave function, which are touched by the target nucleus are set to zero. This means that the nucleus is no longer in its ground state but also in excited states. The projection of this excited state to the continuum states gives the amplitude for diffractive dissociation, see also Eq. (105).

where $k$ is the momentum of the projectile and $\vec{q} = \vec{k}_i - \vec{k}_f$. The profile function $S$ depends on the individual impact parameters $b_i = b - \xi_{i\perp}$. It is given by the product of the individual profile functions

$$S(b, \xi_\perp) = \prod_i S_i(b_i) = \prod_i \exp(i\chi_i(b_i)). \tag{104}$$

It is possible to evaluate this expression numerically with fully microscopic wave function $\phi_0$ and $\phi_m$, see e.g. [129].

An intermediate model, which is well suited for halo nuclei, is the *Serber model* [101], improved by Glauber [102], see also [103]; in this model only the relevant clusters are taken into account in the Glauber multiple scattering model.

In the eikonal DWBA, see Eq. (94), a global projectile-target profile function is used to describe the c.m. motion of the projectile. In the improved Serber model, see Eq. (105) below, one uses individual profile functions $S_i(b_i)$ for each fragment $i$, e.g., the core $c$ and the halo neutron $n$ [130, 131, 132, 133, 97]. The individual profile functions can then be calculated in the same way as in Eqs. (96), (97) or (100). The differential cross section for the elastic breakup (*diffraction*) is then found to be, see also Eq. (103),

$$f_{fi}(q) = \frac{k}{2\pi i} \int d^2 b \exp(i\vec{q}\vec{b}) \langle f | \exp\left(i\chi_c(b_c)\right) \exp\left(i\chi_n(b_n)\right) - 1 | i \rangle, \tag{105}$$

where $b_c = b + m_n/(m_n + m_c)r_\perp$ and $b_n = b - m_c/(m_n + m_c)r_\perp$ are the individual impact parameter of the core and the neutron with the target, respectively. In this way the most important parts of the internal structure of the projectile nucleus are taken into account. This approach can easily be extended also to the case of more than two clusters [134, 135]. Only initial and final state wave functions but no intermediate states are needed in this way.

A simple picture of the diffractive breakup can be found in the limit of the "black disc" model, where the individual profile functions are approximated by black discs, see Fig. 11.

## 5.5  *Coulomb-Nuclear Interference*

Nuclear effects enter most sensitively through the interference of the nuclear and Coulomb amplitudes. This has been addressed in the past in a number of papers, some recent references are [136, 137, 138, 139].

A simple (analytic) result is given in [7] for a neutron halo nucleus. The amplitude of Coulomb excitation in first order (Eq. (3.4.16) of [7]) is combined with the nuclear breakup amplitude of Akhiezer and Sitenko [140] (Eq. (3.4.14) of [7]). In this way a good estimate of the interference effect can be found.
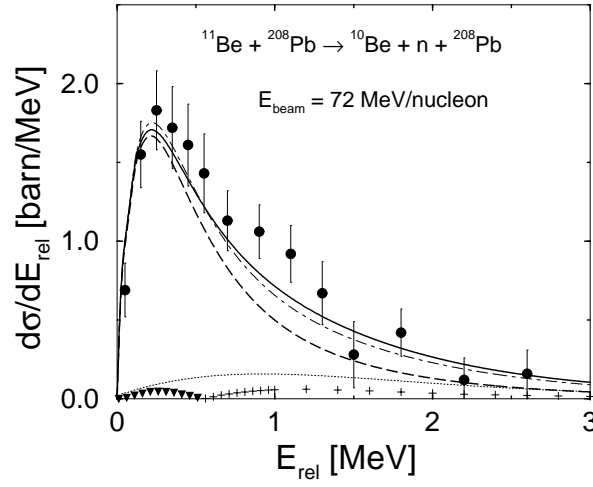
Figure 12: Fingerprints of Coulomb-nuclear interference: effects of nuclear and Coulomb-interference are shown for the breakup of $^{11}$Be on $^{208}$Pb at 72 $A$MeV. Shown are the contribution from pure Coulomb (dashed), nuclear (dotted) and their incoherent (dashed-dotted) and coherent sum (solid line). The magnitude of negative and positive Coulomb-nuclear interference terms are shown as inverted triangles and plus signs, respectively. The experimental results are taken from [67]. This figure is adapted from [137].
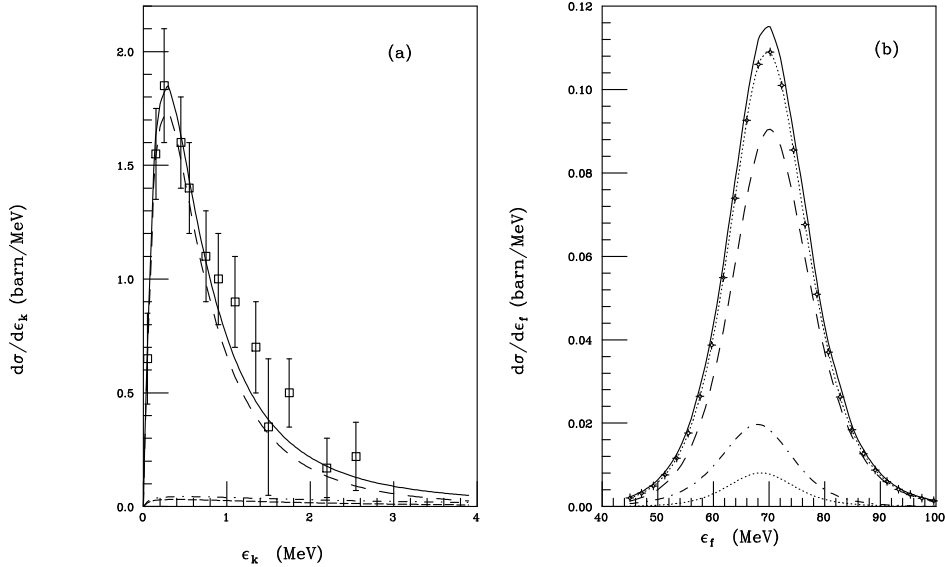


Figure 13: Effects of nuclear and Coulomb-nuclear interference are shown for the breakup of $^{11}$Be on $^{208}$Pb at 72 $A$MeV in the projectile (left)and target (right) frame. Shown are the results for nuclear breakup (dot-dashed), Coulomb (long-dashed) and Coulomb-nuclear interference (dotted) and the sum (solid line). The experimental results are taken from [67]. This figure is taken from [136], Fig. 4 there.

More detailed calculations have been done in the mean time. E.g., in [136, 141] a calculation within Glauber theory is presented. In [138] the time-dependent Schrödinger equation in the semiclassical approximation is solved numerically and compared to a first order calculation and to the eikonal approximation.

In the case of halo nuclei the condition of *no nuclear penetration* may not be well fulfilled and the decomposition of the Coulomb interaction into $r_<$ and $r_>$ parts (see Eq. (4)) may not be reliable, as shown in [138] for the case of $^8$B.

We illustrate the fingerprints of Coulomb-nuclear interference and nuclear effects from two recent theoretical model calculations. The results shown in Fig. 12 are based on a post-form DWBA approach, see Sec. 4. The results shown in Fig. 13 are based on a Glauber type calculation, see Eq. (105), taking higher orders in the nuclear interaction together with the Coulomb interaction in lowest order into account.

In both cases breakup of $^{11}$Be on a $^{208}$Pb target at 72 $A$MeV are shown in comparison to the experimental data of [67]. One sees that both nuclear and Coulomb-nuclear effects are rather small in this case.

# 6   Coulomb Dissociation and Nuclear Structure

## 6.1   *Primakoff Effect*

We want to recall first at this point that the strong nuclear Coulomb field has also been used in particle physics to study photon interactions with (unstable) particles. Typically a high energy secondary beam, like a beam of $\Lambda$ particles hits a heavy target nucleus. In the nuclear Coulomb field, high energy $\Sigma^0$ hyperons are produced in the reaction

$$\Lambda + Z \to \Sigma^0 + Z. \tag{106}$$

The cross section for this process is proportional to the $B(M1)$- value for the $\Lambda \to \Sigma^0$ electromagnetic excitation. From the measurement of this cross section the lifetime of the $\Sigma^0$ is obtained. For further details of the analysis see [7], where further references and other applications of the *Primakoff effect* (like the determination of the pion polarizability) are given. A more recent example is the radiative decay width measurement of neutral Kaon excitations using the Primakoff effect by the KTeV Collaboration [142]. They used $K_L$ mesons in the 100-200 GeV energy range to produce the axial vector ($1^+$) mesons $K_1(1270)$ and $K_1(1400)$ in the nuclear Coulomb field of a Pb target. In this way the radiative widths for the decay of these particles into $K^0 + \gamma$ could be determined. For further details we refer to this paper [142]. This approach is very similar to the one used nowadays in nuclear physics: an exotic (unstable) nucleus is excited by the quasireal photons provided by the nuclear Coulomb field.

We mention a second example to illustrate the use of equivalent photons: At Fermilab the Primakoff effect is used for a determination of the proton polarization of a 185 GeV/$c$ proton beam by means of azimuthal asymmetry measurements [143]. This method could also be useful for antiproton beams. For further details we refer to this reference [143]. From this work one can see that it is possible to study the photon-proton interaction in the nucleon resonance region using equivalent photons. In Fig. 14 we show the invariant mass spectrum of the $\pi^0 - p$ system in the reaction $p + Pb \to \pi^0 + p + Pb$ for a momentum transfer $|t| < 1 \times 10^{-3}(GeV/c)^2$. One can clearly recognize the nucleon-resonances (especially the $\Delta$-resonance) which are excited with the continuous equivalent photon spectrum provided by the Coulomb field of the Pb target nucleus. Since the Lorentz factor $\gamma$ of the proton is about 200 in this experiment, the corresponding equivalent photon spectrum is quite hard: (see the discussion in Sec. 2.2 about the cutoff in the photon spectrum at $\omega_{max} \sim \gamma/R$) we can roughly take $1/R \sim 30$ MeV and obtain a maximum photon energy of about 6 GeV.
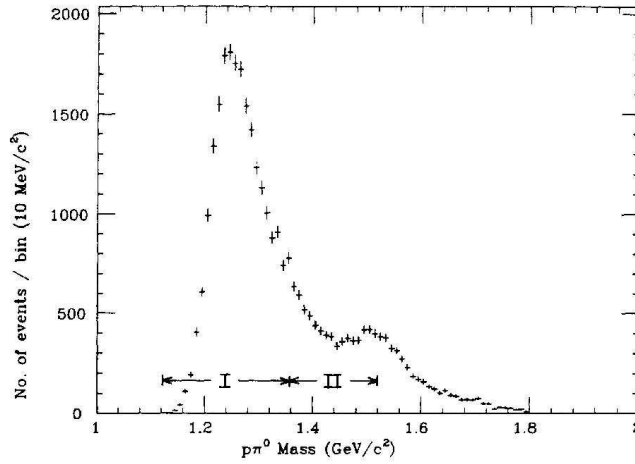
Figure 14: The invariant mass spectrum of the $\pi^0 - p$ system in the reaction $p + \text{Pb} \rightarrow \pi^0 + p + \text{Pb}$ with a 185 GeV/$c$ proton for a momentum transfer of $|t| < 1 \times 10^{-3}(\text{GeV}/c)^2$ is shown. These small momentum transfer values ensure that photon exchange is the dominant excitation mechanism. Peaks due to the $\Delta^+(1232)$ and $N^*(1520)$ resonances are clearly seen. Reproduced from Fig. 2 of [143], to which we refer for further details. Copyright (1990) by the American Physical Society.

## 6.2 *Some Aspects of Electromagnetic Excitation in Relativistic Heavy Ion Collisions*

Electromagnetic excitation is also used at (ultra-) relativistic heavy ion accelerators to obtain nuclear structure information. Recent examples are the Coulomb fission studies of radioactive nuclei at GSI [144, 145] and Coulomb fission of $^{208}$Pb [146] at SPS/CERN. Due to the logarithmic rise of the cross-section with beam energy, cross-sections for the excitation of the giant dipole resonance (*Weizsäcker-Williams process*) at the relativistic heavy ion colliders RHIC and the forthcoming LHC(Pb-Pb) at CERN are huge [147, 148, 149], of the order of 100 b for heavy systems (Au-Au or Pb-Pb).

The neutrons from GDR decay were observed at RHIC [150]. In this reference mutual Coulomb dissociation was measured in $\sqrt{s_{NN}} = 130$ GeV Au-Au collisions. This is shown in Fig. 15 (taken from [150]).

The two classes of events are defined according to the number $n_{BBC}$ of hits in the BBC (*beam beam counters*) photomultipliers. The PHENIX (one of the detectors at RHIC) BBC measures the relativistic charged particles produced in cones around each beam with a rapidity range $3.05 < |\eta| < 3.85$) with $2\pi$ azimuthal coverage. For *hadronic* events we have $n_{BBC} > 1$ in each arm, for *Coulomb* events there is $n_{BBC} \leq 1$ in at least one arm. We see that the "Coulomb" events tend to have a low neutron multiplicity. This is easily understood qualitatively: Coulomb events are mainly due to the electromagnetic excitation of the GDR (in $^{197}$Au) in ultraperipheral collisions (*UPC*). The GDR decays subsequently by the emission of one (or only a few) neutrons. See [150] for further details.

In colliders, this effect leads to a loss of the beam, due to the particle (neutron) decay of the GDR. Even worse, this effect can lead to a localized beam pipe heating in Pb-Pb collisions at LHC, as was noticed in [151]. (An even more severe process in this context, limiting the maximum luminosity that can be achieved at the LHC, is the electromagnetic process of bound-free electron pair production.) On the other hand, this effect can also be useful as a luminosity monitor by detecting the neutrons in the forward direction as first proposed in [152] and demonstrated in [150]. One measures the neutrons which are produced in the decay of the giant dipole resonance, which is excited in each of the ions (*mutual excitation*). Since this process has a steeper impact parameter dependence than the single excitation cross-section, there is more sensitivity to the cut-off radius and to nuclear effects. The neutrons from
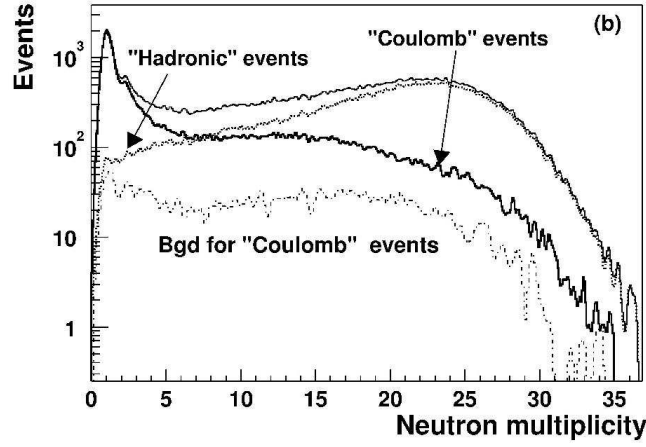
36

Figure 15: Single arm ZDC (Zero Degree Calorimeter) neutron multiplicity spectrum for Coulomb and hadronic events. The two types of neutron emission can be separated from each other as hadronic production also leads to charged particle production in the more central parts of the detector. See text and [150] for details. Reproduced from Fig. 2 of [150]. Copyright (2001) by the American Physical Society.

the GDR decay can also serve as a trigger on the ultraperipheral collisions. For details and further references, see [148, 149].

UPCs are also of great interest in particle and hadron physics: at RHIC and LHC the equivalent photon spectrum extends to about 500 GeV and 1 PeV ($10^3$ TeV), respectively, in the rest frame of one of the ions. This leads to many interesting applications like the coherent production of vector mesons [153, 154]. Coherent $\rho^0$ production with and without simultaneous GDR excitation has been observed at RHIC [155]. This is a very hot topic, but it is outside the scope of the present article, we refer to the reviews in [156, 148, 149, 157].

## 6.3 *Intermediate Energy Coulomb Excitation of Discrete Levels and Gamma Decay*

Electromagnetic excitation is a very clean and efficient way to excite nuclear states. Interesting nuclear structure properties like the position of energy levels, as well as, electromagnetic transition matrix elements can be determined. The general features of electromagnetic excitation have been given in Sec. 2. Collective states, i.e., those with large electromagnetic matrixelements, are most strongly excited. While in Coulomb excitation below the barrier one can only populate low lying states like rotational or low lying vibrational states (see discussion in Sec. 2), it becomes possible at intermediate energies to excite also high lying states, the prime example being the GDR. The main features are shown in Fig. 16, taken from [3], see also Figs. 3.3 and 3.7 of [7]. In these figures the excitation cross section of an exotic nucleus with typical values for structure parameters (whose exact values do not matter now) is shown. The low lying $2^+$-collective level is excited most strongly at the low energies, while the GDR takes over at the higher energies. Two- and three-phonon GDR's (labelled 2-ph GDR, and 3-ph GDR) are excited with smaller cross-sections (see Sec. 3.1). They tend to a constant in the limit of high beam energies. The one-photon GDR excitation cross section first rises quite steeply with increasing energy, overcoming the adiabatic cut-off criterion; eventually it will show the asymptotic rise with $\ln \gamma$, see Eq. (21). The (high lying) isoscalar quadrupole excitation is also given. The cross section for the low lying $2^+$ excitation shows a $1/v^2$-behaviour, while its logarithmic rise will only occur at extremely high energies (see the remarks in Sec. 2). These excited states can decay by photon- (or, at
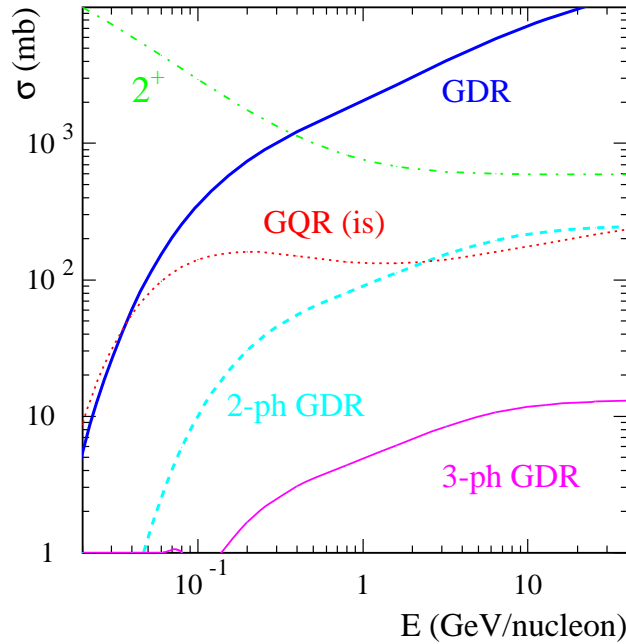
37

Figure 16: Cross sections for the electromagnetic excitation of collective states of an exotic nucleus on a Pb target. Typical nuclear structure parameters for a medium mass nucleus were adopted. This figure is taken from [3], p. 128.

sufficiently high excitation energies, by particle-) emission.

Photons emitted in-flight from intermediate energy projectiles can be distinguished with modern gamma ray detectors from $\gamma$-rays originating from the target. In order to accomplish this, the information on the emission angle is used to correct for the Doppler broadening. The development of position-sensitive $\gamma$-detectors was a key to the success of this method. For a detailed description of this field we refer to the review by Glasmacher [158] and more recently [159] and [3].

This method is very well suited for radioactive beams and very valuable information about the nuclear structure of unstable nuclei has been obtained and is expected to be obtained in the future.

Many interesting examples of the investigation of nuclear structure effects of unstable nuclei with this method are given in [159]. We refer to this reference for more details. Let us mention here only some points:

Electromagnetic excitation of intermediate energy (exotic) beams has been developed into a useful spectroscopic tool [160, 161]. This method is ideal to study the behaviour and onset of collectivity (deformation) for $0^+ \rightarrow 2^+$ transitions in nuclei far from stability. By measuring the excitation energies of the first $2^+$ states and the corresponding $B(E2)$–values, nuclear structure effects like deformation, can be studied in a unique way for nuclei far off stability.

Electromagnetic excitation of the $1^{st}$ excited state in $^{11}$Be has been studied experimentally at GANIL [162], RIKEN [163] and MSU [164]. This is a good test case, since the $B(E1)$–value of the corresponding ground-state transition is known independently. Theoretical calculations [165, 166] show that higher order effects are small. They decrease with increasing beam energy, as expected.

Subsequently, many interesting nuclear structure studies followed at RIKEN, GANIL, MSU/NSCL and GSI with this method, which can be considered as well established by now.

We mention here that the neutron-rich nucleus $^{34}$Mg has been studied recently via Coulomb excitation using a radioactive beam on a Pb target [167]. The high $B(E2)$ value for the excitation of the $2_1^+$ state corresponds to a quadrupole deformation parameter $\beta_2$ of 0.58(6), implying an anomalously large deformation of $^{34}$Mg.

The work done at MSU can be found at [168]. Let us mention one of their latest results: The $0^+_{gs} \to 2^+$ excitations in the mirror nuclei $^{32}$Ar and $^{32}$Si were compared to each other. This is a sensitive test of isospin symmetry which could be extended to a $T = 2$ isobaric multiplet [169].

In this context it is worth mentioning that a computer program for scattering at intermediate energies has recently been published in [34]. Nuclear, as well as, Coulomb excitation processes are calculated using the eikonal approximation and semiclassical coupled channels methods. The eikonal method is very appropriate for intermediate energies: it is both numerically accurate and fast (as opposed to DWBA methods, where also the relative center of mass motion, with its huge number of partial waves, is treated in a quantum-mechanical way). The general problem of the coupled channels method is to find the important states to be included. In many practical cases this proves to be possible. In any case, as we have shown above, the strength parameter is proportional to $1/v$, i.e., higher order effects tend to be small for intermediate and high beam energies. On the other hand this also means that one cannot have efficient multiple Coulomb excitation for intermediate beam energies. The two-photon excitation of the strongly collective DGDR discussed above is an interesting exception. For low energy Coulomb excitation, the multiple excitation of rotational bands is a very well known feature. Angular distributions of elastically and inelastically scattered particles, as well as, angular distributions of $\gamma$-rays are also calculated in [34].

## 6.4  *Intermediate Energy Coulomb Dissociation, Invariant Mass Spectroscopy and Low Lying $E1$ Strength*

Nuclei in the valley of stability show a prominent collective mode, the Giant Dipole Resonance (GDR). In this mode, all protons oscillate against all neutrons. This state has an excitation energy of about $E_{GDR} \approx 80\text{MeV } A^{-1/3}$ and exhausts the classical energy-weighted Thomas-Reiche-Kuhn (TRK) sum rule to a large extent. As a consequence of this, low lying $E1$-strength is strongly hindered. In [170] it was shown that this hindrance of $E1$-transition strength disappears when loosely bound nucleons are involved. This is, e.g., the case in neutron halo nuclei. A classic case is the $E1$-strength in the prototype of a neutron halo nucleus: the deuteron. Using simple zero range wave functions, the $E1$ strength is calculated in [171]. A similar calculation for neutron halo nuclei is given in [7], which clearly shows how the low-lying $E1$-strength is obtained in a single particle model. With the zero range bound state wave function, see Eq. (58) above or Eq. (3.4.11) of [7]

$$\Psi_i(r) = \sqrt{\frac{\kappa}{2\pi}} \exp(-\kappa r)/r \tag{107}$$

and the continuum wave function, see Eq. (62) or Eq. (3.4.12) of [7], (for the relevant partial waves ($l > 0$) this corresponds to the spherical Bessel functions, which describe a free particle) we obtain for the electromagnetic matrix-element Eq. (7) (see Eq. (3.4.19) of [7]):

$$M(Elm) = e\sqrt{2\pi\kappa}(-i)^l l! 2^{l+1}(Z_1\beta_1^l + (-1)^l Z_2\beta_2^l)\frac{q^l}{(\kappa^2 + q^2)^{l+1}}Y_{lm}(\hat{q}), \tag{108}$$

with $\beta_1 = m_2/(m_1 + m_2)$ and $\beta_2 = m_1/(m_1 + m_2)$ and $Z_1$ and $Z_2$ denote the charge numbers of the two clusters.

A general discussion of dipole strength in neutron rich nuclei is given by Hansen and Jonson [172] and Ikeda [173]. A significant low-lying $E1$ strength is found. These modes are sometimes called *soft dipole state* or *"pigmy resonance"*, see Fig. 17. An early discussion of the disappearance of the hindrance of $E1$-transitions involving loosely bound nucleons is given in [170].

A measure of the $E1$-strength of certain configurations is given by the *cluster sum rule*: in the usual
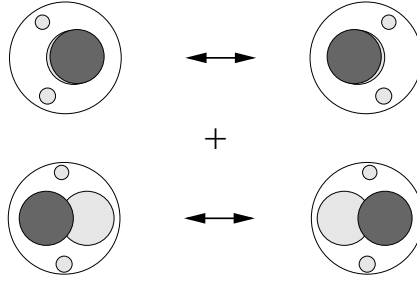
Figure 17: In the GDR all neutrons move against all protons (*hard mode*, lower figure). In a nucleus which contains also loosely bound nucleons, e.g., in a 2-neutron halo nucleus like $^{11}$Li, a new type of oscillation, called the *soft dipole mode* (upper figure), can occur. In this mode the two loosely bound neutrons oscillate against the inert core of strongly bound protons and neutrons. This gives rise to $E1$ strength at low energies. Figure adapted from [173].

TRK sum-rule the relevant degrees of freedom of the nucleus are the neutrons and protons [2]. In this case the TRK sum rule tells us that

$$\sum_n (E_n - E_0)|D_{n0}|^2 = \frac{3\hbar^2}{2m_N}\frac{NZ}{A}, \tag{109}$$

where $N$,$Z$, and $A$ denote the neutron, proton and mass number of the nucleus and where $D_{n0}$ is the dipole matrix-element between the ground state 0 and the excited state $n$. In this equation we have neglected the effect of exchange forces in the nucleon-nucleon interaction, which is of the order of some 10%. We can determine the contribution of certain cluster configurations to the energy-weighted sum rule by a so-called cluster sum rule: assuming an inert core with mass $M$ and charge $Z$ and some valence neutrons with mass $m$ as the relevant degrees of freedom, one can write down a *cluster sum rule*, taking those as the relevant degrees of freedom. In this sum rule the factor $NZ/A$ in Eq. (109) is replaced by $\frac{(Z_1 N_2 - Z_2 N_1)^2}{(A_1+A_2)A_1 A_2}$, where $N_i$,$Z_i$ and $A_i = (N_i + Z_i)$ are the neutron, proton, and nucleon number of each cluster [175]. In the case of a neutron halo ($Z_2 = 0$, either single neutron or more) this gives a factor $\frac{Z_1^2 N_2}{(A_1+A_2)A_1}$.

Effective field theories ($EFT$) are nowadays also used for the description of halo nuclei, see [176]. The relative momentum $k$ of the neutron and the core is indeed much smaller than the inverse range of their interaction $1/R$ and $kR$ is a suitable expansion parameter. (In our model of the pure-Coulomb breakup of a bound state bound by a zero range force, see Sec. 4 above, we have $R = 0$, i.e., $kR = 0$ and we have the zero order contribution of the expansion). Effective range theory seems a natural starting point. This aspect was pursued in [177, 178]. In [178] radiative capture cross sections into $s$-, $p$- and $d$-bound states are calculated in simple models, and the cross sections depend only on a few low energy parameters. The neutron halo effect on direct neutron capture and photodisintegration of $^{13}$C was studied in [179] and [180]. In their figures it can very well be seen that the radial integrals are dominated by the outside region. While they find a sensitivity on neutron optical model parameters for $s \to p$ capture, this sensitivity is strongly reduced for the $p \to s$ and $p \to d$ capture cases. In [176] it is remarked that the EFT approach *"is not unrelated to traditional single-particle models"* and that *"it remains to be seen whether these developments will prove to be a significant improvement over more traditional approaches."* With a wealth of data on halo nuclei to be expected from the future rare ion beams we can be confident that these questions will be answered. An interesting effect is known from the deuteron, the mother (prototype) of all halo nuclei: for very low energies, there is an $M1$ $s \to s$

---

[2]On a more microscopic scale the relevant degrees of freedom are the quarks, see also Exercise 3 of [174]. The nucleon resonances, see Fig. 14 are a manifestation of these degrees of freedom
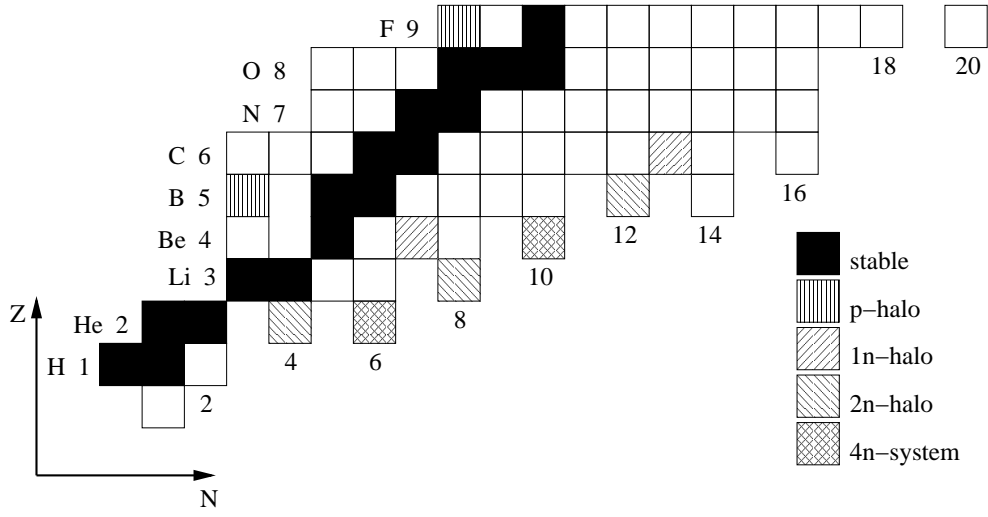
Figure 18: Chart of the (particle stable) light nuclei. Stable nuclei, one- and two-neutron halo nuclei, four-neutron cluster nuclei and proton halo nuclei are marked. The deuteron (marked in black) is the prototype of a one-neutron halo nucleus. Coulomb dissociation experiments of most of those nuclei are discussed in the present and the following sections.

transition, which dominates over $E1$ [171]. It remains to be seen whether a similar situation will be found in other halo nuclei.

In Fig. 18 we give a part of the chart of nuclides. We concentrate on the light nuclides and indicate one- and two-neutron halo nuclei. On the proton rich side, $^8$B (and probably also $^{17}$F, at least its $1/2^+$ first excited state) can be considered as a proton halo nucleus. $^8$He, as well as, $^{14}$Be can be regarded as four-neutron cluster nuclei.

Coulomb dissociation of exotic nuclei is just the right tool to study this nuclear structure problem. By this method one determines the electromagnetic matrix elements between the ground state and the nuclear continuum. A classic example is the $^{11}$Be Coulomb dissociation. The excitation energy spectrum of the $^{10}$Be$+n$ system in the Coulomb dissociation of the one-neutron halo nucleus $^{11}$Be on a Pb target at 72 $A$MeV was measured [67], from which we show Fig. 1a-c as Fig. 19.

Low lying $E1$-strength was found. It shows the shape of the $B(E1)$ distribution obtained from the simple zero range model of Eq. (108). This distribution of low lying $E1$-strength is one of the most convincing demonstrations of the neutron halo phenomenon.

The Coulomb dissociation of the extremely neutron-rich nucleus $^{19}$C was recently studied in a similar way [66]. From the shape of the dipole distribution, the neutron separation energy of $^{19}$C could also be determined to be $530 \pm 130$ keV. As can be seen from Eq. (108), this shape depends directly on the binding energy parameter $\kappa$.

We note the similarity of the shape of the low lying $B(E1)$ strength in the case of $^{11}Be$ (Fig. 19), $^{19}$C (Fig. 5 above) and also for the deuteron (see Fig. 4.1, p. 609 in [171]). The reason is that all these nuclei are halo nuclei: the ground state wave function is an $s$-wave function with a small binding energy parameter $\kappa$ and it is rather well described by Eq. (107) or (58). The neutron spends most of its time in the classically forbidden region. The continuum is a $p$-wave function which differs little from the spherical Bessel function which describes a free neutron. At the low relevant neutron energies there is only little interaction with the strong short range force in the $p$- or higher partial wave channels. In this case, the electric transition dipole moment is given by Eq. (108) above.

The $E1$-strength in other neutron-rich carbon isotopes has also been studied experimentally: Coulomb dissociation of $^{15}$C is again well described by a model with a $^{14}$C-core coupled to an $s_{1/2}$ neutron. The analysis of [181] gave a spectroscopic factor of 0.75, consistent with the one found from $(d,p)$-
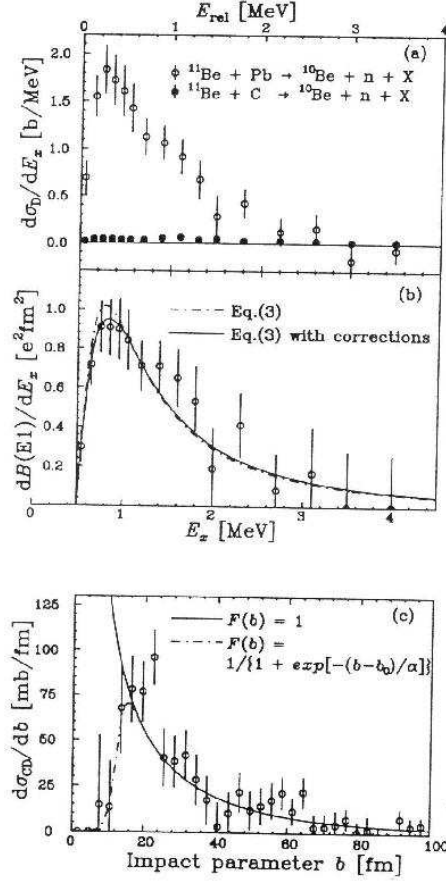
Figure 19: Fig1(a) Dissociation cross sections of $^{11}$Be on a Pb target as a function of the excitation energy $E_x$ for the $^{10}Be+n$ system. Data from a C target are also indicated. (b) Dipole strengths deduced from the $d\sigma_{CD}/dE_x$ spectrum are shown by the open circles. (c) Impact parameter dependence of the Coulomb dissociation cross section. The low lying $E1$ strength in $^{11}$Be is clearly seen. This figure is taken from [67], Fig. 1 there, where further details can be found.
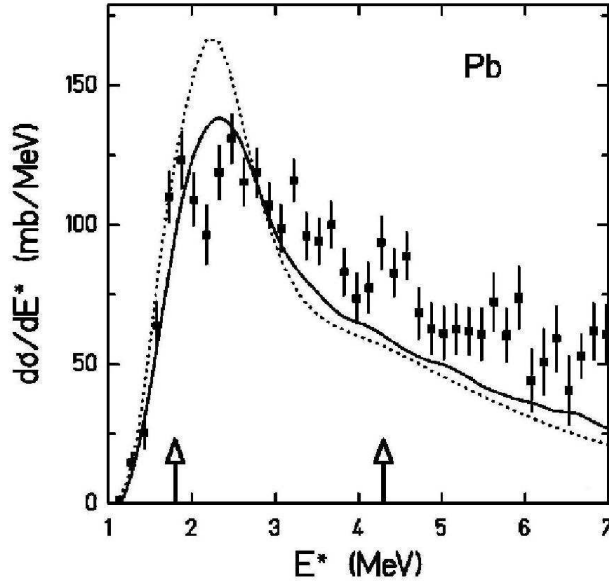
Figure 20: The excitation cross section $d\sigma/dE^*$ is shown for the breakup of $^6$He at 240 $A$MeV on a Pb target, where $E^*$ has been reconstructed from the invariant mass of the $\alpha + n + n$ fragments. The dotted curve shows the result of a semiclassical perturbative calculation using the $dB(E1)/dE*$ distribution from the three body model of [186], the solid one shows the convolution of the dotted curve with the instrumental response. The two arrow show two $2^+$ resonances, a known one at an energy of $E^* = 1.80$ MeV and a predicted one at $E^* = 4.3$ MeV [187]. Reproduced from Fig. 3 of [188], where further details can be found. Copyright (1999) by the American Physical Society.

reactions. It would be of interest to compare their results obtained with a 606 $A$MeV $^{15}$C beam to those of [182], see also Sec. 7.

The Coulomb dissociation of $^{17}$C was also studied. One can adopt a model of a neutron coupled to a $^{16}$C core. The importance of the $2^+$-core excited state is directly evident from the Coulomb dissociation measurement: Coulomb dissociation is dominantly accompanied by the emission of photons from the 1.77 MeV $\gamma$-line from the deexcitation of the $2^+$ state in the $^{16}$C core. A sizeable $s$-component of the neutron coupled to the $2^+$ core is found, and it is concluded that the ground state spin of $^{17}$C is either $3/2^+$ or $5/2^+$. For further details we refer to [181].

It is appropriate to mention at this point also a different exotic nucleus: the hypernucleus $^3_\Lambda$H. The binding energy $B_\Lambda$ of the hyperon to the deuteron core is $0.06 \pm 0.06$ MeV. The Coulomb disintegration of this hypernucleus depends sensitively on its binding energy, see [183, 184, 185].

Quite similarly, the Coulomb dissociation of the $2n$-halo nuclei can be studied experimentally in order to investigate the low lying $E1$-strength. Certainly, this is a richer field than the study of single-neutron halo nuclei, where essentially single particle effects show up. Now there are in addition interesting correlation effects. E.g., $^{11}$Li and also other $2n$-nuclei like $^6$He are so-called *Borromean systems*: the core-$2n$-system is bound, whereas none of the binary subsystems ($n$-$n$, or core-$n$) are bound.

The most prominent example is $^{11}$Li (for $^6$He see below), which was studied experimentally in various laboratories [191, 192, 193]. The momentum distributions for the ($^{11}$Li,$^9$Li$+n+n$) breakup reaction were studied theoretically in [194] and [195]. In an experiment at MSU [196], the correlations of the outgoing neutrons were studied. Within the limits of experimental accuracy, no correlations were found.
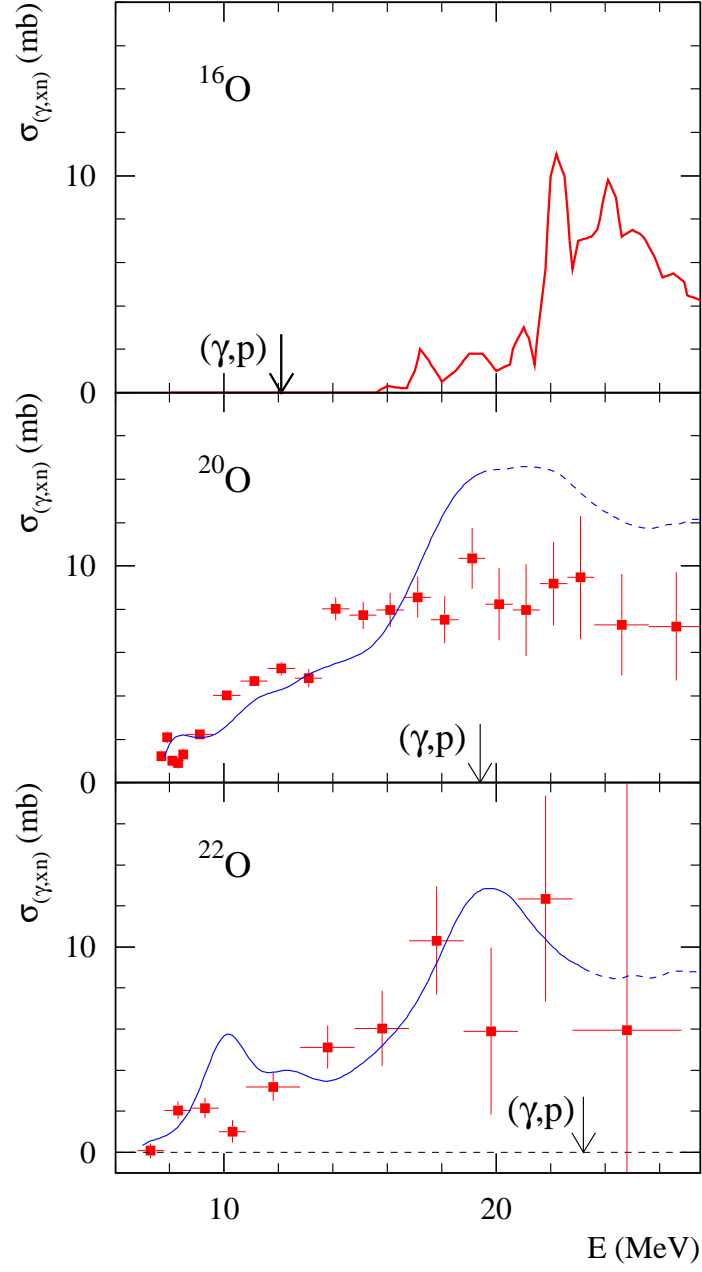
43

Figure 21: Photo-neutron cross sections measured [189] for the unstable oxygen isotopes $^{20,22}$O in comparison to that of the stable isotope $^{16}$O. The data for $^{20,22}$O are compared to shell model calculations [190]. The $(\gamma, p)$ thresholds are indicated by arrows. This figure is taken from [3] p. 86.

(To be sure there must be correlations, as the Borromean effect itself shows, they are just hard to see in the breakup experiments). Further studies were reported in [193]. In this reference invariant mass spectroscopy of $^{10}$Li and $^{11}$Li was performed. It was concluded that *"a strong di-neutron correlation can be disregarded"*. Low lying $E1$- strength was found, it exhausts up to about 8% of the TRK-sum rule below 4 MeV excitation energy which corresponds to 96% of the cluster sum rule assuming a $2n$-halo. Two low lying structures were observed for $^{10}$Li ($n$-$^9$Li final state interaction), see also [197].

The Coulomb breakup of the neutron-rich He-isotopes $^6$He and $^8$He has also been investigated experimentally [198, 188], see also Fig. 20.

The Coulomb dissociation cross-section at 227 $A$MeV on Pb is about a factor of three smaller in $^8$He than in $^6$He. This indicates that $^6$He is a halo-nucleus, with low-lying $E1$-strength, whereas $^8$He is not. The low lying strength in $^6$He (up to an excitation energy of 5 MeV) was found to exhaust $10 \pm 2\%$ of the TRK sum rule, which corresponds to about 40% of the cluster sum rule.

The dissociation reaction $^6$He $\rightarrow \alpha + 2n$ was studied at 23.9 $A$MeV on C, Al, Cu, Sn and Pb targets [199]. For U the Coulomb part accounts for 2/3 of the total two-neutron removal cross section $\sigma_{-2n}$. Only a small correlation between the two neutrons was found. The $B(E1)$-strength found is in agreement with [188], an experiment with about ten times the beam energy of [199].

Similar studies were also carried out in GANIL [200]. The neutron-neutron correlation there was analysed in terms of the radius of the *producing source* and using Dalitz plots, see also [181]. Final state effects are taken into account. Differences between the Coulomb and nuclear breakup are found, which are interpreted as being due to the direct breakup in nuclear dissociation and a resonant breakup in Coulomb dissociation.

Photoneutron cross sections for unstable neutron-rich oxygen isotopes were recently studied in [189]. Their results for the isotopes $^{20,22}$O are shown in Fig. 21, where also the corresponding results for the stable isotope $^{16}$O are given. It was found that there is systematically a considerable fraction of low-lying dipole strength. Low lying $E1$ strength was also found in the proton-rich isotope $^{13}$O by a $^{13}$O $\rightarrow p + ^{12}$N Coulomb dissociation measurement [201]. It is very promising to extend such types of studies to even heavier unstable neutron- (and also proton-) rich nuclei. This is also a challenge for modern nuclear structure theory. While we just discussed the single particle aspect, which is the main point for 1-$n$, or 2-$n$ halo nuclei, the onset of a *pigmy collectivity* is a question for more involved theories. The exploration of the structure of unstable nuclei is a large field for modern nuclear structure theory, which benefits also from the modern high computing power. This field is rapidly expanding, as can be seen from the many conferences which are taking place on this topic; as recent ones let us mention the *"Hirschegg workshop 2003 on Nuclear Structure and Dynamics at the Limits"* [202] or *"INT workshop on Reaction Theory for Nuclei Far From Stability"*[100]. We can refer here only to further references which may, e.g., be found in [3].

# 7 Nuclear Astrophysics

*Du verstehst nicht die Sterne*
*ohne die Kerne.*
*(unknown poet, last century)*

In nuclear astrophysics, radiative capture reactions of the type

$$b + c \rightarrow a + \gamma \tag{110}$$

play a very important role. They can also be studied by the time-reversed reaction

$$\gamma + a \rightarrow b + c \,, \tag{111}$$

at least in those cases where the nucleus $a$ is in its ground state.

Such a photodissociation experiment has been recently performed with a real photon beam by Utsunomiya et al. [203]. They investigated the photodisintegration of $^9$Be with laser-induced Compton backscattered $\gamma$ rays. We refer to this work for further details.

The two cross sections Eqs. (110) and (111) are related to each other by detailed balance

$$\sigma(b + c \rightarrow a + \gamma) = \frac{2(2j_a + 1)}{(2j_b + 1)(2j_c + 1)} \frac{k_\gamma^2}{k_{CM}^2} \sigma(\gamma + a \rightarrow b + c), \tag{112}$$

where the wave number in the $(b + c)$-channel is given by $k_{CM}^2 = 2\mu_{bc}E_{CM}/\hbar^2$, with $\mu_{bc}$ the reduced mass; the photon wave number is given by $k_\gamma = (E_{CM} + Q)/(\hbar c)$, where $Q$ is the Q-value of the capture reaction Eq. (110). One typically has $k_\gamma/k_{CM} \ll 1$ for energies not immediately in the threshold region $k_{CM} \approx 0$. Due to this phase space factor there is a strong enhancement of the dissociation cross section Eq. (111) as compared to the capture cross section Eq. (110).

As a photon beam, we use now the equivalent photon spectrum, which is provided by the Coulomb field of the target nucleus in the fast peripheral collision [16]. There are previous reviews, where both experimental, as well as, theoretical aspects have been given, see [17, 18]. We want to concentrate here on theoretical aspects, but also discuss experimental issues, at least from our point of view as theoreticians. The last review has been written in 1996 and much progress, on the theoretical, as well as, experimental side, has been made in the meantime.

In [204] Austin gives a minireview of various indirect methods in nuclear astrophysics. He remarks that *"it is a common perception that experimental nuclear astrophysics involves long measurements of small cross sections at lower and lower energies, so as to permit a reliable extrapolation to actual astrophysical energies. This perception is only partially correct. Recent developments, especially of radioactive beams, often permit one to obtain equivalent information with higher energy beams. The high energy experiments commonly yield higher event rates and sometimes yield information not available in the classical approach."* Coulomb breakup is a good example.

In non-resonant charged particle reactions the energy dependence of the cross section is dominated by the penetration of the Coulomb barrier. This energy dependence is usually factored out by defining the astrophysical $S$-factor

$$S(E_{CM}) = E_{CM}\sigma(E_{CM})\exp(2\pi\eta), \tag{113}$$

where $\eta$ is the Coulomb parameter Eq. (13).

We want to give here some examples of Coulomb breakup experiments of astrophysical relevance. We also (briefly) explain their astrophysical relevance and the theoretical background of the experiments. In judging the conditions of an actual experiment, it is always useful to keep in mind the values of the basic parameters $\eta$, $\xi$, and $\chi$ of electromagnetic excitation, see Eqs. (10) and (12). In this way it is, e.g., quite clear that Coulomb dissociation of $^8$B is a more favourable case than that of $^{16}$O, with its comparatively high $\xi$-values (see also Fig. 3 of [37]).

## 7.1 *Li Isotopes*

$^6$**Li** $\rightarrow \alpha + d$

The $^6$Li Coulomb dissociation into $\alpha$+d has been a test case of the Coulomb breakup method, see [205] and [16, 17, 18]. These experiments were carried out with a 156 MeV $^6$Li beam at the Karlsruhe Isochronous Cyclotron using the magnetic spectrograph "Little John". This reaction is of astrophysical importance since the $d(\alpha, \gamma)^6$Li radiative capture is the only process by which $^6$Li is produced in the standard primordial nucleosynthesis models. There has been renewed interest in $^6$Li as a cosmological probe in recent years, mainly because the sensitivity of searches for $^6$Li has been increased. $^6$Li has

been found in metal-poor halo stars at a level exceeding even optimistic estimates of how much of it could have been made in the standard big bang nucleosynthesis. For more discussion on this, see [206].

A $^6$Li-breakup experiment on $^{208}$Pb at 60 MeV was performed at the Heidelberg tandem [207]. These authors found that the measured breakup cross section could not be related directly by first-order Coulomb excitation theory to the astrophysically relevant $^4$He$(\alpha, d)^6$Li capture reaction. It would be interesting to redo the analysis with a modern reaction code and see the influence of higher order electromagnetic and nuclear effects.

An experiment at the much higher beam energy of 150 $A$MeV than at Karlsruhe [205] or Heidelberg [207] is under way at GSI. Results from this experiments are eagerly awaited.

For $(N = Z)$-nuclei electric dipole transitions obey the selection rule $\Delta T = 1$. Since the two fragments $d$ and $\alpha$ have isospin $T = 0$ the electric dipole transition is forbidden by isospin selection rules. The contribution from the $E2$ transition should dominate. $E1$ transitions can still occur due to isospin violations.

d$(\alpha, \gamma)^6$Li radiative capture experiments were also performed: Robertson et al. [208] made measurements down to a relative energy of 1 MeV by detecting the recoil $^6$Li ions. Cecil et al. [209] searched for the capture reaction at a relative energy of $E_{cm} = 53$ keV; they obtained an upper limit on the reaction $S$-factor of $2 \times 10^{-7}$ MeV$b$. The direct capture into the $3^+$ resonance was measured also by Mohr et al. [210].


## $^7$Li $\rightarrow \alpha + t$

The reaction $t(\alpha, \gamma)^7$Li is also astrophysically relevant, and many experimental groups have measured this process in direct capture experiments. The nuclide $^7$Li is produced in the early universe via this radiative capture reaction. The Coulomb dissociation method has also been applied under various conditions. We mention here the direct breakup of 70 MeV $^7$Li scattered from a $^{120}$Sn target [211]. It was found that the breakup is dominated by the Coulomb interaction for scattering angles inside the grazing angle. $^7$Li breakup measurements on $^{197}$Au at 54 MeV were performed in [212]. No straightforward analysis in terms of first order Coulomb breakup was found to be possible.

A rather detailed measurement of the $^7$Li $\rightarrow \alpha + t$ breakup was recently performed by Tokimoto et al. [73] with improved experimental techniques. This measurement was also accompanied by a theoretical analysis, where the time dependent Schrödinger equation was solved numerically, see [64] and also the discussion in Sec. 3. In this way, valuable insight into the Coulomb dissociation process, the $E1$ and $E2$ mixtures, its higher order effects (*postacceleration*) and the time-dependence of the tunneling process became possible. We refer the reader to this reference for further details.


## $^9$Li $\rightarrow ^8$Li $+ n$

The cross section for the radiative capture reaction $^8Li(n, \gamma)^9Li$ was studied with the Coulomb dissociation of a $^9Li$ beam of 28.53 $A$MeV at MSU [213].

This reaction is of importance for the nucleosynthesis in inhomogeneous big bang models and in Type II supernovae. While the standard big bang nucleosynthesis ends with $^7$Li, nucleosynthesis in neutron-rich regions could produce an observable amount of $A > 8$ nuclei. The $^8$Li$(n, \gamma)^9$Li reaction is in competition with the $^8$Li$(\alpha, n)^{11}$B reaction in determining the reaction path in the evolution network. This reaction may also play an important role in the explanation of the origin of light neutron-rich nuclei like $^{36}$S, $^{40}$Ar, $^{46}$Ca and $^{48}$Ca. Recently, neutron-star mergers have been proposed as possible alternative sites for an $r$-process [214], where similar reaction chains occur.

This reaction is also of importance in order to determine the different primordial abundances of Li, Be, B, and C, in order to confine the possibility of inhomogeneous big bang nucleosynthesis. In
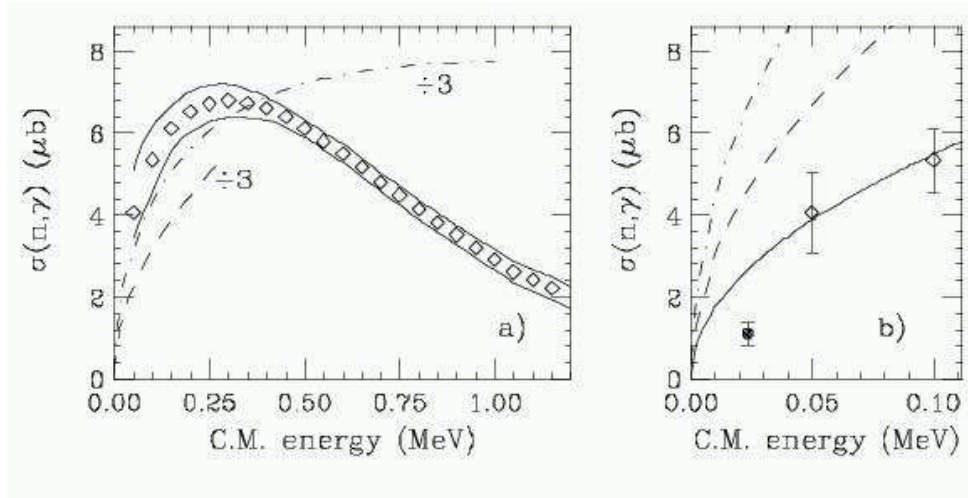
Figure 22: (a) The $(n, \gamma)$ capture cross sections on $^{14}C$ are shown as a function of the c.m. energy. The diamonds enclosed by two solid curves define the region of the experimental results. Plotted as 1/3 of the actual values the dashed curve is a prediction of [220], the dot-dashed curve is a prediction of [221]. (b) Blowup of the low energy region showing the same theoretical curves (not divided by 3), the experimental result of [222] (solid point) and the lowest energy points (diamonds) of [182] with a kinematical fit (solid curve). This is Fig. 8 of [182].

such models the neutron-to-proton ratio is different in different regions in the early universe. In the neutron-rich region this reaction could therefore lead to a different bridging of the mass number $A = 8$.

The half-life of $^8$Li is less than a second (838ms), this probably makes a direct measurement of the capture cross section impossible. One has to rely on indirect methods, like the Coulomb dissociation of $^9$Li (with a half-life of 178 ms, but the Coulomb dissociation still works for such a case, as the $^9$Li beam is produced in a fragmentation reaction). In this experiment [213], only an upper limit could be put on the relevant cross section. Still, this is interesting since it directly rules out two theoretical calculations [215, 216] while the found upper limit is still consistent with the theoretical results of [217, 218]. A new attempt was recently made at MSU [219] to measure the $^8$Li $(\gamma,n)^9$Li cross-section by the Coulomb dissociation of $^9$Li with a more sensitive equipment than in [213]. It considerably lowers the upper bounds found there. We refer to this reference for details.

## $^{11}$Li $\rightarrow^9$ Li $+ 2n$
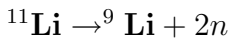
This reaction is mainly of interest for nuclear structure studies due to the Borromean nature of $^{11}$Li. It is discussed in Sec. 6 above. Of general interest with respect to astrophysics is the question of the correlation of the two halo neutrons. This influences the rate of the two-neutron capture reaction. An understanding of this correlation is also of importance for other two-neutron capture reactions to be discussed in the Sec. 8.2.

## 7.2  $^{14}C(n, \gamma)^{15}C$

The nuclear structure aspect of the Coulomb dissociation of $^{15}$C was touched upon in Sec. 6, where a measurement at GSI with a 606 $A$MeV $^{15}$C beam is discussed. In this experiment, the $B(E1)$-distribution in the range of excitation energies from the threshold ($E_{threshold} = 1.2184$ MeV) up to about $E = 8$ MeV was studied.

Now we are interested in thermonuclear energies, i.e., relative $n+^{14}$C energies from about 10 keV up

48

to about 300 keV (corresponding to temperatures between $0.1 - 3 \times 10^9$ K). The Coulomb dissociation of $^{15}$C was discussed in [18] as a way to investigate the radiative capture reaction $^{14}$C$(n, \gamma)^{15}$C. This reaction is important in neutron-induced CNO cycles of stellar evolution phases beyond the main sequence. It is also relevant in inhomogeneous big bang scenarios. A $^{15}$C Coulomb dissociation experiment was performed at MSU [182] where details and further references can be found. The present status is not entirely conclusive, as one can see from Fig. 22 (Fig. 8 of [182]). The excitation function for the $^{14}$C$(n, \gamma)$ cross section was measured in [182] with an $E/A = 35$ MeV beam. This energy is much lower than the energy of 606 $A$MeV used at GSI. It is still high enough to break up the $^{15}$C nucleus and excite the low energy continuum relevant for astrophysics. The deduced excitation function is shown as diamonds in Fig. 22(a). They are enclosed by the two solid curves, which define the region of the experimental results of the Coulomb dissociation experiment of [182]. Plotted as 1/3 of the actual values, the dashed curve is a theoretical prediction of Wiescher et al. [220] and the dot-dashed curve is a prediction of [221]. In Fig. 22(b) a blowup of the low energy region is shown. The result from the direct capture experiment at 23 keV of the Karlsruhe group [222] (solid point) and the low energy points of the MSU experiment with a kinematical fit (solid curve) are shown. For further details see [182].

The excitation function for the $^{14}$C$(n, \gamma)$-reaction, as deduced from the Coulomb breakup, is consistent with an $E_n^{1/2}$ rise, as expected for $p$-wave capture. A fit gives $\sigma_{n,\gamma}(23\text{keV}) = 3.2 \pm 0.9 \mu$b, about three times higher than the result of [222]. Also, the shape of the excitation curve has a peak at around $E_n = 200$ keV. On the other hand, theoretical predictions by Wiescher et al. [220] and Descouvemont [221] increase monotonically in this energy range. Another issue is the radiative capture contribution to the $5/2^+$-excited state at 740 keV. This contribution is not included in the Coulomb breakup measurement. It is estimated to be small on theoretical grounds: the $E_\gamma^3$-dependence of the dipole transitions and the measured spectroscopic factors favour the ground state transition. We conclude that more work is necessary to resolve these questions.

## 7.3 $^{16}O \rightarrow \alpha + ^{12}C$ Coulomb Dissociation

The helium burning reaction $^{12}$C$(\alpha, \gamma)^{16}$O at thermonuclear energies is a key process for the evolution of massive stars and for the nucleosynthesis of $^{16}$O and heavier elements up to Fe. Despite its importance for nuclear astrophysics, the cross section for this reaction is still quite uncertain in the stellar energy domain $(E_{cm} \sim 300$ keV). The reason is the extremely small value of this cross section and the superposition of $E1$- and $E2$-multipole contributions in the capture process. Several direct measurements of the radiative capture reaction, elastic $\alpha + ^{12}$C scattering and $^{16}$N-decay studies have succeeded to determine reasonably well the $E1$-part of the astrophysical $S$-factor. However, the $E2$-part, which is thought to be of about the same magnitude as the $E1$-part, is still quite uncertain.

In this situation, Coulomb breakup seems to be an interesting method, since $E2$-excitations are enhanced as compared to $E1$, see Sec. 2, especially Eq. (23). However, several points render this method quite challenging. The $\alpha + ^{12}$C-breakup threshold $E = 7.162$ MeV is quite high, which means that the $\xi$-values, even at high $^{16}$O beam energies are not small (for the experiment mentioned below we get a value of about $\xi = 0.8$). The relatively low flux of equivalent photons at these high energies leads to a serious competition with nuclear excitation effects. Also, there is $E1$- and $E2$-interference. Undaunted by all this, a breakup experiment was performed at GANIL at a projectile energy of 95 $A$MeV. Assuming only $E2$ Coulomb and $\Delta L = 2$ nuclear excitation the measured breakup cross sections were compared to optical model calculations and an $E2$ $S$-factor was extracted in [223]. This analysis is based on theoretical calculations with the ECIS-code in [224] and calculations of the fragment angular correlations in [225]. Further experimental studies were done recently at KVI , Groningen at 80 $A$MeV [226]. The large angular and momentum acceptances make the spectrometer BBS a very suitable device for such coincidence studies. A further experiment is planned at MSU which can use all the experience

gained from the previous experiments. The difficulties of the experiment were identified in the previous approaches and can hopefully be overcome. Much is at stake. As Wolfgang Pauli said (when he invented the neutrino): *"Nur wer wagt, gewinnt!" ("Nothing ventured, nothing gained").*

## 7.4 Some $(p, \gamma)$-Reactions studied with Coulomb Dissociation

The Coulomb breakup of $^{14}$O has been studied at RIKEN [227] and GANIL [228] in order to determine the $S$-factor of the $^{13}$N$(p, \gamma)^{14}$O capture reaction. It is astrophysically relevant for the hot CNO cycle. The $S$-factor is dominated by the $1^-$ resonance in $^{14}$O which can be reached from the ground state in an $E1$ transition. Such a case is certainly simpler to study than a transition into the (flat) continuum. We refer to previous reviews [17, 18]. We note that there is good agreement with the direct radiative capture measurement at Louvain-la Neuve [229]. This consistency can also be considered as a test of the Coulomb dissociation approach. It is also worth mentioning that as a by-product of the $^{14}$O Coulomb dissociation approach the transition from the $\frac{1}{2}^-$ ground state to the first excited $\frac{1}{2}^+$- state in $^{13}$N was studied in [227]. The corresponding value of the radiative width $\Gamma_\gamma$ was found to be in good agreement with values from a different previous experiment. Again, this can be considered as a confirmation of the Coulomb dissociation method. The accuracy of the RIKEN measurements [227] was improved in new experiments at RIKEN [230]. There is agreement with the previous studies; the reliability of the Coulomb dissociation method has been tested to an accuracy of the order of 10 percent in the $^{12}$C$(p, \gamma)^{13}$N case.

The $^{12}$N $\rightarrow {}^{11}$C$ + p$ breakup reaction was studied at GANIL [231] in order to study the $^{11}$C$(p, \gamma)^{12}$N radiative capture process. This reaction is relevant for the hot $pp$-chain. From the experimental breakup yield, the radiative width of the 1.19 MeV level in $^{12}$N and the spectroscopic factor for the direct proton capture on $^{11}$C have been extracted. The radiative width of the 1.19 MeV level is found to be smaller by more than one order of magnitude compared to a recent theoretical calculation but in rough agreement with an estimate by Wiescher et al. [232]. We refer to this reference for further details. The $^{11}$C$(p, \gamma)^{12}$N reaction was also studied at RIKEN by the Coulomb dissociation method [233, 234]. Their result is consistent with the GANIL measurement [231], the accuracy of the value for the radiative width of the 1.19 MeV level in $^{12}$N is improved; for further details see these references. An experimental study of the $^{22}$Mg$(p, \gamma)^{23}$Al reaction by the Coulomb dissociation method is also reported at RIKEN [235]. This reaction is relevant for the nucleosynthesis of $^{22}$Na in Ne-rich novae.

A very instructive test case would be $^{17}$F-Coulomb dissociation. There are very accurate radiative capture experiments [236] and [237] to which one could compare possible Coulomb breakup measurements. The radiative capture reaction goes to the ground state and the $\frac{1}{2}^+$ excited state, with the Coulomb breakup method one can only study the ground state transition. There are data for the 170 MeV $^{17}$F dissociation into $p + {}^{16}$O [238]. They were analyzed theoretically by Esbensen and Bertsch [22]; substantial higher order effects were found at this energy. Higher $^{17}$F beam energies would reduce these effects and greatly facilitate the analysis. A recent work [239] found large nuclear effects in the dissociation of $^{17}$F on $^{208}$Pb at an energy of 65 $A$MeV. This would make an extraction of the electromagnetic transition matrixelement quite difficult.

## 7.5 $^8B$ Coulomb Dissociation and the Solar Neutrino Problem

### Astrophysical motivation

Two kinds of extraterrestrial neutrinos, solar neutrinos and supernovae neutrinos, have been observed and their measured fluxes, as well as, energy spectra, shed a new light on astrophysics and particle physics [240]. In this context, the $^7$Be$(p, \gamma)^8$B radiative capture reaction is relevant for the solar neutrino problem. It determines the rate of production of $^8$B which leads to the emission of high energy neutrinos.

The SNO experiment [241] has measured the $\nu_e$ flux in the *charged current* (CC) reaction

$$d + \nu_e \rightarrow p + p + e^-, \tag{114}$$

and also the *neutral current* (NC) reaction

$$d + \nu_x \rightarrow p + n + \nu_x \tag{115}$$

was recently measured [242, 243]. The CC reaction is only sensitive to electron neutrinos, whereas the NC reaction is equally sensitive to all neutrino flavours $\nu_x$ where $x = e$, $\mu$, and $\tau$.

The Kamiokande and SNO detectors also measure neutrino *elastic scattering* (ES) on the electrons:

$$\nu_x + e^- \rightarrow \nu_x + e^-. \tag{116}$$

This reaction is sensitive to all kinds of neutrino flavours, mainly to electron neutrinos but also to some extent (to about 14%) to $\nu_\mu$ and $\nu_\tau$ via the neutral current interaction. Comparison of the two neutrino fluxes from SNO and Kamiokande and of the NC and CC results of SNO are a direct proof that there are neutrino oscillations. Some of the Kamiokande and SNO neutrinos come from flavours other than the electron flavour [3].

In this argument the astrophysical $S$-factor $S_{17}$ does not enter, since one considers only the ratios of fluxes. However, this $S$-factor is still of vital importance: it determines the absolute value of theoretical calculations of the solar $^8$B $\nu$ flux and therefore many efforts were undertaken to study the $^7$Be$(p, \gamma)^8$B reaction [245, 246].

In scenarios involving sterile neutrinos it is important to know the standard solar model $^8$B neutrino flux in order to derive which part of the flux has oscillated into the sterile ones. We quote from [247]: *"Thus, the $^8$B plays a crucial role in the interpretation of these experiments. Unfortunately, the predicted value of the $^8$B flux normalization is quite uncertain, mainly due to poorly known nuclear cross sections at low energies."*

For recent developments we refer to [248]. The situation is summarized in [249]: *Improved ($^8$B) production rate predictions are very important for limiting the allowed neutrino mixing parameters, including possible contributions of sterile neutrinos. The astrophysical S factor $S_{17}(0)$ for this reaction must be known to $\pm 5\%$ in order that this uncertainty not be the dominant error in predictions of the solar $\nu_e$ flux.*

### Direct measurements of the $^7$Be$(p, \gamma)^8$B-capture cross section

There are direct reaction measurements, for the recent ones see Ref. [250, 251, 249, 252]. The target is the radioactive nucleus $^7$Be and a major problem is the determination of the thickness of this target. The reaction has been measured at $E_{c.m.} = 185.8, 134.7$ and $111.7$ keV and the zero energy $S$-factor inferred from these data is $18.5\pm2.4$ eVb. This reaction has been studied recently in [253] with a $^7$Be radioactive beam. In this way the target thickness problem is overcome, see also the discussion in [204].

There is an experiment by Junghans et al. from Seattle and TRIUMF [249] with a somewhat high value of the $S$-factor. The cross section values of this paper are currently being revised, see Ref. 11 of [252]. A precision measurement at $E_{lab} = 991$ keV with an implanted $^7$Be target was recently reported in [252].

---

[3]Oscillations of antineutrinos (coming from quite a few nuclear power reactors about 180 km from the detector) were recently also found by the KAMLAND experiment [244].

## Coulomb dissociation of $^8$B

While there are certainly experimental problems with the direct capture experiments, there are (in addition to the specific experimental problems of the Coulomb dissociation method) problems of the theoretical analysis of the experiments in terms of the astrophysical $S$-factor. These theoretical problems can be solved in principle, as peripheral reactions are the ones best understood on a quantitative basis. They are mainly related to higher order electromagnetic effects (see also Sec. 3 above), nuclear effects (see Sec. 5) and the mixture of different multipoles (especially $E1$ and $E2$). Yet, the Coulomb dissociation of $^8$B offers some advantages: at the low binding energy of $^8$B of 137 keV, the relevant photon fluxes are very high. Experiments under various conditions have been performed, which are affected in different ways by the different problems mentioned above. With all these problems identified a consistent picture emerges and an $S$-factor is obtained in an entirely different way as compared to the direct measurements. This in itself is valuable.

The story of the mid-nineties has been vividly told by Taube [254] and efforts to determine the astrophysical $S$-factor $S_{17}$ by many different methods including Coulomb dissociation continue up to now.

We now discuss the various experimental and theoretical contributions: Higher order perturbation theory using the semiclassical approximation was studied in [14, 15]. The semiclassical time-dependent Schrödinger equation was solved in [74, 75]. CDCC calculations were performed in [70], which become increasingly cumbersome for higher beam energies. The reactions at the different radioactive beam facilities have been done under different kinematical conditions, the highest $^8$B beam energy is at GSI, 254 $A$MeV [255], at MSU it is about 40 to 83 $A$MeV [256, 257]. At RIKEN it is about 50 $A$MeV [258].

The measurement at Notre Dame is at a very low $^8$B beam energy of 26 MeV [259]. For such beam energies higher order effects are very important and it is not a simple task to extract a model independent $S$-factor. Nevertheless, these experiments are of great interest since they allow to test the dynamics of the Coulomb breakup process. With modern reaction codes (e.g. solving of the time-dependent Schrödinger equation [64, 22, 139], see also Sec. 3). One can well describe such reactions, however, the connection to the astrophysical $S$-factor is becoming somewhat indirect.

One of the main issues is the contributions of the $E1$ and $E2$ multipoles and their separation. As can be shown from Eq. (23) the $E2$ photon number at intermediate and lower energies is enhanced, therefore they can contribute considerably to the Coulomb breakup cross section, whereas they are a small contribution to the photodissociation (or radiative capture) cross section. At RIKEN, one uses the different angular behaviour of the $E1$ and $E2$ multipolarities in order to disentangle the contributions, see [260, 261, 262]. The $E2$ contribution shows up predominantly at smaller impact parameters, i.e., at larger scattering angles. In Fig. 23 we show some theoretical calculations related to this point [15]. The $E1$ contribution shows a $(\sin \theta)^{-2}$-behaviour, whereas the $E2$ contribution is almost constant, down to a minimum angle $\theta_{adiabatic}$. Nuclear diffraction effects are small. This is used in the RIKEN experiment to determine the $E2$ contribution. We show their result in Fig. 24. These authors conclude that *"although systematic effects could be large, the extracted $E2$ components appear to be quite small"*.

In the MSU method, one uses the asymmetries, which are induced by the $E1$-$E2$ interference effects in order to sensitively determine the $E2$ $S$-factor [263, 257, 264]. We show their longitudinal momentum distribution here in Fig. 25.

An intuitively appealing picture of the Coulomb dissociation process can be gained [257] by plotting $b^2 P_{diss}(b)$, where $P_{diss}(b)$ is the Coulomb dissociation probability with various $^7$Be scattering angle cuts. This is shown in Fig 26; one can clearly see that Coulomb dissociation essentially takes place outside the nuclear interaction region.

In a particle-core model one can see qualitatively the relative importance of the various multipolar-
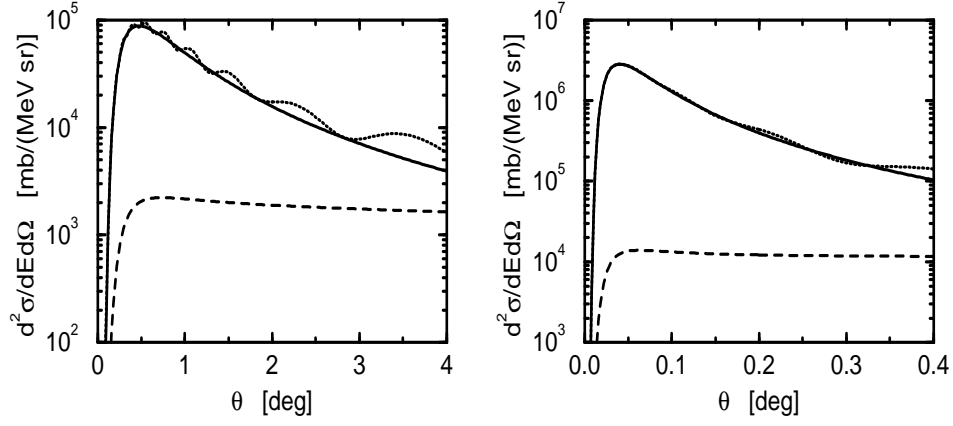
Figure 23: Coulomb dissociation cross section of $^8$B scattered on $^{208}$Pb as a function of the scattering angle for projectile energies of 46.5 $A$MeV (left) and 250 $A$MeV (right) and a $^7$Be-$p$ relative energy of 0.3 MeV. First order results $E1$ (solid line), $E2$ (dashed line) and $E1 + E2$ excitation including nuclear diffraction (dotted line). (From Figs. 4 and 5 of Ref. [15].)
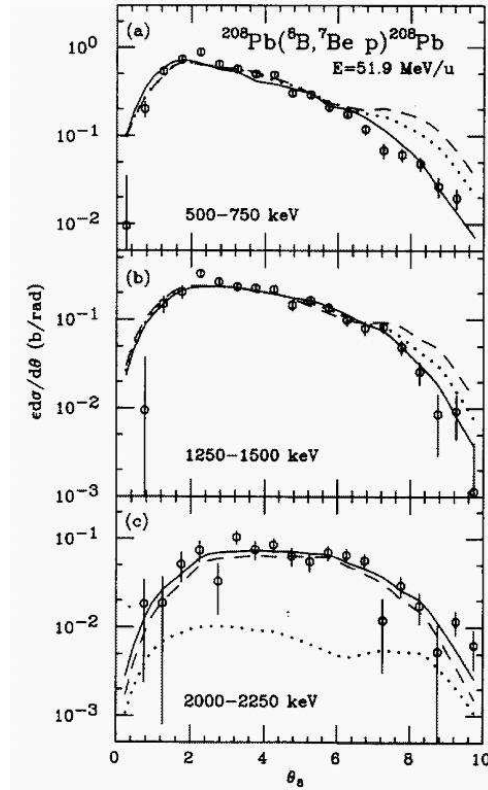


Figure 24: Observed cross sections $\epsilon d\sigma/d\theta$ are shown as a function of the outgoing $^8$B$^*$ scattering angle for the three indicated relative energy bins. The $y$ axis shows the product of the detection efficiency $\epsilon$ and the differential cross section. The solid curve represents the best fit obtained with calculated $E1$ (dashed curve in (c)) and $E2$ (Coulomb and nuclear: dotted curve in (c)) amplitudes. For the first two energy bins shown in (a) and (b), the best fits result in pure $E1$ transitions. Dashed and dotted curves in (a) and (b) correspond to the results calculated with $l = 1$ and $l = 2$ components predicted by some theoretical models. This is Fig. 2 from [260], where further details can be found.
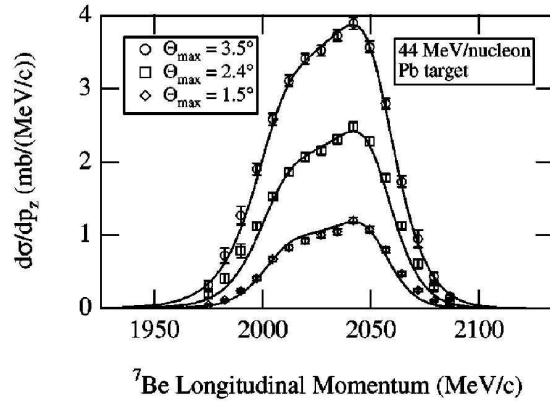
Figure 25: The measured longitudinal momentum distributions of $^7$Be fragments from the Coulomb dissociation of 44 $A$MeV $^8$B on Pb with several maximum $^7$Be scattering angle cuts are shown. The measurements are compared to a first order perturbation theory calculation convoluted with the experimental resolution. The asymmetry due to the $E1$-$E2$ interference is clearly seen. The overall normalization and the ⸱⸱⸱⸱⸱⸱⸱⸱⸱⸱⸱⸱⸱ ⸱⸱⸱⸱⸱⸱⸱⸱⸱⸱⸱⸱⸱ ⸱⸱⸱⸱⸱⸱⸱⸱⸱⸱ roduced from Fig. 8 of [257], to which we refer ⸱⸱⸱⸱⸱⸱⸱⸱⸱⸱⸱⸱⸱⸱⸱⸱⸱⸱⸱⸱⸱⸱⸱⸱⸱⸱⸱⸱⸱⸱⸱⸱⸱⸱⸱⸱⸱⸱⸱⸱⸱ Physical Society.
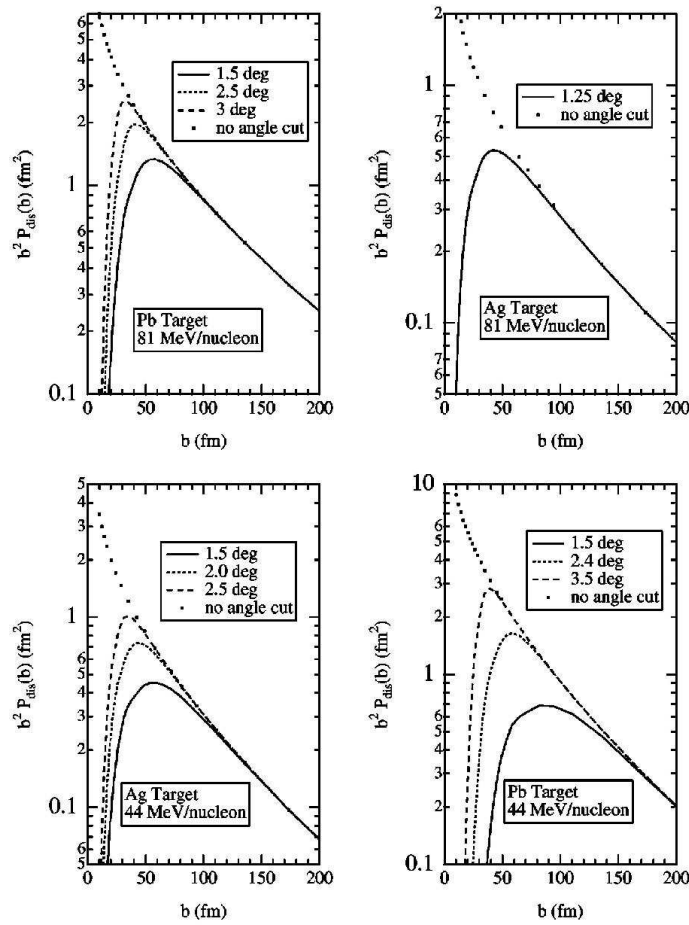


Figure 26: The product of the Coulomb dissociation probability $P(b)$ and $b^2$, where $b$ is the impact parameter are shown as a function of $b$. Various $^7$Be scattering angle cuts are applied, as indicated in the figures. Reproduced from Fig. 10 of [257]. Copyright (2001) by the American Physical Society.
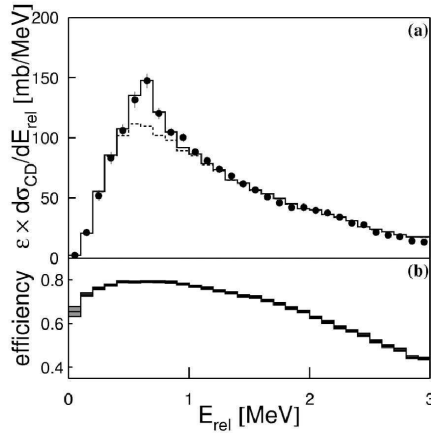
Figure 27: Yields of breakup events (cross section times efficiency) plotted as a function of the relative energy. The solid and dashed histograms denote simulated $E1+E2$ and $E1$ yields respectively. Although the $M1$ contribution is reduced by about a factor of $(v/c)^2$ in the Coulomb dissociation the $M1$ peak (smeared out by the experimental resolution) is clearly seen in the GSI data. Reproduced from Fig. 1 of [255]. Copyright (1999) by the American Physical Society.

ities. The effective charges are given by

$$Z_{eff}^{(\lambda)} = Z_b \left( \frac{m_c}{m_b + m_c} \right)^\lambda + Z_c \left( \frac{-m_b}{m_b + m_c} \right)^\lambda, \tag{117}$$

with the charge numbers $Z_b$ and $Z_c$ and the masses $m_b$ and $m_c$ of the fragments. We see that $E1$ charges are relatively small, $E2$ charges are large: for $^8$B $=^7$Be $+ p$ we have $Z_{eff}^{(1)} = 3/8$ and $Z_{eff}^{(2)} = 53/64$. This can be compared to a neutron-core system: for $^{11}$Be $=^{10}$Be $+ n$ we find $Z_{eff}^{(1)} = 4/11$ and $Z_{eff}^{(2)} = 4/121$. Furthermore, $M1$ transitions are suppressed by about a factor of $(v/c)^2$. This $M1$ peak is nicely seen in the GSI experiment. It is somewhat smeared out due to the resolution in $E_{rel}$ in the $p+^7$Be invariant mass, see Fig. 27.

A new experiment on $^8$B Coulombdissociation was recently completed at GSI [266]. They also pointed out that most extrapolations currently done are based on the cluster model of Descouvement [267], which does not seem to fully reproduce the energy dependence. This could partly explain the discrepancies of the different experiments done at different relative energies. This idea is pursued further in [268] taking into account a full dynamic reaction calculation, as well as, an improved potential model for $^8B$. A recent minireview can also be found in [269], where also a future CERN/ISOLDE measurement using a radioactive $^7$Be beam is briefly discussed.

The experimental results was summarized in Fig 19 of [257]. We have updated this figure with the latest results and show it in Fig. 28. Altogether it is quite remarkable that completely different experimental methods with possibly different systematic errors lead to results that are quite consistent.

# 8   Possible New Applications of Coulomb Dissociation for Nuclear Astrophysics

Radioactive beam facilities all over the world have considerably widened the scope of nuclear physics in the past years. In the previous sections we described the applications of Coulomb excitation and
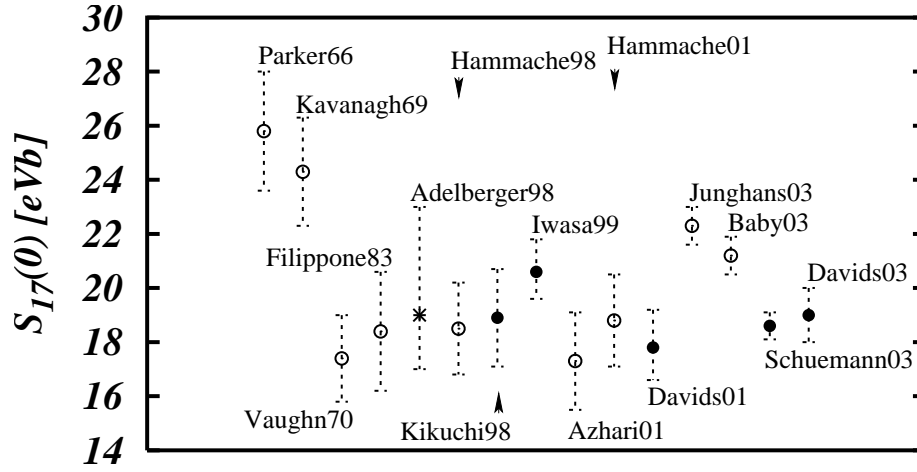
Figure 28: The zero-energy astrophysical $S$-factor $S_{17}$ for the $^7\mathrm{Be}(p,\gamma)^8\mathrm{B}$ reaction is shown from selected direct and indirect methods. The open circle denote results obtained from direct measurements, the full circle those of Coulomb breakup experiments. The star is the value given in [265] as proposed reference value. Adapted from Fig. 19 of [257].

dissociation to nuclear structure and astrophysics. For example halo nuclei and new regions of deformation could be studied in detail for light exotic nuclei. With the new forthcoming generation of RIA's also medium and heavy nuclei will be produced with sufficient intensities, with further opportunities. We mention the project in Europe [3], where a substantial part of the program is in Rare Isotope Beams research. In the US the scientific opportunities with fast fragmentation beams from the Rare Isotope Accelerator are intensively investigated see [4], and also [270]. In Japan, at RIKEN, Wako the construction of a Radio Isotope Beam Factory (RIBF) is underway, see e.g. [6].

A status report is also provided in [271]. The astrophysical scenario is presented by Käppeler et al. in [272]. In the following we indicate some of the future opportunities in this field related to nuclear astrophysics, especially to the $r$- and $rp$-processes.

## 8.1  *Electromagnetic Properties of $r$-Process Nuclei*

Nucleosynthesis beyond the iron peak proceeds mainly by the $r$- and $s$-processes (rapid and slow neutron capture). This is widely discussed in the literature, see e.g. [273, 274] or also [275]. Concise *executive summaries* are provided in [3] (p. 96f) or [4] (p. 54).

In order to assess the $r$-process path, it is important to know the nuclear properties like $\beta$-decay half-lives and neutron binding energies. In the waiting point approximation [273, 274] an (n,$\gamma$)- and ($\gamma$,n)-equilibrium is assumed in an isotopic chain. As the nuclei inside the isotopic chain are assumed to be in a thermal equilibrium, only binding energies and $\beta$-decay halflives are needed.

In general the waiting point approximation should be replaced by a dynamic $r$-process flow calculation, taking into account (n,$\gamma$), ($\gamma$,n) cross sections and $\beta$-decay rates, as well as, time-varying temperature and neutron density for the astrophysical scenario. In this case the knowledge of (n,$\gamma$) cross sections is of importance.

To establish the quantitative details of the $r$-process, accurate energy-averaged neutron-capture cross sections are needed. Such data provide information on the mechanism of the neutron-capture process and time scales, as well as, temperatures involved in the process. The data should also shed light on neutron sources, required neutron fluxes and possible sites of the processes (see Ref. [273]). In this situation, it is very instructive to look at the model studies of [276] and the scenario described in [277]. The dependence of direct neutron capture on nuclear structure models was investigated in [276].
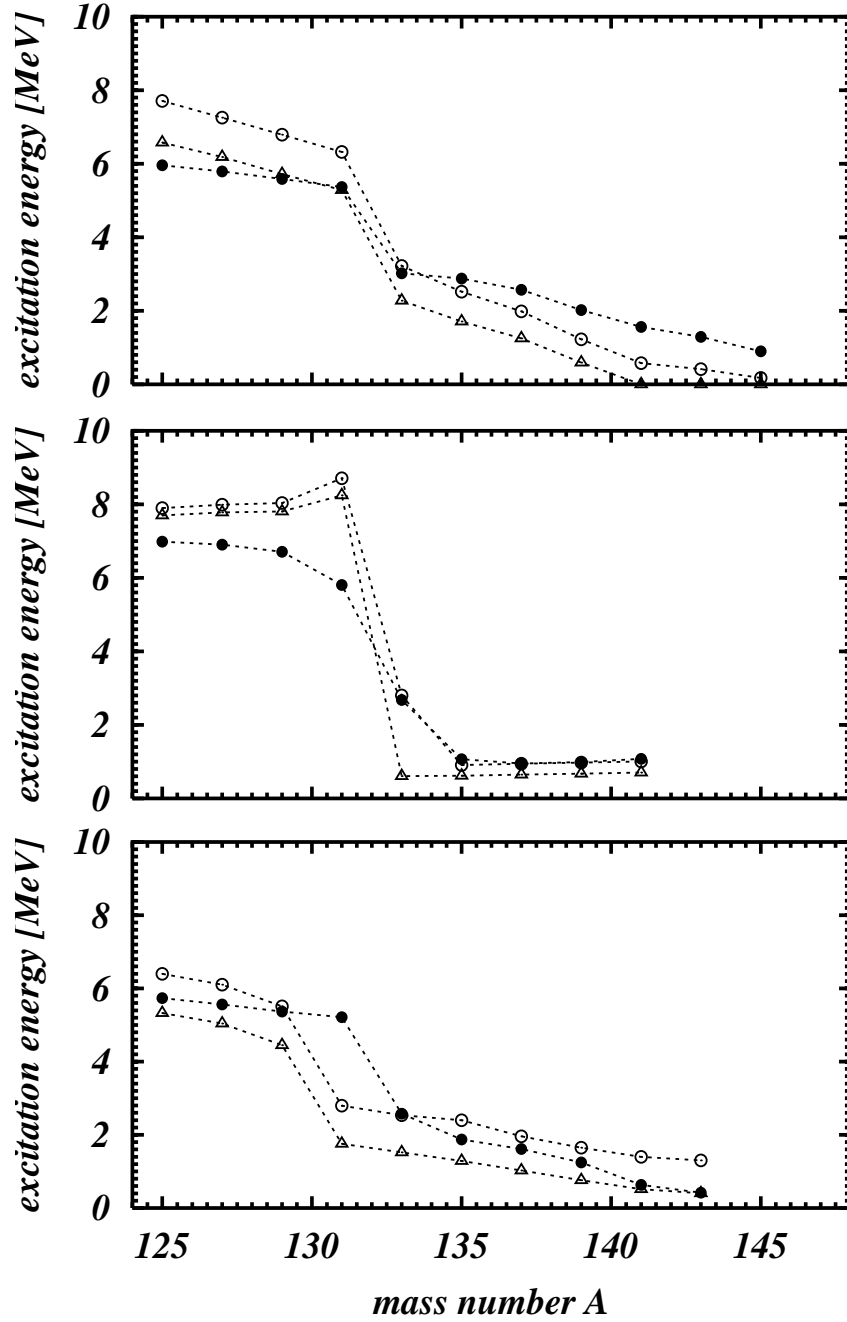
Figure 29: Dependence of level energies on mass number for even-odd Sn isotopes calculated in the Hartree-Fock-Bogolyubov model (HFB) (upper panel), in the Relativistic Mean Field approach (RMF) (middle panel) and in the Finite Range Droplet Model (FRDM) (lower panel). The $1/2^-$ state (open circles), the $3/2^-$ state (triangles) and the calculated neutron separation energy (full circles) are shown. The lines are drawn to guide the eye. These are adapted from the Figs. 10–12 of [276].
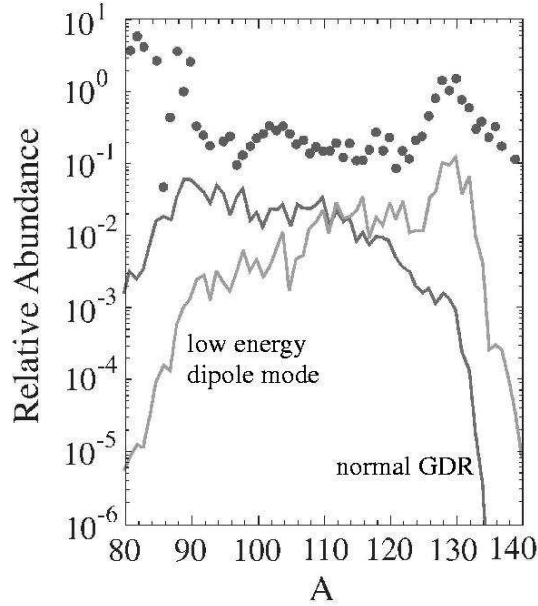
Figure 30: The measured and calculated abundances of nuclei are compared with each other. The dots show the measured abundance which are compared to the one of a calculation including a low energy dipole mode and one with a normal GDR mode. The presence of a low energy GDR leads to higher abundances for larger $A$ (lighter curve), whereas the one with a standard GDR mode has a higher abundance at lower $A$ (darker curve) This is Fig. 24 of [4], which is an adaption from [277].

The investigated models yield capture cross sections sometimes differing by orders of magnitude. The $A$-dependence of level energies and neutron separation energies is illustrated by comparing Figs 10–12 of [276], shown in Fig. 29.

The dependence of the level energies and neutron separation energies on various theoretical models (HFB, RMFT and FRDM) can strikingly be noticed there. This may also lead to differences in the predicted astrophysical $r$-process paths. Because of the low level densities, the compound nucleus model may not be applicable.

The dependence of the $r$-process abundance on nuclear properties and astrophysical conditions is investigated in [277]. The influence of the normal GDR and a GDR, which includes low energy dipole contributions, is strikingly summarized in Fig. 30. Specifically the possible existence of a low-enery $E1$ pigmy resonance is studied. There can also be a problem with the application of the statistical (Hauser-Feshbach) model to neutron rich nuclei: since the number of available resonance states may not be large enough for the application of this model, there could be a possible overestimate of the statistical (Hauser-Feshbach) predictions for resonance-deficient nuclei. The influence of nuclear structure properties on the $r$-process abundance distributions is shown in Fig. 6 of [277] for the astrophysical scenarios $T = 1.0 \times 10^9$ K, $N_n = 10^{20}$ cm$^{-3}$, $\tau = 2.4$ s and $T = 1.5 \times 10^9$ K, $N_n = 10^{28}$ cm$^{-3}$ and $\tau = 0.3$ s, where $N_n$ is the neutron density and $\tau$ the irradiation time. We recall that the astrophysical site of the $r$-process is still under debate. From this study it can be concluded that [277] *"there is an urgent need to carry on investigating theoretically as well as experimentally, the radiative neutron captures by exotic nuclei in order to improve our understanding of the r-process nucleosynthesis."*

In such a situation, the Coulomb dissociation can be a very useful tool to obtain information on $(n,\gamma)$-reaction cross sections on unstable nuclei, where direct measurements cannot be done. Of course, one cannot and need not study the capture cross section on all the nuclei involved; there will be some key reactions of nuclei close to magic numbers. It was proposed in [278] to use the Coulomb dissociation method to obtain information about (n,$\gamma$) reaction cross sections, using nuclei like $^{124}$Mo, $^{126}$Ru, $^{128}$Pd

and $^{130}$Cd as projectiles.

Since the flux of equivalent photons has essentially a $1/\omega$ dependence, low neutron thresholds are favourable for the Coulomb dissociation method. The optimum choice of beam energy is an important issue. It will depend essentially on the actual neutron binding energy. There is a factor of $(c/v)^2$ on the photon flux (see Eq. (20)) favoring the low beam velocities. On the other hand, the beam energy should not be so low that higher order effects become important (the strength paramer $\chi$ has an $1/v$-dependence, see Eq. (12)) or that the adiabaticity criterion is not fulfilled (see Eq. (10)). Note that only information about the $(n,\gamma)$ capture reaction to the ground state is possible with the Coulomb dissociation method. The situation is reminiscent of the loosely bound neutron-rich light nuclei, like $^{11}$Be, $^{11}$Li and $^{19}$C, which were discussed in Sec. 6. We recall that it was possible to determine the neutron binding energy of $^{19}$C from the shape of the low-lying $E1$ strength distribution, see [66] or Sec. 6. The relevant level densities are low, which is also favourable for the Coulomb dissociation method. To first order Coulomb dissociation probabilities are independent of the mass of the core (the recoil is proportional to $1/A$, but the Coulomb force is proportional to $Z$, see Eqs. (43) and (48)), so one can expect that the Coulomb dissociation method works essentially in a quite similar way as for the light ions like $^{11}Be$, or $^{15,17,19}C$.

In [13] the $1^{st}$ and $2^{nd}$ order Coulomb excitation amplitudes are given analytically in a zero range model for the neutron-core interaction (see also Sec. 3). We propose to use this handy formalism to assess, how far one can go down in beam energy and still obtain meaningful results with the Coulomb dissociation method, i.e., where the $1^{st}$ order amplitude can still be extracted experimentally without being too much disturbed by corrections due to higher orders. For radioactive beam facilities, like ISOL or SPIRAL, the maximum beam energy is an important question for possible Coulomb dissociation experiments. (For Coulomb dissociation with two charged fragments in the final state, like in the $^8$B $\rightarrow$ $^7$Be$+p$ experiment with a 26 MeV $^8$B beam [259] it seems to be impossible to obtain such a simple analytical formula and one should resort to the more involved approaches mentioned in Sec. 3.)

There is also another aspect: the radiative neutron capture by neutron rich nuclei at astrophysical energies is given by the low energy tail of the $E1$ strength. Standard values for the Lorentz parameters of the GDR are normally used. The possible existence of a low energy $E1$ pigmy resonance can strongly influence this picture, see [277]. Coulomb dissociation is *the* tool to study this question experimentally; we refer to our discussion of the light ions in Sec. 6. Especially, at the GSI the dipole response of the oxygen isotopes has been studied [189]. It will be very interesting to see the corresponding results for the (medium) heavy nuclei.

With the new radioactive beam facilities (either fragment separator or ISOL-type facilities) some of the nuclei far off the valley of stability, which are relevant for the $r$-process, can be produced. An impression of the future possibilities can be obtained, e.g., from Fig. 2 p.10 of [4]. In the chart of nuclides the production rates predicted for RIA can be seen, along with a line which indicates the $r$-process path. The rates for the future accelerator at the GSI are given in Fig 1.17, p. 106 and on p. 156 in [3].

The estimated minimum intensities of high-energy secondary high energy beams necessary for a certain type of reaction studies are given in Table 1.2, p. 125 of [3]. For Coulomb breakup a rate of the order of $10^3$ ions/$s$ is given as a rough general estimate.

## 8.2 *Two-Particle Capture Reactions and Cross Sections Relevant for the rp-Process*

A new field of application of the Coulomb dissociation method can be two particle capture reactions of the type

$$A + p_1 + p_2 \rightarrow B + \gamma. \tag{118}$$

The most famous reaction of this type is certainly the triple $\alpha$ capture reaction leading, via an $^8$Be unstable state, to a resonance in $^{12}$C, which was predicted by Hoyle [279]. Evidently, such a type of

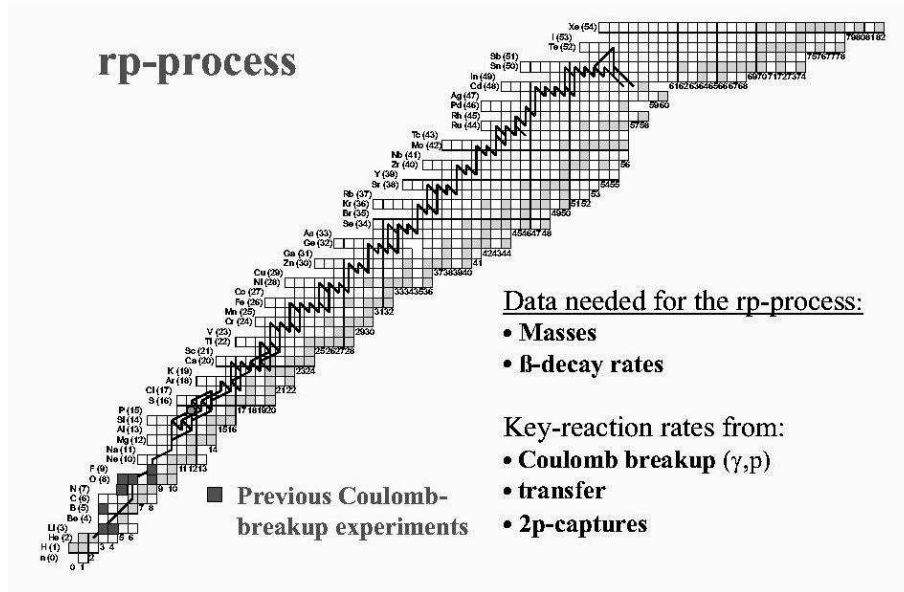Figure 31: The $rp$-process path, including $2p$-captures, for temperatures of $1.9\times10^9$K and densities of $10^6 gcm^{-3}$ [285]. Also shown are stable nuclei and the position of the proton-drip line. This is Fig. 1.14 of [3].

reaction cannot be studied in a direct way in the laboratory. Sometimes this is not necessary, when the relevant information about resonances involved can be obtained by other means (transfer reactions, etc.), like in the triple $\alpha$-process. Another way to investigate such processes can be the Coulomb dissociation method, where the time reversed process $\gamma + B(\text{gs}) \rightarrow A + p_1 + p_2$ is studied using equivalent photons. Let us give some examples:

Two-neutron capture reactions in supernovae neutrino bubbles are studied in Ref. [280]. In the case of a high neutron abundance, a sequence of two-neutron capture reactions, ${}^4\text{He}(2n,\gamma){}^6\text{He}(2n,\gamma){}^8\text{He}$ can bridge the $A = 5$ and $8$ gaps. The ${}^6\text{He}$ and ${}^8\text{He}$ nuclei may be formed preferentially by two-step resonant processes through their broad $2^+$ first excited states [280]. Dedicated Coulomb dissociation experiments can be useful. The ${}^6\text{He}$ Coulomb dissociation is measured in [188]. Astrophysical aspects related to the two-neutron capture on ${}^4\text{He}$ are also discussed there. One can envisage two mechanisms: a nonresonant two-neutron capture and a capture with an unstable ${}^5\text{He}$ resonant intermediate state [281]. A dedicated Coulomb dissociation experiment could shed light on the question which mechanism is dominant.

Another key reaction can be the ${}^4\text{He}(\alpha n,\gamma){}^9\text{Be}$ reaction [280]. The ${}^9\text{Be}(\gamma,n)$ reaction has been studied directly (see Ref. [282]) and the low energy $s_{\frac{1}{2}}$ resonance is clearly established. Despite this, a ${}^9\text{Be}$ Coulomb dissociation experiment could be rewarding (see also Ref. [178]). Other useful information is obtained from $(e, e')$ and $(p, p')$ reactions on ${}^9\text{Be}$ [283]. Recently the photodissociation of ${}^9\text{Be}$ was studied by [284, 203], as was already mentioned.

Another important application is for reactions relevant for the $rp$-process: neutron-deficient nuclei close to the proton drip line play an important role in a variety of astrophysical scenarios such as Nova explosions, $X$-ray bursts, or $X$-ray pulsars. In those scenarios, hydrogen is burnt via a sequence of rapid proton captures and $\beta^+$-decays close to the proton drip line (called the $rp$-process). The impact and perspectives of radioactive beam experiments for the $rp$-process was recently discussed by Wiescher and Schatz [286]. It is noted there that $(p, \gamma)$ capture experiments become increasingly difficult with increasing charge $Z$, and Coulomb breakup, Coulomb excitation and particle transfer reactions in inverse kinematics become promising indirect methods to access the relevant information. We recall that $(p, \gamma)$ reactions on light nuclei were studied by the Coulomb dissociation of ${}^8\text{B}$, ${}^{12}\text{N}$, and ${}^{14}\text{O}$ radioactive

beams, see Sec. 7. For further discussion we refer to [3] p. 98ff and especially Fig. 1.14, shown here as Fig. 31.

In the $rp$-process, two-proton capture reactions can bridge the waiting points [287, 288, 285]. From the $^{15}\mathrm{O}(2p,\gamma)^{17}\mathrm{Ne}$, $^{18}\mathrm{Ne}(2p,\gamma)^{20}\mathrm{Mg}$ and $^{38}\mathrm{Ca}(2p,\gamma)^{40}\mathrm{Ti}$ reactions considered in Ref. [288], the latter can act as an efficient reaction link at conditions typical for $X$-ray bursts on neutron stars. A $^{40}\mathrm{Ti} \rightarrow p+p+^{38}\mathrm{Ca}$ Coulomb dissociation experiment should be feasible. The decay with two protons is expected to be sequential rather than correlated ("$^2\mathrm{He}$"-emission, $2p$-radioactivity). The relevant resonances are listed in Table XII of Ref. [288]. In Ref. [285] it is found that in $X$-ray bursts $2p$-capture reactions accelerate the reaction flow into the $Z \geq 36$ region considerably. In Table 1 of Ref. [285] nuclei, on which $2p$-capture reactions may occur, are listed; the final nuclei are $^{68}\mathrm{Se}$, $^{72}\mathrm{Kr}$, $^{76}\mathrm{Sr}$, $^{80}\mathrm{Zr}$, $^{84}\mathrm{Mo}$, $^{88}\mathrm{Ru}$, $^{92}\mathrm{Pd}$ and $^{96}\mathrm{Cd}$ (see also Fig. 8 of Ref. [287]). It is proposed to study the Coulomb dissociation of these nuclei in order to obtain more direct insight into the $2p$-capture process.

# 9   Conclusions

Peripheral collisions of medium and high energy nuclei (stable or radioactive) passing each other at distances beyond nuclear contact and thus dominated by electromagnetic interactions are important tools of nuclear physics research. The intense source of quasi-real (or equivalent) photons present in such collisions has opened a wide horizon of related problems and new experimental possibilities especially for the present and forthcoming radioactive beam facilities to investigate efficiently photo-interactions with nuclei (single- and multiphoton excitations and electromagnetic dissociation). We have described the basic points of the theory, which rests on very solid grounds: quantum mechanics and the electromagnetic interaction. Problems in the technical description of the process, problems due to nuclear interactions between the ions are identified and can be considered as well understood. Modern computational methods are of great help.

It has sometimes been said about the Coulomb dissociation method, see e.g. [249], that "it is difficult to determine all of their important systematic errors". Certainly, there are systematic effects which one has to take carefully into account. This is the task of nuclear reaction theory which is described in this review. We hope that it has become clear that these effects are well identified and can be calculated. After all, it is essentially the electromagnetic interaction which enters, and there is QED, the best theory we have. We hope that we have shown here that the view expressed in [249] is overly pessimistic.

Certainly, there are also experimental problems: one of them is the accurate determination of the relative energy of the fragments. Due to the influence of the Coulomb barrier, the astrophysical $S$-factors depend very sensitively on this quantity. However, we have to leave such questions to our experimental colleagues.

After these theoretical considerations we discussed experimental results in the field of nuclear structure and nuclear astrophysics. Due to the good theoretical understanding of the electromagnetic excitation, unambiguous conclusions have been drawn from them. Let us mention here the discovery of low lying $E1$ strength in neutron-rich nuclei and the determination of astrophysical $S$-factors of radiative capture processes, like $^7\mathrm{Be}(\mathrm{p},\gamma)^8\mathrm{B}$.

Fast moving heavy nuclei are a bright source of equivalent photons, and we expect a bright future of this subject, especially at the future rare isotope facilities. Coulomb excitation and dissociation is an opportunity to study the interaction of exotic nuclei with photons. It is unique, until electron-ion colliders will become available as a complementary tool.

# 10 Acknowledgments

# A    The Electromagnetic Interaction: the Condition of No Nuclear Contact and Expansion into Electromagnetic Multipoles

Although the following is quite familiar, it seems of interest to deal with some basic physical points which arise in the special case of electromagnetic excitation in nucleus-nucleus collisions. We especially wish to clarify the difference of it to the treatment of electron scattering, which is perhaps even more familiar to most readers.

As was already emphasized, in hadron-hadron collisions the important condition for the dominance of the electromagnetic interaction is $r < r_p$, i.e., there are two *spatially separated* charge distributions, see Fig. 1. In this way strong interactions are avoided, there is only the electromagnetic interaction between the ions and this simple reaction mechanism is not spoiled by nuclear effects. It is useful to take the photon propagator in coordinate space $\vec{r}$ and only Fourier transformed with respect to $t$, i.e. we consider $D_{\mu\nu}(\vec{r}, \omega)$; in this representation the condition of *no nuclear contact* ($r < r_p$) can be implemented easily.

The condition $r < r_p$ is used in the semiclassical approach here, where the projectile on the orbit $\vec{r}_p(t)$ does not overlap with the target. In a distorted wave Born approximation (DWBA) with, e.g., only Coulomb waves (CWBA) the *no nuclear contact* condition $r < r_p$ is also useful: for low collision energies, where the classical turning point is outside the target nucleus, the Coulomb wave function is very small inside the target nucleus and its contribution can be neglected.

As we will see below, the information about the hadronic system to be studied can be expressed in terms of electromagnetic matrix-elements *at the photon point.*

The interaction of two currents is a standard problem in electrodynamics and QED. The electromagnetic field is described by the vector potential $A_\mu$ and its interaction as $M_{int} = \int d^4x \, j \cdot A$. We define the scalar product of two four-vectors as $a \cdot b = g^{\mu\nu} a_\mu b_\nu = a_\mu a^\mu = a_0 b_0 - \vec{a} \cdot \vec{b}$, where we use the metric $g = \text{diagonal}(1, -1, -1, -1)$ throughout this article. In our case the vector potential $A_\mu$ is generated by the moving charge distribution $J_\mu$. It is given by

$$A_\mu(x) = \int d^4x' D_{\mu\nu}(x, x') J_\nu(x'). \tag{119}$$

The Fourier transform of the current distribution is defined as

$$j_\mu(x) = \frac{1}{(2\pi)^4} \int d^4k \exp(ik \cdot x)\hat{j}_\mu(k) \tag{120}$$

$$\hat{j}_\mu(k) = \int d^4x \exp(-ik \cdot x) j_\mu(x), \tag{121}$$

with the notation $d^4k = dk_0 d^3k$ and $k = (k_0 = \omega, \vec{k})$. We have current conservation, which is expressed as

$$\partial_\mu j^\mu = \partial j_0 / \partial x_0 - \vec{\nabla} \cdot \vec{j} = 0, \tag{122}$$

or $k \cdot \hat{j} = 0$ in momentum space.

The electromagnetic interaction between two current distributions $j_1$ and $j_2$ can be written as

$$M_{int} = \iint d^4x \, d^4x' \, j_{1\mu}(x) D_{\mu\nu}(x - x') j_{2\nu}(x'). \tag{123}$$

Alternatively it is given in terms of the Fourier transform of the propagator

$$D_{\mu\nu}(k) = \int d^4x \exp(-ikx) D_{\mu\nu}(x) \tag{124}$$

$$\tag{125}$$

and the currents (see above) as

$$M_{int} = \frac{1}{(2\pi)^4} \int d^4k \, \hat{j}_{1\mu}(-k) D_{\mu\nu}(k) \hat{j}_{2\nu}(k). \tag{126}$$

In the Born approximation which is often used, e.g., in lepton scattering, see Fig. 2, Eq. (126) simplifies as we can use plane waves for initial and final states. We consider the reaction $1 + 2 \to 1' + 2'$, with the four-momenta $p_1 + p_2 = p_1' + p_2'$. The momentum transfer $q$ is given by $q = p_1 - p_1' = -p_2 + p_2'$. The transition currents can be written as $j_{1\mu}(x) = a_\mu \exp(i(p_1 - p_1')x)$ and $j_{2\mu} = b_\mu \exp(i(p_2 - p_2')x')$ where $a_\mu$ and $b_\mu$ are independent of $x$, $x'$. With this we can write $M_{int}$ as

$$M_{int} = (2\pi)^4 \delta(p_1 + p_2 - p_1' - p_2') a_\mu D_{\mu\nu}(q) b_\nu. \tag{127}$$

The fundamental property of the electromagnetic interaction is *gauge invariance:* We can add to any vector potential $A_\mu$ a gradient term of the form $\partial_\mu \chi(x)$. Due to current conservation $\partial^\mu j_\mu = 0$ this leaves the electromagnetic interaction $M_{int}$ invariant. Various gauges exist also for $D_{\mu\nu}$, corresponding to various gauges of $A_\mu$. E.g., [90] gives a very instructive discussion on the application of different gauges, see also [289] p. 109ff. For interesting historical remarks (e.g., that the Lorentz condition is originally due to Lorenz) see [290]. A rather general covariant form of the propagator is given by the *linear lambda gauge*

$$D_{\mu\nu}(k) = \frac{4\pi}{k^2 + i\epsilon} \left( g_{\mu\nu} + \lambda \frac{k_\mu k_\nu}{k^2} \right), \tag{128}$$

where $\lambda$ is an arbitrary parameter.

In the Coulomb gauge (characterized by $\operatorname{div}\vec{A} = 0$) one has explicitly [90]

$$
\begin{aligned}
D_{00} &= -\frac{4\pi}{\vec{k}^2} \\
D_{0i} &= D_{i0} = 0 \\
D_{il} &= -\frac{4\pi}{k^2} \left( \delta_{il} - \frac{k_i k_l}{\vec{k}^2} \right),
\end{aligned}
\tag{129}
$$

(with $k^2 = \omega^2 - \vec{k}^2$ and $\omega = k_0$) where $i, l = 1, 2, 3$ denote the spatial indices. (We leave out the $+i\epsilon$ for simplicity.) In this gauge we have

$$a_\mu D_{\mu\nu}(k) b_\nu = 4\pi \left( \frac{-a_0 b_0}{\vec{k}^2} - \frac{\vec{a} \cdot \vec{b}}{k^2} + \frac{(\vec{k} \cdot \vec{a})(\vec{k} \cdot \vec{b})}{k^2 \vec{k}^2} \right). \tag{130}$$

Using current conservation we can rewrite this as

$$
\begin{aligned}
&= 4\pi \left[ -\frac{\vec{a} \cdot \vec{b}}{k^2} - \frac{a_0 b_0}{\vec{k}^2} \left( 1 - \frac{k_0^2}{k^2} \right) \right] \\
&= \frac{4\pi}{k^2} \left( a_0 b_0 - \vec{a} \cdot \vec{b} \right) = \frac{4\pi}{k^2} a \cdot b.
\end{aligned}
\tag{131}
$$

Due to gauge invariance one obtains the same result in the Coulomb gauge, as well as in the Feynman gauge ($\lambda = 0$), Lorentz gauge ($\lambda = -1$) or in any other gauge, as it should be.

In the general case, which is relevant for electromagnetic excitation with nuclei, the transition currents are not associated with a definite momentum transfer $q$. There is an integration over the momentum transfer $k$, see Eq. (126) above. In the static limit (no retardation, corresponding to $k_0 = \omega = 0$) one gets

$$
\begin{aligned}
M_{int} &= \frac{1}{(2\pi)^4} \int d^4k \left( \frac{\hat{j}_{1,0}(-k)\hat{j}_{2,0}(k) - \vec{\hat{j}}_1(-k) \cdot \vec{\hat{j}}_2(k)}{\vec{k}^2} \right) \\
&= \int dt \iint d^3r_1 d^3r_2 \frac{\rho_1(r_1)\rho_2(r_2) - \vec{j}_1(r_1) \cdot \vec{j}_2(r_2)/c^2}{|\vec{r}_1 - \vec{r}_2|} \\
&= \int dt \, W(1,2),
\end{aligned}
\tag{132}
$$

which corresponds to Eq. (1) in the main text, the starting point for the nonrelativistic Coulomb excitation in [1], see also p.84 of [21].

Now we want to indicate how to express the interaction in terms of the electromagnetic multipole matrix-elements of the charge-current distribution. (The details can be found in the textbooks, see, e.g., [21].) This is possible for non-overlapping charge distributions. We only deal with the monopole-multipole part of the interaction, see Fig. 1. Then we can assume that the charge $Z_p$ is a point charge. The static case is well known, the relativistic case can be handled as well.

In [21] the Lorentz condition is used for the propagator. See especially Sec. 6.1 Eq. (8) and (22) and Sec. 6.2 in that reference. We do not give here all the details of the multipole expansion for interacting charges and currents, see, e.g., [21, 30, 291]. Let us emphasize the main points related to the question of *penetrating* (like in the plane wave case) versus spatially separated charge distributions. The propagator ("Green's function") is expanded into multipoles in analogy to Eq. (4) (see also, e.g., [21], Eq. (23)) [4]

$$
\frac{\exp(i\omega|\vec{r} - \vec{r}_p|)}{|\vec{r} - \vec{r}_p|} = 4\pi i\omega \sum_{LM} j_L(\omega r_<) h_L^{(1)}(\omega r_>) Y_{LM}^*(\hat{r}_<) Y_{LM}(\hat{r}_>),
\tag{133}
$$

where $r_<$ and $r_>$ are the smaller and larger of $r_p$ and r respectively. In the case of spatially separated charge distributions we always have $r_< = r$ and $r_> = r_p$.

This is a generalization of the multipole expansion of the static Coulomb interaction [5],

$$
\frac{1}{|\vec{r} - \vec{r}_p|} = 4\pi \sum_{LM} \frac{1}{2L+1} \frac{r_<^L}{r_>^{L+1}} Y_{LM}^*(\hat{r}_<) Y_{LM}(\hat{r}_>),
\tag{134}
$$

which can be obtained from Eq. (133) by performing the limit $\omega \to 0$ and using the expansion

$$
j_L(x) = \frac{x^L}{(2L+1)!!}, \quad \text{and} \quad h_L^{(1)}(x) = -i\frac{(2L-1)!!}{x^{L+1}}
\tag{135}
$$

---

[4] We follow here the convention of [92] in the definition of the spherical Bessel function, which is $h_L^{(1)}(z) = j_L(z) + iy_L(z)$, where $j_L$ and $y_L$ are the (regular) spherical Bessel and the (irregular) Neumann function. This is different than the one used in [20].

[5] For $L = 0$ we have a term proportional to $1/r_>$. This term gives a contribution to nuclear excitation only if $r > r_p$. Monopole transitions can occur, e.g., in the case of internal conversion, due to the penetration of the electron charge cloud into the nucleus, see, e.g., [292]. In this case we have $r > r_e$, where $r_e$ and $r$ denote the electronic and nuclear variables, respectively. Usually, the electron cloud is outside of the nucleus, i.e. $r < r_e$ and the probability of internal conversion is proportional to the $B(\pi, \lambda)$-value of the corresponding $\gamma$-transition. This is in close analogy to the Coulomb excitation discussed here.

for small values of the argument $x = \omega r$.

On the other hand one can Fourier transform the (retarded) interaction into momentum space by means of the Bethe integral

$$\frac{\exp(i\omega|\vec{r} - \vec{r_p}|)}{|\vec{r} - \vec{r_p}|} = \frac{1}{2\pi^2} \int d^3k \frac{\exp(i\vec{k} \cdot (\vec{r} - \vec{r_p}))}{k^2 - \omega^2 - i\epsilon}, \tag{136}$$

with $\epsilon$ being an infinitesimally small positive number. Using the plane-wave expansion of $\exp(i\vec{k} \cdot \vec{r})$ into multipoles, integrating over the angular part of $\vec{k}$, and making use of the orthogonality of the spherical harmonics we obtain the formula

$$\int_0^\infty dk k^2 \frac{j_L(kr)j_L(kr_p)}{k^2 - \omega^2 - i\epsilon} = \frac{i\pi\omega}{2} j_L(\omega r_<)h_L^{(1)}(\omega r_>). \tag{137}$$

In the static limit $\omega = 0$ one obtains

$$\int_0^\infty dk j_L(kr)j_L(kr_p) = \frac{\pi}{2(2L + 1)} \frac{r_<^L}{r_>^{L+1}}. \tag{138}$$

In [2] the Coulomb gauge is used to derive the full expression for first order Coulomb excitation, see their Sec. II B.1. The result in this approach is the same as in [21], where the Lorentz gauge is used; this must be so due to gauge invariance. It is important to note that the electromagnetic matrix-elements *at the photon point* (see Eqs. (141) and (142) below) enter in the expression for the Coulomb excitation amplitude. In the approach using the Coulomb gauge one also needs the equation (Eq. (2.B.11) in [2])

$$\int_0^\infty dk \frac{j_L(kr)j_L(kr_p)}{k^2 - \omega^2 - i\epsilon} = \frac{i\pi}{2\omega} j_L(\omega r_<)h_L^{(1)}(\omega r_>) - \frac{\pi}{2(2L + 1)\omega^2} \frac{r_<^L}{r_>^{L+1}}, \tag{139}$$

which can either be found in [293] or follows from the identity

$$\frac{k^2}{\omega^2(k^2 - \omega^2)} - \frac{1}{\omega^2} = \frac{1}{k^2 - \omega^2}, \tag{140}$$

together with the two expressions Eqs. (137) and Eqs. (138) above.

These expressions are now used in the calculation of the matrixelements for electromagnetic excitation, either in a semiclassical or in a quantum-mechanical framework (for all the necessary details on the multipole expansion of the electromagnetic field and on vector spherical harmonics see, e.g., [2, 21, 171]). A good discussion of vector spherical harmonics and electromagnetic interactions is also given in [294]. One clearly sees how the separation into the $r$ and $r_p$ parts comes about when we can use the no penetration condition $r_< = r$ and $r_> = r_p$. The expressions factorize naturally into an orbital part (associated with $h_L^{(1)}(\omega r_p)$) and an electromagnetic matrixelement (associated with the $j_l(\omega r)$).

The Coulomb excitation amplitude is expressed in terms of the electromagnetic multipole moments, which are defined as (see, e.g., [2])

$$M(E\lambda\mu, q) = \frac{(2l + 1)!!}{q^{l+1}c(l + 1)} \int d^3r \vec{j} \cdot \vec{\nabla} \times \vec{L} \left( j_l(qr)Y_{lm}(\hat{r}) \right) \tag{141}$$

$$M(M\lambda\mu, q) = -i\frac{(2l + 1)!!}{q^l c(l + 1)} \int d^3r \vec{j}(\vec{r}) \cdot \vec{L} \left( j_l(qr)Y_{lm}(\hat{r}) \right), \tag{142}$$

with $\vec{L} = -i\vec{r} \times \vec{\nabla}$ (see Eqs. (II.1.3), (II.1.4) of [1]).

One can see that the integration over the momenta $k$ (see Eqs. (137) and (138)) conspires in such a way that only the electromagnetic matrixelements at the photon point $k = \omega$ (or the long-wave-length expression, respectively) appear.

An even more intriguing version of an addition theorem to expand the electromagnetic field into multipoles and into $r_<$ and $r_>$ parts is used by Winther and Alder [24] to handle the semiclassic relativistic straight line case. In this case the electromagnetic potential is described by the Liénard-Wiechert potential

$$\phi(\vec{r'}, t) = \frac{Z_p e \gamma}{\sqrt{(b - x')^2 + y'^2 + \gamma^2(z' - vt)^2}}, \quad \vec{A}(\vec{r'}, t) = \frac{\vec{v}}{c} \phi(\vec{r'}, t), \tag{143}$$

which can be Fourier transformed with respect to $t$ as

$$\phi(\vec{r'}, \omega) = \frac{2Z_p e}{v} \exp\left(i \frac{\omega}{v} z'\right) K_0\left(\frac{\omega}{v\gamma} \sqrt{(b - x')^2 + y'^2}\right). \tag{144}$$

One expands this expression into multipole components

$$\phi(\vec{r'}, \omega) = \sum_{\lambda\mu} W_{\lambda\mu}(r', \omega) Y_{\lambda\mu}^*(\hat{r'}). \tag{145}$$

By the use of the Graf addition theorem (see Eq. (9.1.79) of [92]) an analytic expression for $W_{\lambda\mu}$ is obtained. Again a complete separation of the excitation probability in electromagnetic multipole moments and quantities which describe the projectile motion is reached, see Eq. (23) of Sec. 2.

This is to be contrasted to the plane wave case (e.g. commonly used in inelastic electron scattering). In this case there is a definite (space-like) momentum transfer $q = p_1 - p_1'$, see Fig. 2. By varying $q$ one can probe the structure of an object in a way not possible with real photons. An important example is deep inelastic electron scattering.

For small values of $-q^2$ we can think of the exchanged photon as quasireal. For small energy loss and small angle scattering we have the kinematical relation $-q^2 = q_\perp^2 + (\omega/(\gamma v))^2$. As the main contribution to the total cross section comes from small values of $-q^2$ (where the photon propagator becomes very large), this cross section is dominated by values of $-q^2 \approx (\omega/(\gamma v))^2$, which, especially for large values of $\gamma$, can be quite small and therefore $q^2 \approx 0$ (*quasireal*) photons dominate in this case as well.

This kind of equivalent photon approximation is different from the one discussed mainly in this review: here we have used the semiclassical approximation, as it is appropriate for the nucleus-nucleus collisions. This leads to impact parameter dependent equivalent photon spectra. These spectra can be integrated over the impact parameters $b > R_{min}$. Still, the plane-wave and the semiclassical approach have some qualitative features in common, like the logarithmic rise of the photon number with the Lorentz factor $\gamma$. As the name implies, the EPA is an *approximation*, with certain ranges of validity, different for the semiclassical and plane wave approaches, see, e.g., [295] and [296]. In [297] experimental data for electromagnetic excitation with heavy ions were analysed using the EPA spectrum of [296]. In contrast to semiclassical calculations, systematically lower cross sections are obtained that cannot reproduce the experimental results.

How the EPA works and where its limits are, is explicitly studied, e.g., in the case of $\bar{H}^0$ production, [298, 299, 300]; we can only refer to these papers here. The PWBA in the Coulomb gauge is also studied very lucidly in a classic paper by Fano [301]; a more recent work is [302].

# References

[1] K. Alder and A. Winther, *Electromagnetic excitation*, North-Holland, Amsterdam, 1975.

[2] K. Alder, A. Bohr, T. Huus, B. Mottelson, and A. Winther, *Rev. Mod. Phys.* 28 (1956) 432.

[3] H. H. Gutbrod et al., editors, *An International Accelerator Facility for Beams of Ions and an-tiprotons*, Gesellschaft für Schwerionenforschung, Darmstadt, 2001.

[4] National Superconducting Cyclotron Laboratory, Scientific Opportunities with Fast Fragmentation Beams from RIA, available at http://www.nscl.msu.edu/research/ria/whitepaper.pdf, 2000.

[5] National Superconducting Cylcotron Laboratory, Workshops and White Papers, see webpage at http://www.nscl.msu.edu/future/ria/process/whitepapers/.

[6] RIKEN RI Beam Factory, see webpage at http://www.rarf.riken.go.jp/ribf/.

[7] C. A. Bertulani and G. Baur, *Phys. Rep.* 163 (1988) 299.

[8] J. Dreitlein and H. Primakoff, *Phys. Rev.* 125 (1962) 1671.

[9] I. Y. Pomeranchuck and I. M. Shmushkevich, *Nucl. Phys.* 23 (1961) 452.

[10] H. Emling, *Prog. Part. Nucl. Phys.* 33 (1994) 729.

[11] T. Aumann, P. F. Bortignon, and H. Emling, *Annu. Rev. Nucl. Part. Sci.* 48 (1998) 351.

[12] G. Baur and C. Bertulani, *Phys. Lett. B* 174 (1986) 23.

[13] S. Typel and G. Baur, *Nucl. Phys. A* 573 (1994) 486.

[14] S. Typel and G. Baur, *Phys. Rev. C* 50 (1994) 2104.

[15] S. Typel, H. H. Wolter, and G. Baur, *Nucl. Phys. A* 613 (1997) 147.

[16] G. Baur, C. A. Bertulani, and H. Rebel, *Nucl. Phys. A* 458 (1986) 188.

[17] G. Baur and H. Rebel, *J. Phys. G* 20 (1994) 1.

[18] G. Baur and H. Rebel, *Ann. Rev. Nucl. Part. Sci.* 46 (1996) 321.

[19] G. Baur, Photon-Hadron, Photon-Photon Interactions and Nuclear Astrophysics at Heavy Ion Accelerators, lecture held at the "Europäisches Graduiertenkolleg Basel-Tübingen", April 8–12, 2002, see webpage at http://www.physik.unibas.ch/eurograd/Vorlesung/Baur/.

[20] A. Messiah, *Quantenmechanik*, volume 2, Walter de Gruyter, Berlin, New York, 1985.

[21] J. M. Eisenberg and W. Greiner, *Nuclear Theory*, volume 2: Excitation Mechanisms of the Nucleus, North-Holland, Amsterdam, Oxford, New York, Tokyo, third revised edition edition, 1988.

[22] H. Esbensen and G. F. Bertsch, *Nucl. Phys. A* 706 (2002) 477.

[23] H. Esbensen and C. A. Bertulani, *Phys. Rev. C* 65 (2002) 024605.

[24] A. Winther and K. Alder, *Nucl. Phys. A* 319 (1979) 518.

[25] E. Fermi, *Z. Phys.* 29 (1924) 315.

[26] E. Fermi, *Nuovo Cimento* 2 (1925) 143.

[27] E. Fermi, in *Proceedings of the workshop on "Electromagnetic Probes of Fundamental Physics", Erice, Italy, Oct. 16–21, 2001*, edited by W. Marciano and S. White, p. 243, Singapore, 2003, World Scientific, translated from the Italian by M. Gallinaro and S. White, available as e-print hep-th/0205086.

[28] C. F. Weizsäcker, *Z. Phys.* 88 (1934) 612.

[29] E. J. Williams, *Phys. Rev.* 45 (1934) 729.

[30] J. D. Jackson, *Classical Electrodynamics*, John Wiley, New York, 1975.

[31] C. E. Aguiar, A. N. F. Aleixo, and C. A. Bertulani, *Phys. Rev. C* 42 (1990) 2180.

[32] A. N. F. Aleixo and C. A. Bertulani, *Nucl. Phys. A* 505 (1989) 448.

[33] S. K. Charagi and S. K. Gupta, *Phys. Rev. C* 41 (1990) 1610.

[34] C. A. Bertulani, C. M. Campbell, and T. Glasmacher, *Computer Phys. Comm.* 152 (2003) 317, e-print nucl-th/0207035.

[35] C. A. Bertulani et al., Intermediate energy Coulomb excitation as a probe of nuclear structure at radioactive beam facilities, e-print nucl-th/0305001, 2003.

[36] N. Bohr, *Mat. Fys. Medd. Dan. Vid. Selsk.* 18 (1948) No. 8.

[37] A. Mündel and G. Baur, *Nucl. Phys. A* 609 (1996) 254.

[38] C. A. Bertulani and A. M. Nathan, *Nucl. Phys. A* 554 (1993) 158.

[39] H. A. Bethe and R. W. Jackiw, *Intermediate Quantum Mechanics*, Benjamin, New York, 1968.

[40] G. Baur, *Nucl. Phys. A* 531 (1991) 685.

[41] A. Aste et al., An eikonal approach to Coulomb corrections in quasielastic electron scattering on heavy nuclei, (in preparation), 2003.

[42] G. Baur et al., Multiphoton Exchange Processes in Ultra Peripheral Relativistic Heavy Ion Collisions, submitted to Nucl. Phys. A, 2003.

[43] M. Levy and J. Sucher, *Phys. Rev.* 186 (1969) 1656.

[44] F. Hayot and C. Itzykson, *Phys. Lett. B* 39 (1972) 521.

[45] P. Braun-Munzinger, Proposal 814 submitted to the AGS Program Committee, SUNY at Stony Brook, accepted 1985 (unpublished).

[46] E. Merzbacher, *Quantum Mechanics*, Wiley, New York, 2nd edition, 1970.

[47] R. J. Glauber, *Phys. Rev.* 131 (1963) 2766.

[48] J. R. Klauder and B.-S. Skagerstam, *Coherent states*, World Scientific, Singapore, 1985.

[49] C. A. Bertulani and G. Baur, *Nucl. Phys. A* 482 (1988) 313c.

[50] K. Boretzki et al., *Phys. Lett. B* 384 (1996) 30.

[51] J. Ritman et al., *Phys. Rev. Lett.* 70 (1993) 533.

[52] R. Schmidt et al., *Phys. Rev. Lett.* 70 (1993) 1767.

[53] C. A. Bertulani, in *Proceedings of the workshop on "Electromagnetic Probes of Fundamental Physics", Erice, Italy, Oct. 16–21, 2001*, edited by W. Marciano and S. White, p. 203, Singapore, 2003, World Scientific, available as e-print nucl-th/0201060.

[54] G. Baur, C. A. Bertulani, and D. Dolci, *Eur. Phys. J. A* 7 (2000) 55.

[55] J. Z. Gu and H. A. Weidenmüller, *Nucl. Phys. A* 690 (2001) 382.

[56] B. V. Carlson et al., *Ann. Phys.* 276 (1999) 111.

[57] B. V. Carlson et al., *Phys. Rev. C* 60 (1999) 014604.

[58] G. Baur and C. A. Bertulani, in *Proc. Int. School of Heavy Ion Physics, Oct. 12–22, 1986*, edited by R. A. Broglia and G. F. Bertsch, p. 343, Plenum Press, 1986.

[59] P. Chomaz and N. Frascaria, *Phys. Rep.* 252 (1995) 275.

[60] S. Mordechai and C. F. Moore, *Nature* 352 (1991) 393.

[61] V. S. Melezhik and D. Baye, *Phys. Rev. C* 59 (1999) 3232.

[62] H. Esbensen, G. F. Bertsch, and C. A. Bertulani, *Nucl. Phys. A* 581 (1995) 107.

[63] H. Utsunomia et al., *Nucl. Phys. A* 654 (1999) 928c.

[64] S. Typel and H. H. Wolter, *Z. Naturforsch.* 54a (1999) 63.

[65] S. Typel and G. Baur, *Phys. Rev. C* 64 (2001) 024601.

[66] T. Nakamura, *Phys. Rev. Lett.* 84 (1999) 1112.

[67] T. Nakamura, *Phys. Lett. B* 331 (1994) 296.

[68] J. A. Tostevin, in *2nd International Conference on Fission and Neutron Rich Nuclei, St. Andrews, Scotland, June 28 – July 2 1999*, edited by J. H. Hamilton et al., Singapore, 2000, World Scientific.

[69] J. A. Tostevin, S. Rugmai, and R. C. Johnson, *Phys. Rev. C* 57 (1998) 3225.

[70] J. Mortimer, I. J. Thompson, and J. A. Tostevin, *Phys. Rev. C* 65 (2002) 064619.

[71] T. Matsumoto et al., New treatment of breakup continuum in the method of continuum discretized coupled channels, submitted to Phys. Rev. C, available as e-print nucl-th/0302034, 2003.

[72] H. D. Marta et al., *Phys. Rev. C* 66 (2002) 024605.

[73] Y. Tokimoto et al., *Phys. Rev. C* 63 (2001) 035801.

[74] H. Esbensen and G. Bertsch, *Nucl. Phys. A* 600 (1996) 37.

[75] H. Esbensen and G. F. Bertsch, *Phys. Lett. B* 359 (1995) 13.

[76] N. Austern, *Direct Reaction Theory*, Wiley, New York, 1970.

[77] G. Baur and D. Trautmann, *Phys. Lett. B* 42 (1972) 31.

[78] L. Jarczyk et al., *Phys. Lett.* 39B (1972) 191.

[79] G. Baur et al., *Prog. Part. Nucl. Phys.* 46 (2001) 99.

[80] F. Ribycki and N. Austern, *Phys. Rev. C* 6 (1971) 1525.

[81] E. O. Alt, B. F. Igarziev, and A. M. Mukhamedzhanov, *Phys. Rev. Lett.* 90 (2003) 122701.

[82] G. Baur and D. Trautmann, *Nucl. Phys. A* 191 (1972) 321.

[83] A. Galonsky et al., $n - n$ Correlations with exotic nuclei, Preprint MSUCL-951, 1994, available from www.nscl.msu.edu.

[84] G. Baur, M. Pauli, and D. Trautmann, *Nucl. Phys. A* 224 (1974) 477.

[85] G. Baur, C. A. Bertulani, and D. M. Kalassa, *Nucl. Phys. A* 550 (1995) 107.

[86] G. Baur and D. Trautmann, *Phys. Rep.* 25C (1976) 293.

[87] G. Baur et al., *Phys. Rep.* 111 (1984) 333.

[88] R. Shyam, P. Banerjee, and G. Baur, *Nucl. Phys. A* 540 (1992) 341.

[89] G. Baur, K. Hencken, and D. Trautmann, in *Proc. of ENAM 2001, Hämeenlinna, Finland, July 2001*, p. 161, Heidelberg, 2002, Springer.

[90] L. D. Landau and E. M. Lifschitz, *Quantenelektrodynamik*, volume IV of *Lehrbuch der theoretischen Physik*, Akademie Verlag, Berlin, 1986.

[91] A. Nordsieck, *Phys. Rev.* 93 (1954) 785.

[92] M. Abramowitz and I. A. Stegun, *Handbook of Mathematical Functions*, National Bureau of Standars, Washington, DC, 1964.

[93] D. Trautmann, K. Hencken, and G. Baur, A realistic solvable model for the Coulomb breakup of Neutron Halo Nuclei, to be published, 2003.

[94] P. Banerjee et al., *Phys. Rev. C* 65 (2002) 064602.

[95] A. Bonaccorso, D. M. Brink, and C. A. Bertulani, Proton vs. neutron halo breakup, Pisa preprint IFUP-TH 11/2003, available as e-print nucl-th/0302001, 2003.

[96] A. Bonaccorso, *Phys. Rev. C* 60 (1999) 054604.

[97] K. Hencken, G. Bertsch, and H. Esbensen, *Phys. Rev. C* 54 (1996) 3043.

[98] F. Schiller, *Wilhelm Tell*, J. B. Cotta'sche Buchhandlung, Tübingen, 1804.

[99] W. E. Frahn, *Diffractive Processes in Nuclear Physics*, Clarendon Press, Oxford, 1985.

[100] "Reaction Theory for Nuclei Far From Stability", INT Workshop 02-26W, Seattle, September 16 - 20, 2002, see webpage at http://int.phys.washington.edu/~int_talk/WorkShops/int_02_26W/.

[101] R. Serber, *Phys. Rev.* 72 (1947) 1008.

[102] R. J. Glauber, *Phys. Rev.* 99 (1955) 1515.

[103] A. G. Sitenko, *Theory of Nuclear Reactions*, World Scientific, Singapore, 1990.

[104] P. G. Hansen, *Phys. Rev. Lett.* 77 (1996) 1016.

[105] J. Hüfner and M. C. Nemes, *Phys. Rev. C* 23 (1981) 2538.

[106] P. G. Hansen and B. M. Sherrill, *Nucl. Phys. A* 693 (2001) 133.

[107] I. Tanihata, *J. Phys. G* 22 (1996) 157.

[108] P. G. Hansen, A. S. Jensen, and B. Jonson, *Annu. Rev. Nucl. Sci.* 45 (1995) 591.

[109] A. Bonaccorso, Reaction Mechanisms with Exotic Nuclei, Pisa preprint IFUP-TH 7/03, available as e-print nucl-th/0301030, 2003.

[110] A. Bonaccorso, Theoretical developments for low energy experiments with radioactive beams, Pisa preprint IFUP-TH 6/03, available as e-print nucl-th/0301031, 2003.

[111] C. A. Bertulani, G. Baur, and M. S. Hussein, *Nucl. Phys. A* 526 (1991) 751.

[112] C. M. Perrey and F. G. Perrey, *At. Data and Nucl. Data Tables* 17 (1976) 1.

[113] R. L. Varner et al., *Phys. Rep.* 201 (1991) 57.

[114] A. J. Koning and J. P. Delaroche, *Nucl. Phys. A* 713 (2003) 231.

[115] A. M. Kobos et al., *Nucl. Phys. A* 384 (1982) 65.

[116] M. E. Brandan and G. R. Satchler, *Nucl. Phys. A* 487 (1988) 477.

[117] G. Bertsch et al., *Nucl. Phys. A* 284 (1977) 399.

[118] D. T. Khoa, R. Satchler, and W. van Oertzen, *Phys. Rev. C* 51 (1995) 2069.

[119] M. S. Hussein, R. Rego, and C. A. Bertulani, *Phys. Rep.* 201 (1991) 279.

[120] L. Ray, *Phys. Rev. C* 20 (1979) 1857.

[121] R. J. Glauber, in *Lectures in Theoretical Physics*, edited by W. E. Brittin and L. C. Dunham, volume 1, p. 315, Interscience, New York, 1959.

[122] C. J. Joachain and C. Quigg, *Rev. Mod. Phys.* 46 (1974) 279.

[123] H. Esbensen and G. F. Bertsch, *Phys. Rev. C* 59 (1999) 3240.

[124] Y. Sakuragi, M. Yahiro, and M. Kamimura, *Prog. Theor. Phys. Suppl.* 89 (1986) 136.

[125] A. M. Moro et al., *Phys. Rev. C* 66 (2002) 024612.

[126] M. Yahiro et al., *Prog. Theor. Phys.* 67 (1982) 1464.

[127] M. Yahiro et al., *Prog. Theor. Phys. Suppl.* 89 (1986) 32.

[128] N. Austern et al., *Phys. Rep.* 154 (1987) 125.

[129] K. Varga et al., *Phys. Rev. C* 66 (2002) 034611.

[130] C. A. Bertulani and K. W. McVoy, *Phys. Rev. C* 46 (1992) 2638.

[131] P. Banerjee and R. Shyam, *Phys. Lett. B* 349 (1993) 421.

[132] H. Sagawa and N. Takigawa, *Phys. Rev. C* 50 (1994) 985.

[133] F. Barranco, E. Vigezzi, and R. A. Broglia, *Z. Phys. A* 356 (1996) 45.

[134] Y. Ogawa, K. Yabana, and Y. Suzuki, *Nucl. Phys. A* 543 (1992) 722.

[135] Y. Ogawa, Y. Suzuki, and K. Yabana, *Nucl. Phys. A* 571 (1994) 784.

[136] J. Margueron, A. Bonaccorso, and D. M. Brink, *Nucl. Phys. A* 703 (2002) 105.

[137] R. Chatterjee and R. Shyam, *Phys. Rev. C* 66 (2002) 061601(R).

[138] H. Esbensen and G. F. Bertsch, *Nucl. Phys. A* 706 (2002) 383.

[139] H. Esbensen and G. F. Bertsch, *Phys. Rev. C* 66 (2002) 044609.

[140] A. I. Akhiezer and A. G. Sitenko, *Phys. Rev.* 106 (1957) 1236.

[141] J. Margueron, A. Bonaccorsa, and D. M. Brink, *Nucl. Phys. A* 720 (2003) 337.

[142] A. Alavi-Harati et al., *Phys. Rev. Lett.* 89 (2002) 072001.

[143] D. Carey et al., *Phys. Rev. Lett.* 64 (1990) 357.

[144] K.-H. Schmidt et al., *Nucl. Phys. A* 665 (2000) 221.

[145] A. Heinz et al., *Nucl. Phys. A* 713 (2003) 3.

[146] M. C. Abreu et al., *Phys. Rev. C* 59 (1999) 876.

[147] G. Baur and C. A. Bertulani, *Nucl. Phys. A* 505 (1989) 835.

[148] G. Baur, K. Hencken, and D. Trautmann, *Topical Review, J. Phys. G* 24 (1998) 1657.

[149] G. Baur et al., *Phys. Rep.* 364 (2002) 359.

[150] M. Chiu et al., *Phys. Rev. Lett.* 89 (2002) 012302.

[151] S. R. Klein, *Nucl. Instrum. Methods* A59 (2001) 51.

[152] A. Baltz, C. Chasman, and S. N. White, *Nucl. Instrum. Methods* 417 (1998) 1.

[153] K. Hencken and S. White, *Cern Courier* 42 (2002) 15.

[154] S. Klein and J. Nystrand, *Phys. Rev. C* 60 (1999) 014903.

[155] C. Adler et al., *Phys. Rev. Lett.* 89 (2002) 272303.

[156] F. Krauss, M. Greiner, and G. Soff, *Prog. Part. Nucl. Phys.* 39 (1997) 503.

[157] G. Baur et al., in *Proceedings of the workshop on "Electromagnetic Probes of Fundamental Physics", Erice, Italy, Oct. 16–21, 2001*, edited by W. Marciano and S. White, p. 235, Singapore, 2003, World Scientific, available as e-print hep-ex/0201034.

[158] T. Glasmacher, *Annu. Rev. Nucl. Part. Sci.* 48 (1998) 1.

[159] T. Glasmacher, *Nucl. Phys. A* 693 (2001) 90.

[160] T. Motobayashi et al., *Phys. Lett. B* 346 (1995) 9.

[161] H. Scheit et al., *Phys. Rev. Lett.* 77 (1996) 3967.

[162] R. Anne et al., *Z. Phys. A* 352 (1995) 397.

[163] T. Nakamura et al., *Phys. Lett. B* 394 (1997) 11.

[164] M. Fauerbach et al., *Phys. Rev. C* 56 (1997) R1.

[165] C. A. Bertulani, L. F. Canto, and M. S. Hussein, *Phys. Lett. B* 353 (1995) 413.

[166] S. Typel and G. Baur, *Phys. Lett. B* 356 (1995) 186.

[167] H. Iwasaki, *Phys. Lett. B* 522 (2001) 227.

[168] Homepage of Thomas Glasmacher, see webpage at www.nscl.msu.edu/∼glasmacher.

[169] P. D. Cottle et al., *Phys. Rev. Lett.* 88 (2002) 172502.

[170] T. Uchiyama and H. Morinaga, *Z. Phys. A* 320 (1985) 273.

[171] J. M. Blatt and V. F. Weisskopf, *Theoretical nuclear physics*, Springer, New York, 1979.

[172] P. G. Hansen and B. Jonson, *Europhys. Lett.* 4 (1987) 409.

[173] K. Ikeda, *Nucl. Phys. A* 538 (1992) 355c.

[174] G. F. Bertsch, in *Trends in nuclear physics, 100 years later*, edited by H. Nifenecker et al., volume Session LXVI of *Les Houches*, p. 123, Elsevier, Amsterdam, 1998.

[175] Y. Alhassid, M. Gai, and G. Bertsch, *Phys. Rev. Lett.* 49 (1982) 1482.

[176] C. A. Bertulani, H.-W. Hammer, and U. van Kolck, *Nucl. Phys. A* 712 (2002) 37.

[177] D. M. Kalassa and G. Baur, The effective range approach to the electromagnetic dissociation of loosely bound nuclei, in *Proc. of the Int. Conference on "Physics with GeV-Particle Beams"*, edited by H. Machner and K. Sistemich, p.468, Singapore, 1994, Forschungszentrum Jülich, World Scientific.

[178] D. M. Kalassa and G. Baur, *J. Phys. G* 22 (1996) 115.

[179] A. Mengoni et al., *Phys. Rev. C* 52 (1995) R2334.

[180] T. Otsuka et al., *Phys. Rev. C* 49 (1994) R2289.

[181] T. Aumann et al., *Nucl. Phys. A* 687 (2001) 103c.

[182] A. Horvath et al., *Astrophys. J.* 570 (2002) 926.

[183] G. Bohm and F. Wysotzki, *Nucl. Phys. B* 15 (1970) 628.

[184] M. Juric et al., *Nucl. Phys. B* 52 (1973) 1.

[185] V. L. Lyuboshits, *Sov. J. Nucl. Phys.* 51 (1990) 648.

[186] B. V. Danilin et al., *Nucl. Phys. A* 632 (1998) 383.

[187] B. V. Danilin et al., *Phys. Rev. C* 55 (1997) R577.

[188] T. Aumann et al., *Phys. Rev. C* 59 (1999) 1252.

[189] A. Leistenschneider et al., *Phys. Rev. Lett.* 86 (2001) 5442.

[190] H. Sagawa and T. Suzuki, *Phys. Rev. C* 59 (1000) 3116.

[191] T. Kobayashi et al., *Phys. Lett. B* 232 (1989) 51.

[192] S. Shimoura et al., *Phys. Lett. B* 348 (1995) 29.

[193] M. Zinser et al., *Nucl. Phys. A* 619 (1997) 151.

[194] H. Esbensen, G. F. Bertsch, and K. Ieki, *Phys. Rev. C* 48 (1993) 326.

[195] H. Esbensen and G. Bertsch, *Phys. Rev. C* 46 (1992) 1552.

[196] K. Ieki et al., *Phys. Rev. C* 54 (1996) 1589.

[197] G. F. Bertsch, K. Hencken, and H. Esbensen, *Phys. Rev. C* 77 (1998) 1366.

[198] M. Meister et al., *Nucl. Phys. A* 700 (2002) 3.

[199] J. Wang et al., *Phys. Rev. C* 65 (2002) 034036.

[200] F. M. Marquez et al., *Phys. Rev. C* 64 (2001) 061301.

[201] T. Minemura et al., *RIKEN Accel. Prog. Rep.* 35 (2002) 59.

[202] "Nuclear Structure and Dynamics at the Limits", Hirschegg, Kleinwalsertal, January 12–18, 2003 see webpage at http://theory.gsi.de/hirschegg/.

[203] H. Utsunomiya et al., *Phys. Rev. C* 63 (2001) 018801.

[204] S. Austin, in *EMI 2001 Int. Symp. Electromagnetic Interactions in Nuclear and Hadron Physics*, Singapore, 2002, World Scientific, available as e-print nucl-th/0201010.

[205] J. Kiener et al., *Phys. Rev. C* 44 (1991) 2195.

[206] K. M. Nollett, M. Lemoine, and D. N. Schramm, *Phys. Rev. C* 56 (1997) 1144.

[207] J. Hesselbarth and T. K. Knöpfle, *Phys. Rev. Lett.* 67 (1991) 2773.

[208] R. G. H. Robertson et al., *Phys. Rev. Lett.* 47 (1981) 1867.

[209] F. E. Cecil et al., *Phys. Rev. C* 53 (1996) 1967.

[210] P. Mohr et al., *Phys. Rev. C* 50 (1994) 1543.

[211] A. Shotter et al., *Phys. Rev. Lett.* 53 (1984) 1539.

[212] S. B. Gazes et al., *Phys. Rev. Lett.* 68 (1992) 150.

[213] P. D. Zecher et al., *Phys. Rev. C* 57 (1998) 959.

[214] S. K. Rosswog, C. Freiburghaus, and F.-K. Thielemann, *Nucl. Phys. A* 688 (2001) 344.

[215] Z. Q. Mao and A. E. Champagne, *Nucl. Phys. A* 522 (1991) 568.

[216] R. A. Malaney and W. A. Fowler, *Astrophys. J.* 345 (1989) L5.

[217] T. Rauscher et al., *Astrophys. J.* 429 (1994) 499.

[218] P. Descouvement, *Astrophys. J. Lett.* 405 (1993) 518.

[219] H. Kobayashi et al., *Phys. Rev. C* 67 (2003) 015806.

[220] M. Wiescher, J. Görres, and F. Thielemann, *Astrophys. J.* 363 (1990) 340.

[221] P. Descouvement, *Nucl. Phys. A* 675 (2000) 559.

[222] H. Beer et al., *Astrophys. J.* 387 (1992) 258.

[223] J. Kiener, in *NATO Advanced Study Institute: Nuclei Far from Stability and Astrophysics*, edited by D. N. Poenaru, H. Rebel, and J. Wentz, p. 271, New York, 2001, Plenum.

[224] V. Tatischeff et al., *Phys. Rev. C* 51 (1995) 2789.

[225] G. Baur and M. Weber, *Nucl. Phys. A* 504 (1989) 352.

[226] F. Fleurot, $^{16}O$ *Coulomb dissociation: a means to determine* $^{12}C + \alpha$ *fusion rate in stars*, PhD thesis, Rijksuniversiteit Groningen, 2002, (unpublished), available from http://www.ub.rug.nl/eldoc/dis/science/f.fleurot/.

[227] T. Motobayashi et al., *Phys. Lett. B* 264 (1991) 259.

[228] J. Kiener et al., *Nucl. Phys. A* 552 (1993) 63.

[229] P. Decrock et al., *Phys. Rev. Lett.* 67 (1991) 808.

[230] M. Serata et al., *RIKEN Accel. Prog. Rep.* 35 (2002) 62.

[231] A. Levebvre et al., *Nucl. Phys. A* 595 (1995) 69.

[232] M. Wiescher and F. Thielemann, *Astrophys. J.* 343 (1989) 352.

[233] T. Motobayashi et al., *Eur. Phys. J. A* 13 (2002) 207.

[234] T. Minemura et al., *RIKEN Accel. Prog. Rep.* 35 (2002) 58.

[235] T. Gomi et al., *RIKEN Accel. Prog. Rep.* 35 (2002) 69.

[236] C. Rolfs, *Nucl. Phys. A* 217 (1973) 29.

[237] R. Morlock et al., *Phys. Rev. Lett.* 79 (1997) 3837.

[238] J. F. Liang et al., *Phys. Lett. B* 491 (2000) 23.

[239] C. A. Bertulani and P. Danielewicz, *Nucl. Phys. A* 717 (2003) 199.

[240] The Royal Swedish Academy of Sciences, The Nobel Prize in Physics 2002, see webpage at http://www.nobel.se/physics/laureates/2002/.

[241] Q. Ahmad et al., *Phys. Rev. Lett.* 87 (2001) 071301.

[242] Q. Ahmad et al., *Phys. Rev. Lett.* 89 (2002) 011301.

[243] Q. Ahmad et al., *Phys. Rev. Lett.* 89 (2002) 011302.

[244] K. Eguchi et al., *Phys. Rev. Lett.* 90 (2003) 021802.

[245] J. N. Bahcall, M. H. Pinsonneault, and S. Basu, *Astrophys. J.* 555 (2001) 990.

[246] J. N. Bahcall, S. Basu, and M. H. Pinsonneault, *Phys. Lett. B* 433 (1998) 1.

[247] V. Barger, D. Marfatia, and K. Whisnant, *Phys. Rev. Lett.* 88 (2002) 011302.

[248] Homepage of John N Bahcall, see webpage at http:/www.sns.ias.edu/∼jnb/.

[249] A. R. Junghans et al., *Phys. Rev. Lett.* 88 (2002) 0411011.

[250] F. Hammache et al., *Phys. Rev. Lett.* 80 (1998) 928.

[251] F. Strieder et al., *Nucl. Phys. A* 696 (2001) 219.

[252] L. T. Baby et al., *Phys. Rev. Lett.* 90 (2003) 022501.

[253] F. Terrasi et al., *Nucl. Phys. A* 688 (2001) 539.

[254] G. Taube, *Science* 266 (1994) 1157.

[255] N. Iwasa et al., *Phys. Rev. Lett.* 83 (1999) 2910.

[256] J. H. Kelley et al., *Phys. Rev. Lett.* 77 (1996) 5020.

[257] B. Davids et al., *Phys. Rev. C* 63 (2001) 065806.

[258] T. Motobayashi et al., *Phys. Rev. Lett.* 73 (1994) 2680.

[259] J. von Schwarzenberg et al., *Phys. Rev. C* 53 (1996) R2598.

[260] T. Kikuchi et al., *Phys. Lett. B* 391 (1997) 261.

[261] N. Iwasa et al., *J. of Phys. Soc. of Japan* 65 (1996) 1256.

[262] T. Kikuchi et al., *Eur. Phys. J. A* 3 (1998) 213.

[263] B. Davids et al., *Phys. Rev. Lett.* 81 (1998) 2209.

[264] B. Davids et al., *Phys. Rev. Lett.* 86 (2001) 2750.

[265] E. G. Adelberger et al., *Rev. Mod. Phys.* 70 (1998) 1265.

[266] F. Schümann et al., *Phys. Rev. Lett.* 90 (2003) 232501.

[267] P. Descouvement and D. Baye, *Nucl. Phys. A* 567 (1994) 341.

[268] B. Davids and S. Typel, Electromagnetic dissociation of $^8B$ and the astrophysical $S$ factor for $^7Be(p, \gamma)^8B$, submitted to Phys. Rev. C, available as e-print nucl-th/0304054, 2003.

[269] M. Gai, Solar Fusion and The Coulomb Dissociation of 8B; What Have We Learned and Where Do We Go From Here?, Paper for the 19th Conf. on Nuclear Dynamics, Breckenridge, Colorado, available as e-print nucl-th/0303009, 2003.

[270] Opportunities in Nuclear Astrophysics, Conclusions of a Town Meeting held at the University of Notre Dame 7–8, June 1999.

[271] Radioactive Nuclear Beam Facilities, NuPECC Report, 2000.

[272] F. Käppeler, M. Wiescher, and F. Thielemann, *Annu. Rev. Nucl. Part. Sci.* 48 (1998) 175.

[273] C. E. Rolfs and W. S. Rodney, *Cauldrons in the Cosmos*, University of Chicago Press, Chicago, 1988.

[274] J. J. Cowan, F.-K. Thielemann, and J. W. Truran, *Phys. Rep.* 208 (1991) 267.

[275] Homepage of Thomas Rauscher, see webpage at http://quasar.physik.unibas.ch/~tommy/.

[276] T. Rauscher et al., *Phys. Rev. C* 57 (1998) 2031.

[277] S. Goriely, *Phys. Lett. B* 436 (1998) 10.

[278] M. Gai, ISOL workshop, Columbus/Ohio, July 30 – August 1, 1997, 1997.

[279] F. Hoyle, *Astrophys. J.* Suppl. 1 (1954) 121.

[280] J. Görres et al., *Phys. Rev. C* 52 (1995) 2231.

[281] V. D. Efros et al., *Z. Phys. A* 355 (1996) 101.

[282] F. Ajzenberg-Selove, *Nucl. Phys. A* 490 (1988) 1.

[283] G. Kuechler, A. Richter, and W. von Witsch, *Z. Phys. A* 326 (1987) 447.

[284] H. Utsunomia et al., in *EMI 2001 Int. Symp. Electromagnetic Interactions in Nuclear and Hadron Physics*, Singapore, 2001, World Scientific.

[285] H. Schatz et al., *Phys. Rep.* 294 (1998) 167.

[286] M. Wiescher and H. Schatz, *Nucl. Phys. A* 693 (2001) 269.

[287] I. Baraffe et al., Nuclear and Particle Astrophysics, F.-K. Thielemann (convener), in NuPECC Report: *Nuclear Physics in Europe: Highlights and Opportunities*, 1997.

[288] J. Görres, M. Wiescher, and T.-K. Thielemann, *Phys. Rev. C* 51 (1995) 392.

[289] T. D. Lee, *Particle Physics and Introduction to Field Theory*, Harwood academic publishers, London, 1981.

[290] J. D. Jackson and L. B. Okun, *Rev. Mod. Phys.* 73 (2001) 663.

[291] K. Alder and A. Winther, editors, *Coulomb Excitation*, Perspectives in Physics, Academic Press, New York, London, 1966.

[292] A. I. Achieser and W. B. Berestezki, *Quanten-Elektrodynamik*, Teubner-Verlag, Leipzig, 1962.

[293] G. N. Watson, *Theory of Bessel Functions*, Cambridge University Press, New York, 1944.

[294] A. Bohr and B. Mottelson, *Nuclear Structure*, volume I: Single Particle Motion, Benjamin, New York, 1969.

[295] G. Baur and C. Bertulani, *Phys. Rev. C* 56 (1997) 581.

[296] C. J. Benesh, A. C. Hayes, and J. L. Friar, *Phys. Rev. C* 54 (1996) 1404.

[297] T. Rubehn, W. F. J. Müller, and W. Trautmann, *Phys. Rev. C* 56 (1997) 1165.

[298] C. T. Munger, S. J. Brodsky, and I. Schmidt, *Phys. Rev. D* 49 (1994) 3228.

[299] H. Meier et al., *Eur. Phys. J. C* 5 (1998) 287.

[300] C. A. Bertulani and G. Baur, *Phys. Rev. D* 58 (1998) 034005.

[301] U. Fano, *Annu. Rev. Nucl. Sci.* 13 (1963) 1.

[302] A. B. Voitkiv and J. Ullrich, *J. Phys. B* 34 (2001) 4513.